Endogenously expressed bestrophin-1 modulates calcium signaling in the retinal pigmented epithelium

DISSERTATION ZUR ERLANGUNG DES DOKTORGRADES DER NATURWISSENSCHAFTEN (DR. RER. NAT.) DER NATURWISSENSCHAFTLICHEN FAKULTÄT III
– BIOLOGIE UND VORKLINISCHE MEDIZIN
DER UNIVERSITÄT REGENSBURG

vorgelegt von

Néstor Más Gómez

aus La Habana, Cuba

im Jahr 2012

Die vorliegende Arbeit entstand im Zeitraum von August 2008 bis June 2012 unter der Anleitung von Herrn Prof. Dr. rer. nat. Olaf Strauß in der Abteilung für Experimentelle Ophthalmologie des Universitätsklinikums Regensburg.

_____

Néstor Más Gómez

Promotionsgesuch eingereicht am:	20.06.2012
Die Arbeit wurde angeleitet von:	Herr Prof. Dr. Olaf Strauß
Prüfungsausschuss:	Herr Prof. Dr: Richard Warth (Vorsitzender)
	Herr Prof. Dr. Olaf Strauß (1.Prüfer)
	Herr Prof. Dr. Stephan Schneuwly (2.Prüfer)
	Herr Prof. Dr. Rainer Schreiber (3.Prüfer)

Summary

Mutations in the BEST1 gene lead to a variety of retinal degenerations. To understand the function of the BEST1 gene product, bestrophin-1, represents the first step in the investigation of patho-mechanisms leading to BEST1-associated retinal degenerations. Bestrophin-1 is a protein expressed in the cells of the retinal pigment epithelium (RPE), a monolayer of epithelial cells in the outer retina which closely interact with the photoreceptors. Thus, it is likely that mutant bestrophin-1 changes the RPE function which in turn leads to photoreceptor degeneration. So far the properties of bestrophin-1 were identified by functional analysis of over-expressed proteins. In these studies bestrophin-1 was identified as a Ca^{2+}-dependent Cl channel in the plasma membrane. However, this result could not explain observations made in animal models for bestrophin-1 or cellular function analysis in relation to presence of endogenously expressed bestrophin-1. The few studies on the function of endogenously expressed bestrophin-1 indicated that it may have an intracellular function in relation to Ca^{2+}signaling. The aim of the study was to investigate the function of endogenously expressed bestrophin-1 in mouse models and in a newly developed *in vitro* model of porcine RPE cells.

Since the retina of bestrophin-1 knock-out mice or $Best^{+/Y227N}$ knock-in mice showed no degeneration, the susceptibility of these retinae to light-damage at the threshold to light-damage was tested. Here, no differences between wild-type and transgenic mice were found. Also the ATP-dependent Ca^{2+}-Signals in RPE cells from these mouse strains were not changed. In the porcine RPE cell model siRNA bestrophin-1 was investigated. Ca^{2+}-signaling was ignited by induction of store-operated Ca^{2+}-entry (SOCE). Pharmacological analysis and siRNA knock-down of Orai-1 expression reveled that SOCE was dependent on the activation of Orai-1 channels by stim-1 (stromal interacting molecule-1). Reduction of bestrophin-1 expression did not change the expression of stim-1 or orai-1 expression but reduced the SOCE amplitude. Measuring amplitude of Ca^{2+}-release from intracellular Ca^{2+} stores in response to inhibition of sarcoplasmaic Ca^{2+}-ATPase (SERCA) and quantification of the amount of Ca^{2+} releasable from ER Ca^{2+} stores revealed that after bestrophin-1 knock-down the amount of Ca^{2+} in these stores was strongly decreased. In addition

to these functional data also the analysis of subcellular bestrophin-1 localization by means of immunocytochemistry or electron-microscopy revealed that bestrophin-1 is an intracellular protein which co-localizes with stim-1. However, bestrophin-1 and stim-1 did not physically interact.

In summary, we found that bestrophin-1 is likely an intracellular Cl channel in the membrane of cytosolic Ca^{2+} stores which are localized close to the basolateral membrane. As a Cl channel bestrophin-1 can Ca^{2+}-dependently conduct the counter-ion for Ca^{2+} to accumulate Ca^{2+} in ER stores. The reduced Ca^{2+} amount in Ca^{2+}-stores decreases the activation SOCE and therefore changes intracellular Ca^{2+} signaling which controls RPE function. With these conclusions we can open a new route to understand the chain of events leading to retinal degeneration in BEST1-associated diseases.

Acknowledgments/Agradecimientos

Before to start to give my thanks to all those people who have been with me during these four years of challenges, I would like to give my special thanks to a friend who without his support, I wouldn´t be here today. Thank you very much to Professor Georg Büldt for being such a great person.

I want to give also special thanks to my mentor Prof. Dr. Olaf Strauß, who gave me the chance to join his group. Your confidence and patient in my steps forward were vital for me. Many thanks too, not only because of teaching me physiology but also to show me how to do science.

I want to thank one of my best friends Rene Barro Soria who was also one of the key collaborators who helped me to start my studies in Germany. El Rene…gracias mi bro por ayudarme en todo lo que estuvo a tu alcance, además de los buenos tiempos que fueron bastante.

Thank you very much to Prof. Dr. Stephan Schneuwly, Prof. Dr. Rainer Schreiber, Prof. Dr. Richard Warth and Prof. Dr. Wolf Hayo to accept to be part of my thesis committee.

Many thanks to the FOR 1075 which supported my research during my PhD studies.

Many thanks to Prof. Dr. Ernst Tamm and the technical assistant Margit Schimmel for the assistance provided with the electron microscope.

Many thanks as well to Prof. Dr. Ralph Witzgall and Uwe Devries for giving me the chance to use the confocal microscope.

I would like to give many thanks to: Elfriede Eckert, Andrea Dannullis and Renate Föckler who taught to me how to deal with the laboratory and many basic techniques.

I must say that I was very lucky to have Claudia Müller as a colleague in my group and also as a daily friend in Regensburg. You made my time in Germany very special.

I would like to give special thanks to Joana Raquel Delgado Martins who made the whole formatting of this thesis. Also for all the great time we shared in Regensburg along these years. “Ohe y el vino donde está?”.

To my huge intercultural team of people like: Dianilla, la Noki, la Ana Marta, el Arthur, Der Markus, el David, Dannette, Shimpei, Julia, Simon, Isabelita and many more, thank you to all for the great times we have lived in Regensburg.

And my deepest thanks to my parents. Gracias por todo el apoyo y el amor que me han dado durante todos estos infinitos días de separación. Sin su presencia espiritual no hubiera tenido las fuerzas necesarias para enfrentarme a esta gran meta en mi vida. Les dedico mi doctorado a ustedes. Les quiero y les llevo siempre conmigo.

Abbreviations

%	per cent
°	degree
^{2}	square
2-APB	2-Aminoethoxydiphenyl borate
aa	amino acid
ARPE-19	human RPE cell line (arising RPE from a 19 years old male)
ATP	adenosine triphosphate
Ba^{2+}	barium
BEST1	bestrophin-1 gene
bp	base pair
BSA	bovine serum albumin
BVMD	Best Vitelliform Macular Dystrophy
C terminus	carboxyl terminus
C	Celsius
Ca^{2+}	calcium
CAMKII	Ca^{2+}/calmodulin-dependent protein kinase II
cAMP	cyclic adenosine 3',5'-monophosphate
cDNA	complementary desoxyribonucleic acid
CFTR	cystic fibrosis transmembrane conductance regulator
Cl^-	chloride
CLCs	chloride channel(s)
cm	centimetre
cmr	canine multifocal retinopathy
CO_2	carbon dioxide

CPA	cyclopiazonic acid
DIC	differential interference contrast
DMEM	Dulbecco's modified Eagle's medium
EDTA	ethylene-diamine-tetraacetic acid
EGTA	ethylene glycol tetraacetic acid
EOG	electro-oculogram
ER	endoplasmic reticulum
ERG	electro-retinogram
FAK	focal adhesion kinase
FBS	fetal bovine serum
Fig.	figure
Glut	glucose transporter
H^+	Hydrogen
HCO_3	bicarbonate
HEK	human embryonic kidney cell line
HRP	horseradish peroxidase
I_{crac}	Orai channel current
IP_3	inositol 1,4,5-trisphosphate
IP_3R	inositol 1,4,5-trisphosphate receptor
K^+	Potassium
K_d	dissociation constant
KI	knock-in
KO	knock-out
LD	light damage
LP	light peak
m	milli, meter, mouse

M	mol/liter
MDCK	Madin-Darby Canine Kidney
MerTK	Mer tyrosine kinase
Min	minute(s)
mRNA	messenger ribonucleic acid
N	amino terminus
n	nano, number
n.s	not significant
Na^+	sodium
Orai	ORAI calcium release-activated calcium channel
P2X	purinergic receptor P2X, ligand gated ion channel
P2Y	purinergic receptor P2Y, G-protein coupled
PBS	phosphate buffered saline
Pen	penicillin
PLC	phospholipase C
POS	photoreceptor outer segment
qPCR	quantitative polymerase chain reaction
RPE	retinal pigment epithelium
RT	reverse transcriptase, room temperature
RYR	ryanodine receptor
SAM	sterile alpha motif
SDS-PAGE	sodium dodecyl sulphate polyacrylamide gel electrophoresis
S	second(s)
SERCA	sarco-endoplasmic reticulum ATPase
siRNA	small interfering RNA
SOCE	store-operated Ca^{2+} entry

STIM	stromal interaction molecule
Strep	streptomycin
TG	thapsigargin
TMDs	transmembrane domains
VMD2	vitelliform macular dystrophy
WT	wild-type
M	micro
Ω	ohm

Index

1 Introduction

The human visual system is able to receive and process an important amount of information about the world. The first step in the process of seeing starts when the optics of the eye focuses an image onto the light-sensitive retina. In the retina, photons are detected by photoreceptive cells which transduce light energy to an electrical signal (**Fig. 1**). This new signal is refined by synaptic interactions within the neural circuits of the retina and it is processed through the central visual pathways in the brain.

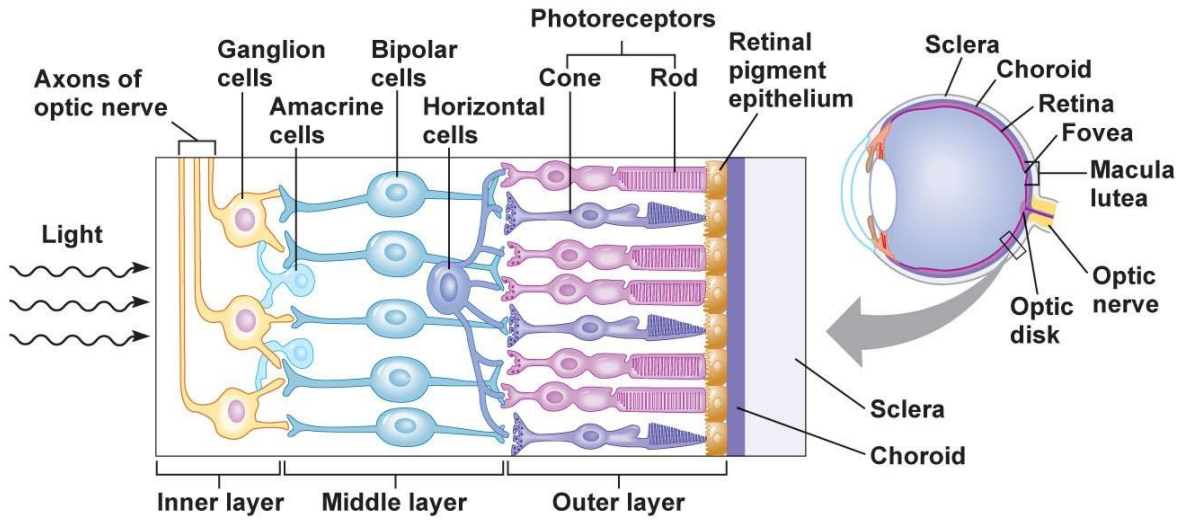

http://virtual.yosemite.cc.ca.us/rdroual/Course%20Materials/Physiology%20101/Chapter%20Notes/Fall%202007/chapter_10%20Fall%202007.htm

Fig. 1 Structure of a human retina.

1.1 RPE functions.

In the animal kingdom, pigmented and photoreceptive cells together have been described as the simplest light detecting organ in the evolution of the eye [1]. So the interaction between pigmented cells and photoreceptor cells is important for visual function [2-5]. In addition, during embryonic development, the functional differentiation of the photoreceptor layer and the retinal pigment epithelium layer (RPE) depend on each other [6, 7].

In the vertebrate eye, the retinal pigmented epithelium (RPE) is a continuous monolayer of cuboidal densely packed cells which plays a central role in retinal physiology [2, 8]. These fully pigmented cells are located between photoreceptors and Bruch´s membrane [8]. The apical membrane contains long microvilli which are in close interaction with photoreceptor outer segments [2].This close interaction makes the RPE able to support photoreceptors function. Furthermore, impaired functions of the RPE lead to photoreceptor degeneration [9-15]. On the other hand, lateral membranes of these cells are joined by a continuous belt of tight junctions which form the outer blood-retina barrier [16, 17]. Due to its localization and characteristics, the RPE is able to fulfill many functions that are essential for visual function [5, 18-20] (**Fig. 2**). These functions are: light absorption, epithelial transport, spatial ion buffering, visual cycle, phagocytosis, secretion and immune modulation.

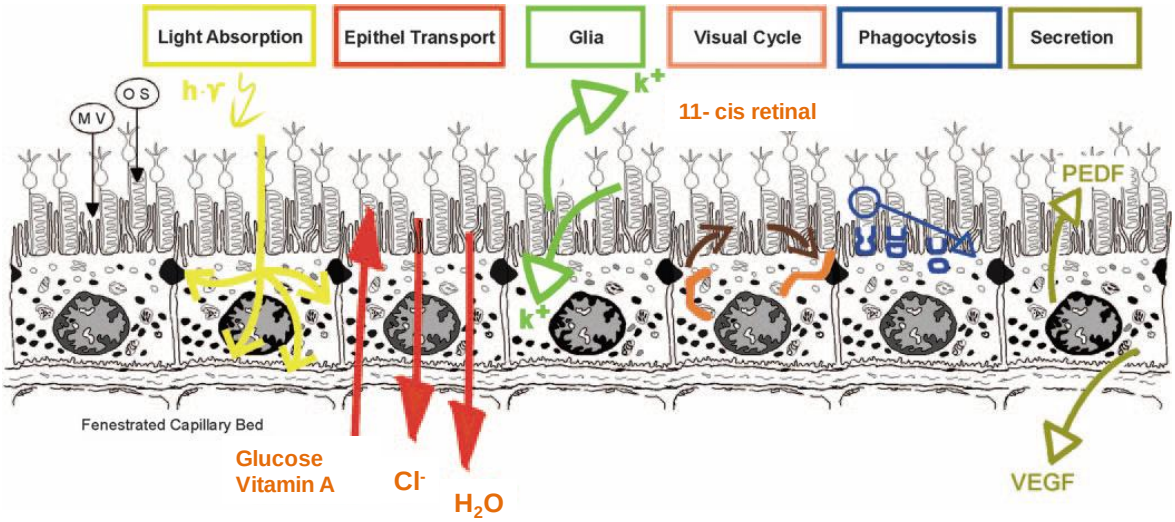

Strauß O. 2005 *Physiol Rev*

Fig. 2 A summary of retinal pigmented epithelium (RPE) functions. VEGF, vascular epithelium growth factor; PEDF, pigment epithelium-derived growth factor.

1.1.1 Light absortion

RPE cells are characterized by their heavy pigmentation. By this, they form a dark wall which is covering the inner of the bulbus. Thus, the RPE is capable to absorb scattered light in the eye which enhances the optic quality [2]. On the other hand, light energy is concentrated in the macula by the lens. The RPE is exposed to an oxygen-rich environment due to the high levels of oxygen in the blood in choriocapillaris [21-23]. This compromises high photo-oxidative activity and subsequent photo-damage in the RPE [2, 8]. Phagocytosis of photoreceptor outer segments further increases the generation of reactive oxygen species in RPE cells [24].

However, the RPE has evolved several lines of defense against all these simultaneous process of oxidative damage, [2, 8].For this purpose, RPE cells contain various pigments that are specialized in filtering different wavelengths [25]. For example, melanin in melanosomes works as a neutral density filter reducing light levels at the RPE [26]. In addition, photoreceptors cells contain the carotenoids lutein and zeaxanthin which are in charge of the absorption of blue light [27, 28]. The blue light appears to be the most dangerous for RPE cells because it promotes catalysis by the photo-oxidation of lipofuscin components into cell toxic substances [29, 30]. Interestingly, the absorption of light by melanosomes and blue light absorbing pigments are only responsible for the absorption of 60% of the light energy [26, 31]. This suggests the involvement of other pigments that have not been described yet. Another mechanism which protects the RPE from light is done by enzymatic (ex: superoxide dismutase and catalase) and non enzymatic (ex: glutathione, ascorbate, α-tocopherol, carotenoids, melanin) antioxidants. These antioxidants neutralize reactive oxygen species before they can cause damage to cellular macromolecules [32, 33]. Despite all these mechanisms of defense, still some oxidative damage remains. However, the RPE is able to recognize damaged DNA, lipids and proteins which can be rapidly repaired or replaced [34].

1.1.2 Epithelial transport

RPE cells have the structural properties of water and ion transporting epithelium [35]). These characteristics are determined by the presence of tight junctions. Therefore, RPE shows an apical to basolateral polarity by structure, organization of organelles and the distribution of membrane proteins [5, 36, 37]. The asymmetric distribution and regulation of these proteins ensure that the RPE transports water, ions and metabolites from the subretinal space to the choroid, and glucose and other nutrients from the blood stream to the photoreceptors [38-40].

The transport of water across the RPE occurs mainly via the transcellular route because of the high resistance formed by the tight junctions. Thus, the RPE expresses aquaporin-1 at the apical and basal membranes for the movement of water [41, 42].The apical transport is driven by the Na^+-K^+-ATPase which localizes apically in the RPE [43-46]. This pump generates the gradient for the uptake of Cl^- and K^+ through the Na^+-K^+-$2Cl^-$ co-transporter [47-52] resulting in a high intracellular Cl^- activity [50, 53, 54]. Cl^- can leave the cell across the basolateral membrane via Ca^{2+}-dependent Cl channels, ClC-2 channel or/and CFTR channel [55-58]. The regulation of pH occurs by the combined activity of the Na^+/H^+ exchanger together with the Na^+/HCO3 co-transporter in the apical membrane and a Cl^-/HCO3 co-transporter at the basolateral membrane [2].

The transport of retinol between the photoreceptors and blood stream is carried out by RPE cells [8]. This process is very important because it is directly coupled to the visual cycle [59]. The transport of glucose in the RPE is passive and is determined by a high amount of glucose transporter Glut-1 and Glut-3 distributed in the apical and basolateral membranes [38-40].

1.1.3 Spatial ion buffering

The light-dependent changes of the photoreceptors activity lead to fast changes in the ion composition in the subretinal space, which requires a fast and capacitative compensation by the RPE [60]. The normal transepithelial transport would be too slow for these changes. In support of this, the RPE has two possible mechanisms to compensate for these changes. One is related with the decrease of K^+ concentration in the subretinal space during light-dependent activation of photoreceptors. The decrease of subretinal K^+ concentration hyperpolarizes the apical membrane of the RPE [61-63].This hyperpolarization in turn leads to the activation of inwardly rectifying K^+ channels which generate the efflux of K^+ back into the subretinal space [64-67]. The second mechanism compensates for volume changes in the subretinal space. This compensation is based on the activity of the apical Na^+/HCO_3^- co-transporter which is voltage-dependent [68]. The light-induced hyperpolarization of the apical membrane decreases the Na^+/HCO_3^- co-transporter activity. This in turn leads to intracellular acidification followed by Cl^- efflux and a subsequent movement of water [69-71].

1.1.4 Visual cycle

The transduction of light into an electrical signal starts with the absorption of a photon by rhodopsin in the photoreceptor outer segment [72-74]. The rhodopsin is composed by a transmembrane G-protein coupled receptor, the opsin and its chromophore 11-*cis* retinal [75]. After bleaching of rhodopsin, 11-*cis* retinal isomerizes to all-*trans* retinal which in turn actives opsin and ignites the signal transduction cascade [74, 76]. Rhodopsin can only be activated again when all-trans retinal is exchanged by 11-cis retinal so the regeneration of all-*trans* retinal to 11-*cis* retinal is vital for the visual function [1, 77]. Since the RPE expresses the isomerase for 11-cis-*trans* retinal, and not the photoreceptor cells, the re-isomarization takes place in the RPE. For this purpose, all-*trans* retinal is delivered to the RPE where it is re-isomerized to 11-*cis* retinal by the RPE65 isomerase and transported back to photoreceptor outer segment. This process is called the visual cycle of retinal [78]. Mutations in the RPE65 isomerase lead to retinal degenerations [13-15].

1.1.5 Phagocytosis

The renewal of photoreceptor outer segment (POS) in concert with the phagocytosis of mature POS by the RPE is a process which is required for proper retinal function [79]. In addition, the turnover of POS is regulated by circadian rhythms [80, 81].

The POS phagocytosis compromises different steps: the recognition and binding, the RPE signaling which in turn leads to the engulfment of POS, and the degradation of the POS [79]. The following receptors have been identified to be responsible to regulate phagocytosis: the surface receptor Mer tyrosine kinase (MerTK), the scavenger receptor CD36, and the integrin adhesive receptor αvβ5 [2]. The event of binding, mediated by αvβ5 [19, 82-84], is transduced into an intracellular signal, a rise in inositol 1,4,5-trisphosphate, which in turn leads to the ingestion of the bound POS [85]. Although, the signal transduction is carried out by MerTK receptor, this mechanism is coordinated by the interaction of integrin and MerKT through a focal adhesion kinase (FAK) [83].The engulfment of POS involves the macrophage receptor CD36 [84, 86-88]. After the internalization, the fusion of phagosomes with lysosomes results in the degradation of the ingested POS by different lysosomal proteases [8, 89].

1.1.6 Secretion

The RPE is known to produce and to secret a large variety of growth factors and signaling molecules [90]. Some of these factors are: ATP, fas-ligand (fas-L), fibroblast growth factors (FGF-1, FGF-2, and FGF-5), transforming growth factor-β (TGF-β), insulin-like growth factor-1 (IGF-1), ciliary neurotrophic factor (CNTF), platelet-derived growth factor (PDGF), vascular endothelial growth factor (VEGF), lens epithelium-derived growth factor (LEDGF), members of the interleukin family, tissue inhibitor of matrix metalloprotease (TIMP) and pigment epithelium-derived factor (PEDF) [2]. Many of them are essential for the maintenance of structural integrity of the retina and choriocapillaris [91, 92].

1.1.7 Immune modulation

RPE is able to modulate immune responses in the eye [18, 93]. This function is supported in two ways. First, RPE works as a barrier separating blood stream from the inner eye and second it can communicate with the immune system in order to suppress immune reactions in the eye. For this purpose, the RPE is able to secrete immune modulatory factors such as interleukin-8 (IL-8) [94], complement factor H (CFH) [95] or monocyte chemotactic protein-1 (MCP1) [96].

1.2 Calcium and cell function in general

When cells respond to an external stimuli such as membrane depolarization, stretch, noxious stimuli, extracellular agonists, etc, this external information is translated into internal second messenger such as Ca^{2+}, which is a major player in intracellular information processing [97]. Ca^{2+} can regulate many cellular processes such as: fertilization, proliferation, development, contraction and secretion [98]. For these aims, cells have an extensive signaling toolbox to create Ca^{2+} signals with specialized spatial and temporal properties [98]. Cells can generate Ca^{2+} signals by using both internal and external sources of Ca^{2+}. The internal stores are held within the endoplasmic reticulum (ER), acidic endosomes or mitochondria. The release of Ca^{2+} from ER stores is controlled by different channels such as $InsP_3R$ and Ryanodine receptor (RYR). At low level of stimulation, only few single $InsP_3Rs$ and RYRs are opened and these single-channel events have been recorded as quarks [99] or blips [100], respectively. On the other hand, high stimulation results in a coordinated opening of InsP3R and RYRs clusters known as puffs [101] or sparks [101], respectively. The sparks and puffs contribute to the Ca^{2+} wave that sweep through cells. To generate a wave, $InsP_3Rs$ and RYRs must be sensible enough to respond to each other through the process of Ca^{2+}-induced Ca^{2+} release [98]. This Ca^{2+} wave can spread from cell to cell through gap junctions [102]. Another important characteristic in Ca^{2+} signaling is that cells often respond to changes in stimuli intensity by varying the frequency of Ca^{2+} waves. In some cases, individual spikes are sufficient to trigger cellular response such as the contraction of skeletal muscle or neurotransmitter release. On the other hand, when longer periods of signaling are

needed, spikes are repeated to give waves with different frequencies in the range between 1-60 seconds to 24 hours [98]. For decoding frequency-encoded Ca^{2+} signal, cells have two Ca^{2+}-sensitive proteins which are : Ca^{2+}/calmodulin-dependent protein kinase II (CAMKII) [103] and protein kinase C [104].

1.2.1 Calcium signaling in the RPE

High levels of calcium, up to 15mM, have been reported in RPE cells [105, 106]. The presence of melanosomes in the RPE enable the storage of larger Ca^{2+}amount compared to other cell types [8, 31]. Interestingly, the release of Ca^{2+} from this compartment is through IP_3Rs and RYRs as in the ER compartment. Therefore, melanosomes can regulate Ca^{2+} concentration in the RPE [106, 107]. On the other hand, to handle large increases in cytosolic Ca^{2+} due to extracellular stimuli, the RPE has different mechanisms to remove Ca^{2+} out of the cell. The presence of Na^{+}/Ca^{2+} exchanger and Ca^{2+}-ATPase are carrying out this function. In addition, sarco-endoplasmic reticulum ATPase (SERCA) is in charge of the uptake of Ca^{2+} into ER compartment. Furthermore, RPE cells are connected each other by gap junctions channels which make RPE able to spread increases of intracellular Ca^{2+} from one cell to its neighbor [108-110].

There are many RPE functions which are regulated by increases in intracellular Ca^{2+} [111]. These are: transepithelial transport of ions and water, phagocytosis, secretion and differentiation. Some of these functions are modulated by Ca^{2+} channels [112, 113].

1.2.1.1 Calcium channels in RPE

RPE cells have different types of calcium channels that can be found and classified depending on their features in: voltage-dependent calcium channels, transient receptor potential (TRP) channels, ligand-gated calcium channels and non-selective cation channels [111].

1.2.1.1.1 Voltage-dependent calcium channels

Voltage-dependent calcium channels (**Fig. 3**) are mainly activated by plasma membrane depolarization [114-117].

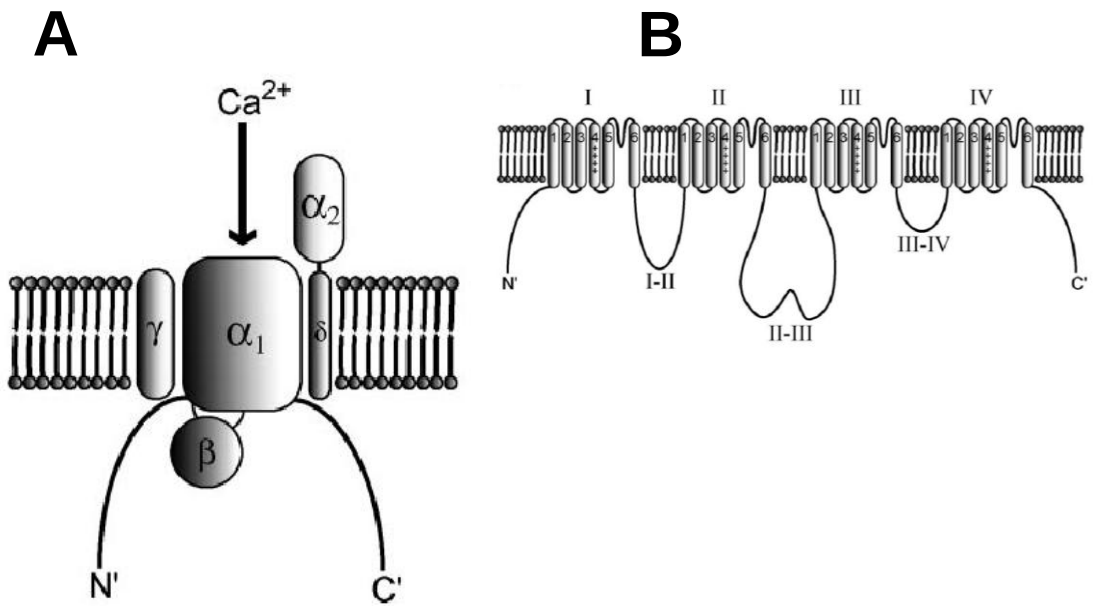

H. WILLIAM TEDFORD AND GERALD W. ZAMPONI **2006** *Pharmacol Rev*

Fig. 3 A voltage-gated Calcium Channel. **a**: Schematic representation of the subunit composition and membrane topology of a typical high-voltage-activated calcium channel. **b**: Schematic representation of structural features of the α1 subunit of the voltage-gated calcium channel.

To date, by means of RT-PCR, L-type ($Ca_v1.1$, $Ca_v1.2$, and $Ca_v1.3$) and T-type ($Ca_v3.1$ and $Ca_v3.3$) calcium channels have been found in ARPE-19 cell line and in freshly isolated human RPE cells [118]. Also the presence of $Ca_v1.2$ (α1C) and $Ca_v1.3$ (α1D) subunit have been shown by mean of western blot technique [119, 120]. However, electrophysiological analysis of currents suggested that Cav1.3 contributed to the whole-cell current of voltage-dependent Ba^{2+} currents [121]. This was based on the low dihydropyridine sensitivity, the fast time-dependent activation and the voltage-dependent activation at rather negative membrane voltages found in these currents [122, 123]. Furthermore, using whole-cell recording of Ba^{2+} currents it was possible to identified T-type channels currents in fresh isolated RPE cells [118]. These currents showed a fast inactivation and no significant changes in the presence

of dihydropyridine derivatives. So far, the function of T-type calcium channels in the RPE is unknown. On the contrary, L-type calcium channel has been more investigated and indeed, it has been found to play a role in phagocytosis and also in the secretion of VEGF in the RPE [113, 119].

1.2.1.1.2 TRP channels

From the subfamily of the TRPC calcium channels (Canonical), TRPC1 and TRPC4 were found in ARPE cell line [124]. In freshly isolated human RPE cells in addition TRPC7 calcium channel was found. Since these channels mediate the basal Ca^{2+} entry in the RPE, it is likely they could be involved in the secretion of cytokines. From the subfamily of The TRPV (vanilloid receptor-type) calcium channels, TRPV1, TRPV2, TRPV3 and TRPV4 were also found in ARPE-19 and in fresh isolated human RPE [112]. Currents of these channels were trigged by application of IGF-1 or heat which in turn leads to secretion of VEGF-A [112]. It seems that from all these TRPV channels, TRPV2 has a dominant role in RPE cells.

1.2.1.1.3 ATP receptors

ATP receptors are classified in two types: P2X which is a ligand-gated ion channel and P2Y which is a G protein-coupled receptor [111, 125, 126]. There are several studies showing that ATP-dependent signaling plays a role in the regulation of transepithelial ion and water transport, and phagocytosis in RPE cells [127-129]. Moreover, RPE is able to secret ATP in response to different stimuli such as: hypotonic challenge or bFGF [128-130]. The ATP secreted by RPE can work as autocrine messenger by binding either P2Y or P2X receptors [128-130].

1.2.1.1.4 Glutamate receptors

There are two types of glutamate receptors: one is a ligand-gated ion channel and the other one works via G protein-coupling [131-133]. Different studies have shown

the presence of glutamate receptors in the RPE [134, 135]. RPE cells also express NMDA receptor which has been found to stimulate the release of ATP by the RPE [136]. In the dark, it could be that part of the glutamate released by photoreceptors in the synaptic terminal reaches the RPE. This communication enable RPE cells to adapt their functions to the requirements of photoreceptors function in dark [111].

1.2.1.1.5 Store-operated calcium entry (SOCE)

Increases of cytosolic Ca^{2+} by the activation of SOCE trigger many cellular responses [137]. These include for example: gene expression, secretion, phagocytosis, cell growth and proliferation [138, 139]. Several studies have shown that the molecular basis of SOCE activation relies on Stim and Orai proteins [140-144] (**Fig. 4**). There are two Stim homologues: Stim-1 and Stim-2 and three orai homologues: Orai-1, Orai-2 and Orai-3 [145, 146]. The interaction between Stim-1 and Orai-1 activates SOCE [145]. Stim-1 is a membrane protein with one transmembrane domain that is localized predominantly in the ER membrane [140-142, 147]. Thus, its N-terminus faces the lumen of the ER with EF-hand motif which binds Ca^{2+} and its C-terminus faces the cytoplasm [137, 148, 149]. In resting conditions stim-1 forms dimers stabilized by coiled-coil interaction at the C-terminus [137]. During depletion of the ER, EF-Hand motif releases the bound Ca^{2+} and subsequently oligomerization of stim-1 occurs at the N-terminus by the SAM domain [137]. Thus, oligomers of stim-1 translocate closely to the plasma membrane [137]. Orai-1, a Ca^{2+} channel formed by four subunits localizes in the plasma membrane [144, 150, 151].Translocation of stim-1 activates orai-1 allowing the influx of extracellular Ca^{2+} into the cell. This activation is due to interaction of the crac activation domain (CAD) on stim-1 protein with Orai-1 channel [137]. The physical interaction between these proteins has been demonstrated by co-immunoprecipitation experiments [152].

So far, there is only one study done with ARPE-19 and fresh isolated human RPE cells which shows the presence of Orai channels [153]. In this study, by means of RT-PCR expression of all ORAIs and STIMs genes was detected. Accordingly to

patch clamp experiments performed in this study, it was discussed that I_{crac}-mediated Ca^{2+} signal was mediated by Orai-1 and /or Orai-2.

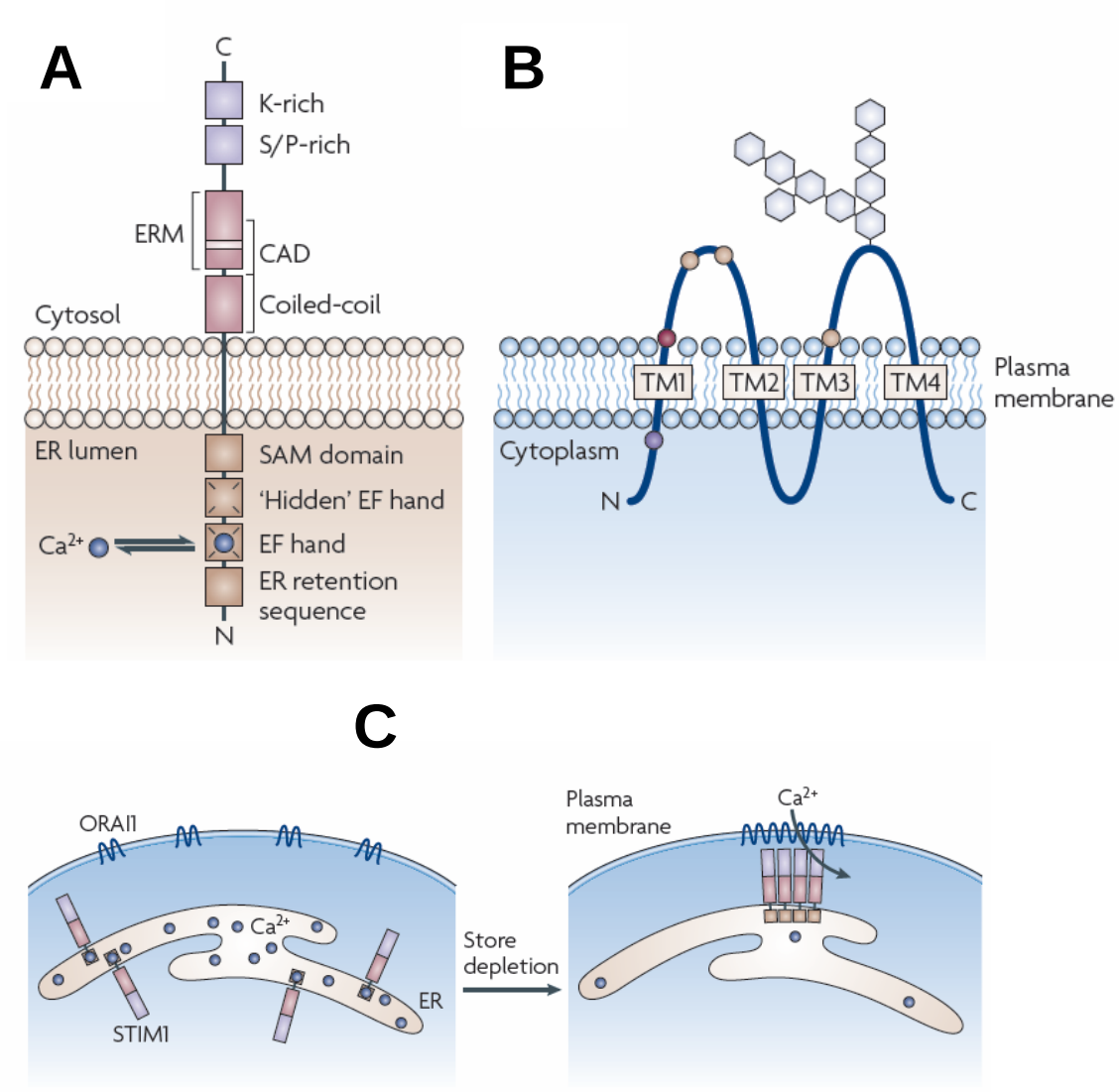

Parekh, A. B. 2010 *Nature Rev*

Fig. 4 Store-operated calcium entry (SOCE). **a:** Stim-1 a single transmembrane protein localizes in the ER. Its N-terminus facing the ER lumen it has an EF-hand Ca^{2+}-dependent domain which senses luminal levels of Ca^{2+} in the ER. Its C-terminus faces the cytosol and it has a CRAC-Activated domain (CAD) which interacts and actives Orai-1 channel at the plasma membrane. **b:** Orai-1 channel at the plasma membrane. It has four transmembrane domains and both, C and N-terminus are facing the cytosol. **c:** Mechanism of SOCE activation. After depletion of the endoplasmic reticulum (ER), Stim-1 translocates into proximity of the plasma membrane and activates Orai-1 calcium channel in the plasma membrane by direct interaction through the CAD domains, allowing extracellular Ca^{2+} to enter the cell.

1.3 RPE diseases

Disruption of RPE cell functions lead to retinal degenerations. The close interaction between RPE and photoreceptor forms a functional unit [2]. Thus, mutations in genes which are expressed in photoreceptor cells can lead to a primary RPE disease followed by a secondary loss of photoreceptors. On the other hand, mutations in genes which are expressed in RPE can lead to primary photoreceptors degeneration. For example, mutations in the *ABCA4* gene which is expressed in the photoreceptor lead to Stargardt's disease which starts with the degeneration of the RPE [154-156]. Furthermore, mutations in several genes expressed in the RPE can lead to retinal degeneration such as: retinitis pigmentosa (RP), age-related macular degeneration (AMD) and Best's vitelliform macular dystrophy (BVMD) [2].

1.3.1 Best's Vitelliform macular dystrophy

Best's vitelliform macular dystrophy (BVMD) is an autosomal inherited dominant juvenile-onset macular degeneration. BVMD was first described in 1905 by a German ophthalmologist Friedrich Best (Best, 1905). BVMD is caused by mutations in BEST1 gene which was independently identified in 1998 by Petrukhin et *al*. [157] and by Marquardt et *al*. [158]. The onset of BVMD is variable, ranging from the first decade to beyond the sixth decade of live [159-161]. As a main symptom patients experience a reduction of the visual acuity, but also symptoms such as photophobia, metamorphopsia and night blindness [162]. Large accumulation of lipofuscin in the RPE characterized Best´s patients [163, 164].

There are several classifications of BVMD based on the ophthalmoscopic aspect of the lesions [160, 165, 166]:

Stage 0 (normal): Normal fovea, abnormal electro-oculogram (EOG)

Stage 1 (previtelliform): RPE defects in macula

Stage 2 (Yellow cyst):

Stage 2a (vitelliform): Round smooth cyst filled with yellow material

Stage 2b (Scrambled egg): Uneven yellow material with irregular borders

Stage 3 (Pseudohypopyon): Yellow material accumulating in the bottom of the cyst

Stage 4 (arrophic):

Stage 4a (atrophy of RPE): Atrophic macular with hypopigmented RPE

Stage 4b (Scar): Subretinal fibrous tissue in macular area

Stage 4c (neovascularization): Subretinal neurovascularization in macular area.

1.3.1.1 Electro-oculogram

The electro-oculogram (EOG) is an electrophysiological test of the retinal pigment epithelium. The EOG measures the change in the electrical potential between the cornea and the ocular fundus when changing from dark and light [167]. This potential is mainly derived from the RPE, and it changes in response to retinal illumination. The potential decreases for 8-10 minutes in darkness. Subsequent retina illumination causes an initial fall in the standing potential followed by a slow rise. This phenomenon is known as the light-peak and arises from increase in Cl conductance across the basal RPE membrane [167]. This is usually expressed as a ratio between the light -peak amplitude and dark potential, known as the Arden ratio [168]

Generally, Best´s patients show absence of the light-peak in the EOG [165]. An abnormal EOG is considered as a hallmark for diagnosis of BVMD in patients with vitelliform lesions [169]. However, although most of Best´s patients share this criterion, many studies have shown that EOG can also be normal in the first stages of the disease, even in those who are clinically affected [161, 170].

1.4 Bestrophin

The human genome contains four bestrophin paralogs (BEST1, BEST2, BEST3 and BEST4) [171, 172]. The four bestrophins share in homology a highly conserved arg-phe-pro RFP motif [173].Bestrophin-1 protein, consisting of 585 amino acids is encoded by BEST1 gene [158, 172, 174-176]. BEST1 locates on chromosome 11q13 and contains 11 exons of which 10 are protein-coding [157, 158]. By mean of RT-PCR, BEST1 has been found in different tissues such as: brain, spinal cord, RPE, heart, lungs, liver, spleen, kidney, colon, skeletal muscle and testicles [157, 158, 177-179]. Protein expression for hBest-1 is found mainly in RPE where localizes basolaterally in this monolayer of cells [174, 180]. Moreover, hBest-1 has been reported in human airways epithelial cells and in addition, mBest-1 has been also reported in colon [181].

Regarding bestrophin-1 structure there are two different topology models (**Fig. 5**) In the model proposed by Tsunenari et *al.* [172] using hydropathy analysis, bestrophin-1 was determined to have six hydrophobic domains, from which domains: 1, 2, 4 and 6 are transmembrane domains (TMs).Domains 3 and 5 make cytosolic and extracellular loops respectively. On the contrary, the model described by Milenkovic et *al.* [176] bestrophin-1 has as TMs: 1, 2, 5 and 6, and domains 3 and 4 make an intracellular loop.

Since bestrophin-1 has been categorized as an ion channel, some studies have investigated whether bestrophin-1 forms oligomers. Heterologously expressed bestrophin-1 has shown tetrameric or pentameric oligomerization in human embryonic Kidney cells (HEK) [182]. However, endogenously expressed porcine bestrophin-1 from RPE cells was found to form only dimers [183]. This discrepancy was clarified when porcine bestrophin-1 was over-expressed in HEK cells. Here, the author concluded that the result of tetramer or pentamer structures were artifacts of over-expression.

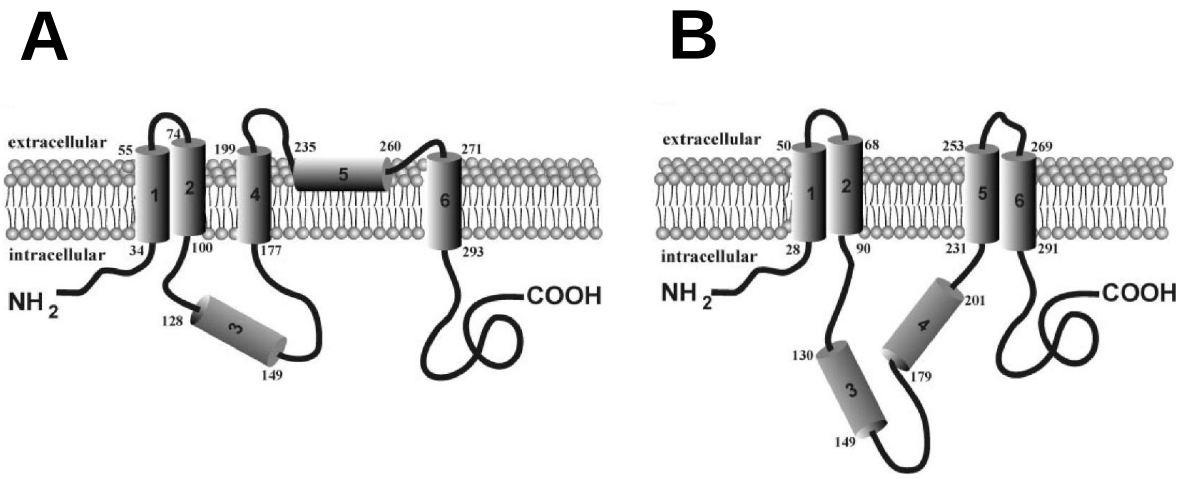

Fig. 5 Human bestrophin-1 topology models. a: Tsunenari et *al*.[172] model predicted six domains of which 1,2,4 and 6 are transmembrane domains (TMs). Domains 3 and 5 make an intracellular and extracellular loop respectively. **b**: Milenkovic et *al*. [176] model predicted domains 1,2,5 and 6 as TMs whereas domains 3 and 4 make an intracellular loop (CITA).

Originally bestrophin-1 was identified as a Cl channel and this was based on different observations. First, as a hallmark for diagnosis, Best´s patients show a reduction of the light-peak (LP) in the EOG. The LP reflects the transmembranal potential across the basolateral membrane of the RPE. In light, photoreceptors release a hypothetical light-peak substance which binds to a receptor at the apical membrane of the RPE. This in turn leads probably to the activation of PLC and the subsequent increase of intracellular Ca^{2+} by the activation of InsP3 receptors in the ER. The increase of Ca^{2+} activates Ca^{2+}-dependent Cl channels localized in the basolateral membrane of the RPE. [171]. When the Cl conductance increases, the basolateral membrane is depolarized. Since bestrophin-1 also localizes basolaterally in the RPE it is expectable that bestrophin-1 could be the Ca^{2+}-dependent Cl channel which is responsible for the LP activation. Therefore mutations in bestrophin-1 could be responsible for the reduction of the LP in Best´s patients.

Studies with heterologously expressed bestrophin-1 showed that bestrophin-1 function as a Cl channel. For example, Sun et *al*. [182] showed that non-transfected HEK cells Cl currents were very small compared to those with hBest-1 transfected

cells. In addition, HEK cells transfected with hBest-1 showed Cl currents activated by increases in cytosolic Ca^{2+} concentration. Furthermore, there are studies where the dominant negative effect of mutant bestrophin-1 was observed [184, 185]. Here the authors transfected HEK cells with wild type and mutant´s bestrophin-1. The result was that mutant bestrophin-1 was able to inhibit Cl currents of the wild type bestrophin-1. In addition, another study done in mouse trachea also reported that not only in bestrophin-1 knock-out but also in cells treated with siRNA against bestrophin-1, Cl conductance was reduced [186].

In addition to evidences that bestrophin-1 is a Cl channel, new hints came from other groups. In the study done by Rosenthal et *al*. [121] using patch clamp technique it was found that wild type hBest-1 transfected in RPE-J cells induced an acceleration of the activation kinetic of Ba^{2+} current through L-type channels, and a shift of the voltage-dependent activation to more negative values. In addition, systemic application of L-type calcium channel blocker nimodipine reduced the LP amplitude in rats and mice in the electro-retinogram (ERG). These results were supported by Marmorstein et *al*. [175] when a bestrophin-1 knock-out mouse showed larger LP at low stimulus luminescence in the ERG compared with wild type animals. In addition, mice injected with nimodipine showed a reduction of the LP. In both, lethargic mice which have loss of function mutation in the voltage-gated Ca^{2+} channel β4 subunit and mice lacking $Ca_v1.3$ subunit of voltage-gated Ca^{2+} channel, the LP was strongly suppressed. The study concluded that bestrophin-1 is not necessary to directly generate the LP but it can antagonize it, by modulation of L-type Calcium channel kinetics. Recently, there was a study published in man which showed that L-type calcium channel contributed to the light-rise of the EOG [187].

The interaction between bestrophin-1 and $Ca_v1.3$ calcium channel has been further demonstrated in different studies. In the first study, done by Kuai Yu et *al*. [188], showed that hBest-1through its proline-rich domain had a functional interaction with SH3 domain of the β subunit of $Ca_v1.3$ calcium channel. The second study, done by Reichhart et *al*. [189] demonstrated for the first time that full-length bestrophin-1 co-immunoprecipitated with Ca^{2+} channel β4-subunit through the interaction of proline-

rich motif/SH3-binding domain respectively. In this study it was also observed that mutant bestrophin-1 (lacking the proline-rich domain) could not reach the cell membrane and therefore could not interact and modulate L-type calcium channel. In addition, a study done by Milenkovic et *al*. [190] described a new proline-rich motif in the C-terminus of bestrophin-1 which interacts withβ4-subunit. Interestingly was also found that through this new interaction bestrophin-1 helps to maintain the function ability of β4-subunit to regulate surface expression of pore-forming Ca_v calcium channel subunit.

Regarding the function of endogenously expressed bestrophin-1, not so much is known. First insight came from bestrophin-1 knock-out mouse which has been investigated in two independent studies [175, 180]. In the first study freshly isolated sheet of RPE cells from wild type and bestrophin-1 KO animals were examined. Here they found that bestrophin-1 KO mice exhibited higher increase in intracellular Ca^{2+} in response to ATP stimulation compared to that of wild-type animals. In addition, Cl currents did not differ between cell types. The second study, using the same animal model showed that confluent cells from bestrophin-1 KO mice exhibited higher resting Ca^{2+} compared with wild type cells. The kinetic of ATP release from Ca^{2+} store also differed between animals, when ATP-induced Ca^{2+} rose faster and decayed slower in bestrophin-1 KO mice compared with in wild type [180]. In addition, in the same study, porcine bestrophin-1 was found after differential centrifugation in the fraction enriched of cytosolic ClC-3 Cl channel and Myosin-7A which are known as intracellular markers [180]. The conclusion of this study was that a proportion of bestrophin-1 localized in the ER influenced the uptake of Ca^{2+} into Ca^{2+} store. This finding was in agreed with another study where over-expressed bestrophin-1 co-localized and interacted with over-expressed Stim-1, a native protein from the ER Ca^{2+} store.

1.5 Mutant bestrophin-1.

To date, more than 100 different BEST1 mutations have been reported in BVMD [191]. The majority (92%) of mutations identified in BVMD are missense mutations

located in the N-terminal half on the protein [165]. Curiously, the N-terminus exhibits the highest evolutionary conservation between paralogs [173]. In contrast, the C-terminus differs between them [173]. Moreover, BVMD is not the only eye disease associated to BEST1 mutations. Eye diseases caused by BEST1 mutations are: adult-onset foveomacular vitelliform dystrophy (AFVD), autosomal dominant vitreoretinochoroidopathy (ADVIRC), autosomal recessive bestrophinopathy (ARB), MRCS syndrome (microcornea, rod-cone dystrophy, cataract syndrome) and age-related macular degeneration (AMD) which are also associated to BEST1 mutations [165]. Some of these mutations are shown in the **figure 6**.

The functional consequences of these mutations remain unclear. There are several studies in different animal models and also in vitro which have tried to identify and/or explain possible patho-mechanisms. For example, a study done by Kuai Yu et *al*. [185] showed with heterologously expressed bestrophin-1 how different mutations even reaching the plasma membrane showed different Cl channel function. On the contrary, a recently study done with 13 disease-associated BEST1 mutant proteins in polarized Madin-Darby Canine Kidney cells (MDCK II) found that indeed most of these mutants bestrophin-1 exhibited a defective trafficking. Thus, mutants were retained in the cytoplasm, whereas wild type bestrophin-1 reached the cell membrane [192]. In addition, this study reported that all mutants exhibited a reduction of anion conductance.

Recently, Zhang and colleagues [193], published a study with a bestrophin-1 knock-in mouse carrying the BVMD-causing mutation W93C, which is the same mutation found in a well characterized family of Swedish originally [194-196]. In this study, both, homozygous and heterozygous bestrophin-1 KI animals showed differences compared with the wild-type mice. For example, the LP was reduced and enhanced depending on the stimulus intensity in both homo- and heterozygous animal compared with the wild type which did not show this modulation. Furthermore, an enhanced accumulation of lipofuscin in the RPE was found in both homo- and heterozygous mice compared with wild-type. Curiously, in heterozygous animals there was more accumulated material compared with homozygous mice. On the

other hand, isolated RPE cells from bestrophin-1 KI mice showed no differences in the Cl conductance compared to isolated RPE cells from wild type mice. In addition, ATP-stimulated changes in intracellular Ca^{2+} was relatively suppressed compared with wild-type RPE cells. In this study, the authors concluded that these bestrophin-1 KI mice reconstitute several of the hallmark symptoms of BVMD and therefore they constitute a viable model for further studies in this retinal disorder.

It is worth to say that is unclear to what extent the mouse model can be extrapolated to human. For example, mBest-1 shares only 63% homology with the hBest-1 [197]. On the other hand mouse does neither have a macula and nor shows the retina lesions known in humans. Curiously, there is in dogs an autosomal recessive eye disorder called canine multifocal retinopathy (*cmr*) which has been in detail characterized and the clinical phenotype and pathology closely resemble lesion of BVMD [198]. In this animal, transcripts of canine BEST1 were found in brain, retina and also in RPE/choroid and the protein was only detected basolaterally in the RPE. Interestingly, distinct mutations in canine BEST1 have been associated to *cmr* disease [198-200]. Since, it is likely that the canine bestrophin-1 protein resembles in many ways to the human bestrophin-1 protein, the authors strongly proposed these mutants dogs as a novel animal model of human inherited retinopathy.

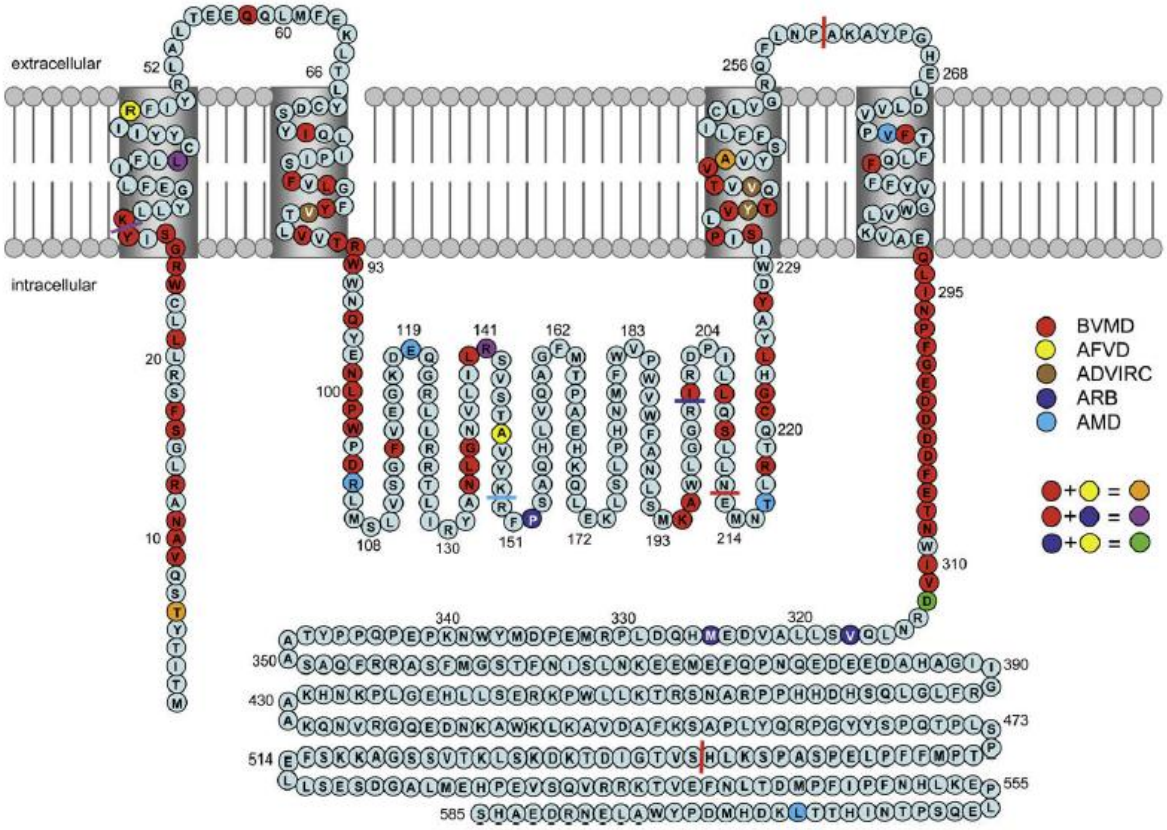

Boon et *al.* 2009 *Prog Retin Eye Res*

Fig. 6 Protein model of bestrophin-1 (adapted to Milenkovic et *al*. [176] model). The known human disease-associated mutations are indicated with colors. The protein variants found in age-related macular degeneration are also shown, although functional studies question their significance in disease pathogenesis. Colored residues: missense mutation or in-frame deletion. Colored bars: nonsense or frameshift mutation. Abbreviations: BVMD, Best's vitelliform macular dystrophy; AFVD, adult-onset foveomacular vitelliform dystrophy; ADVIRC, autosomal dominant vitreoretinochoroidopathy; ARB, autosomal recessive bestrophinopathy; AMD, age-related macular degeneration.

2 Objectives of the work

Knowing the physiological function of bestrophin-1 protein in RPE cells will help to clarify the patho-mechanism of mutant bestrophin-1. Since very little is known about the function of endogenous bestrophin-1 in the RPE, the aim of the present work is to elucidate the role of endogenously expressed bestrophin-1 in retina degeneration and in calcium signaling in the RPE. For this, the present work is divided in three parts:

- Using light damage paradigm experiments we challenge bestrophin-1 knock-out mice retinas in order to investigate possible susceptibility to light-damage and thus a possible mechanism of degeneration due to the absence of bestrophin-1 protein.
- Few studies suggested that endogenous bestrophin-1 has a cytosolic localization and from there it can modulate intracellular Ca^{2+} signals. Using of primary RPE cell culture from bestrophin-1 knock-out mouse we investigate the involvement of bestrophin-1 in calcium signaling triggered by ATP applications.
- Since bestrophin-1 was found to localize in ER Ca^{2+} stores and furthermore also interacting with Stim-1 protein we want to investigate the role of bestrophin-1 in store-operated calcium entry in primary porcine RPE cell culture by mean of siRNA experiments.

3 Material and methods

3.1 Mice models

For light damage (LD) and calcium imaging experiments, wild type and transgenic animals belong to the black 6 mouse line were used. These ones followed all sterile conditions for living and breeding in the animal facility of the Human Genetics at the Universitätklinikum Regensburg, Germany.

Transgenic bestrophin-1 Knock-in mouse carrying the mutation Y227N (KI $^{+/Y227N}$) and bestrophin-1 knock-out (bestrophin-1$^{-/-}$) were provided by Prof. Dr. Bernhard Weber from the institute of Human Genetic, Regensburg, Germany.

3.1.1 Mouse genotype

The genotype of the animals was done in mice 3-4 weeks old. A piece of tail (≈ 2,5 mm) was cut and incubated for 5-7 hours at 55 ^{o}C or overnight in shaking bath at 37 ^{o}C in a lysis buffer (**Table I**). In the next step, the tube containing the digested piece of tail was spinned for 5 minutes at 10-13 K/min and transferred the supernatant into a new tube. One volume of isopropanol was added to the lysate and mixed until the precipitation of DNA was completely (viscosity was gone). The precipitated DNA was washed with ethanol 70 % and the dry pellet was dissolve in distilled water.

Table I Lysis buffer used for the genotype (to make 25 ml)

Stock Solution	Concentration	Volumen
1 M Tris-HCl pH 8-8.5	100 mM	2.5 ml
500 mM EDTA pH 8	5 mM	0.25 ml
20 % SDS	0.2 %	0.25 ml
5 M NaCl	200 mM	1.0 ml
Distilled H_2O		20.7 ml
Proteinase K (20 mg/ml)	250 µg/ml	0.312 ml

For the PCR, 3 µl template of isolated genomic DNA was used in the master-mix of 22 µl containing 12,2 µl H2O, DMSO 1,3 µl, 10x Buffer S incl. MgCl 15 mM, dNTPs 2,5 µl, primers forward and reverse 1µl per each and 0,1µl Tag-polymerase (**Fig. 7**). DNA was amplified using a Touchdown program protocol (**Table II**). For the bestrophin-1 KO two different pair of reverse primers were used (**Table III**).

Table II PCR Program used for the bestrophin-1 $KI^{+/Y227N}$ mouse genotype Touchdown (TD) 60-50^{o}C.

Cycles	Temperature	Time
1x	94°C	2 min
9x	94°C	30 sec
	60-50°C	30 sec
	72°C	30 sec
24x	94°C	30 sec
	50°C	30 sec
	72°C	30 sec
1x	72°C	8 min
1x	15°C	Final Hold

Table III Primer used for bestrophin-1 $KI^{+/Y227N}$ and bestrophin-1 $^{-/-}$mice genotype

Gene	Acc.no.	sequence	length
mBEST1	NC_000085.6	Forward: CAGCCAAAGCTGCTCCATTAG	
		Reverse: CTCCATGGGCCCATGCTGAGGCATCC	550
		Reverse (LacZ): GCTGAAGGCGATTAAGTTGGGT	376

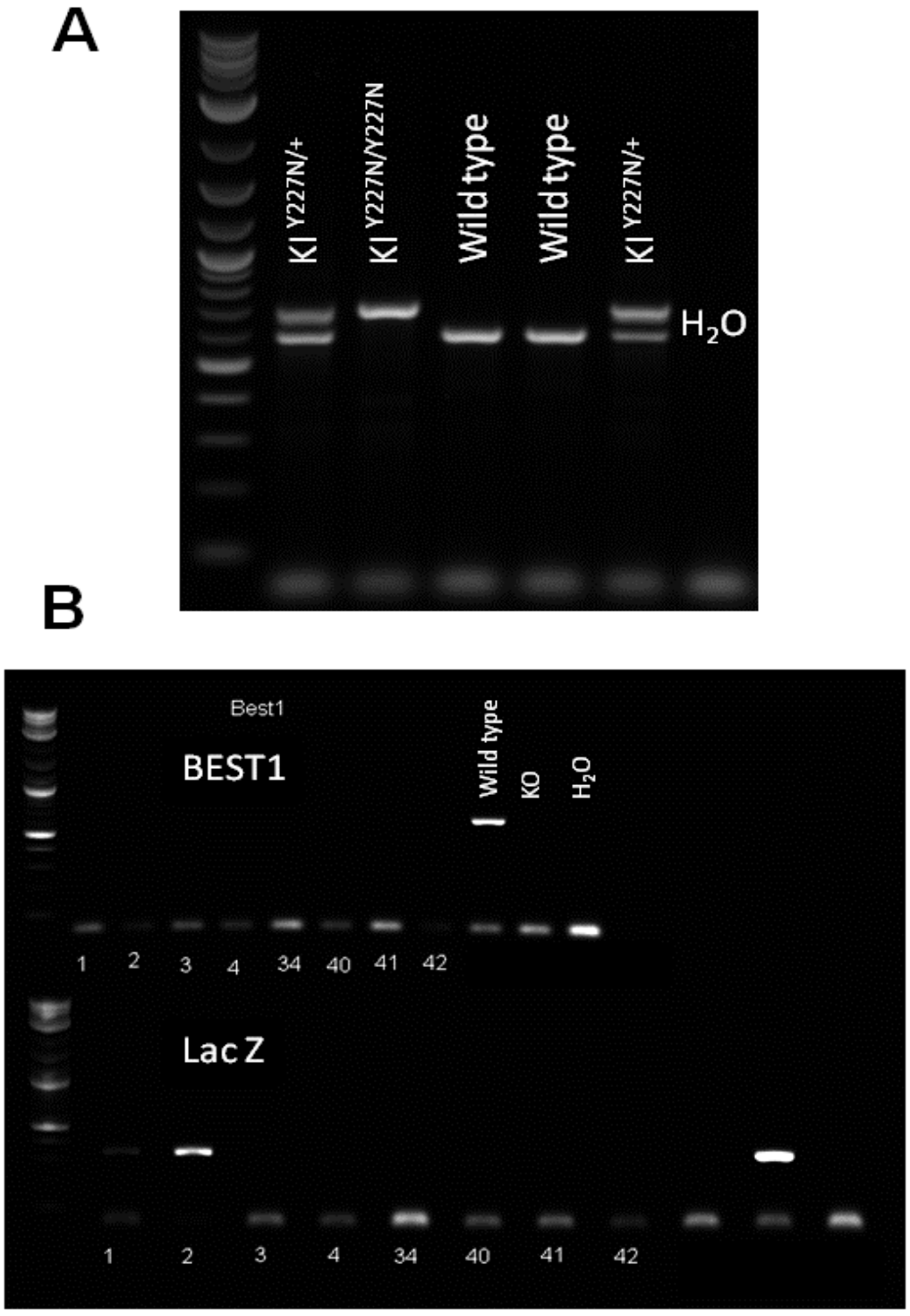

Fig. 7 Genotypes of bestrophin-1 KI $^{+/Y227N}$ and bestrophin-1 $^{-/-}$. **a:** Wild type, KI homozygous and heterozygous from the same breeding after 3-4 weeks old. **b:** bestrophin-1 $^{-/-}$ animals after 3-4 weeks old.Bestrophin-1 $^{-/-}$ mouse was created with a LacZ sequence after the 6th coding exon in order to disrupt bestrophin-1 protein synthesis. Thus, Bestrophin-1 $^{-/-}$ mouse does not express bestrophin-1 protein, instead, it expresses LacZ.

3.1.2 Ligh damage experiment

At the age of 6-8 weeks mice were isolated and stayed in dark for 48 hours before the experiment. 45 minutes before the experiment started, Atropin 0.5% was carefully applied into the eyes at dim light conditions. Mice were exposed at the intensity of light of 800 Lux for 30 minutes. By 9 days after the LD experiment, eyes were removed and followed different histological steps.

3.1.2.1Light damage histology

Eyes were immediately fixed using a Karnovsky fixant (4 % glutaraldehyde or 3 % paraformaldehyde + 0.1 % glutaraldehyde) for 2 hours at room temperature. After this, eyes were rinsed with cacodylate buffer (10 mM, pH= 7.2-7.4) 3 times 5 minutes each and incubate for 2 hours osmium fixant (1 % osmium + cacodylate buffer) at room temperature. After these 2 hours eyes were rinsed again 3 times 5 minutes each and 5 minutes extra in distilled water followed by incubation in propylenoxid over night. Then dehydration was done by a gradient of different ethanol concentrations (30%- 15-30 minutes, 50%-15-30 minutes, 70%-15-30 minutes, 90%-15-30 minutes, 96%-15-30 minutes, 100%-30 minutes) and followed by the application of propylene oxide 2 times 30 minutes each. After dehydratation, the eyes started to be infiltrated by a mixture of propylene oxide and Epon (1:1) for 3 hours or overnight. Next day a fresh prepared Epon was applied to the eyes and incubated for 12-16 hours and after this they were cooked at 65^{o}C for 2 days in order to polymerize the samples.

3.2 Primary mouse retinal pigmented epithelial cells isolation

Eyes were opened through an incision along the *Ora serrata* and the vitreous was removed. Eye cups were incubated with PBS-EDTA (1mM) pre-warmed for 30 minutes waiting until the retina was detached and removed. After that, eye cups were incubated again in PBS-EDTA for 30 minutes which was followed by incubation in an enzyme solution composed by L-Cys (10x, 260 mM), BSA (100mg/ml) and Papain

(Worthington) for 23 minutes at 37^{o}C. The harvest of the RPE was done by suction/pipetting up and down with cell-culture medium: 500 ml Hams F12/ DMEM (with Glutamin) (PAA: E15-813), 10 % fetal calf serum Gold (PAA), 1 % pen-strep. (PAA: P11-010), 250 µl Insulin/Transferrin, 5 ml non-essential amino acids, 2,5 ml 1 M HEPES to stop the activity of the papain. After that, primary mouse RPE cells were washed and plated using 100µl of fresh medium culture in 12 wells plate on 18-mm ø glass cover-slips overnight. Next day, wells were refilled with 1 ml of the corresponding medium. For all experiments cells grew for 1-2 weeks till they got confluent. Cultures were maintained at 37°C and 5%CO_2 in open air.

3.3 Primary porcine retinal pigmented epithelial cells isolation

Eyes were opened through an incision along the *Ora serrata* and the vitreous was removed. Eye cups were incubated with PBS-EDTA (1mM) pre-warmed for 30 minutes waiting until the retina was detached and removed. After that, eye cups were incubated again in PBS-EDTA for 30 minutes which was followed by incubation in an enzyme solution composed by L-Cys (10x, 260 mM), BSA (100mg/ml) and Papain (Worthington) for 23 minutes at 37^{o}C. The harvest of the RPE was done by suction/pipetting up and down with cell-culture medium: 500 ml MEM α modif. (Sigma M-4526), fetal calf serum Gold (PAA), 5 ml glutamin-penicillin-streptomycin. (Sigma G-1146), 5 ml N1-Supplement (Sigma N-6530), 5 ml non-essential amino acids, THT (hydrocortisone (20µg/L), taurine (250 mg/L), and triiodo-thyronin (0.013 µg/L)) to stop the activity of the papain. After that primary porcine RPE cells were washed and plated using 100µl of fresh medium culture in 12 wells plate on 18-mm ø glass cover-slips overnight in a concentration of 1.0-1.2 x 10^6 cells per ml. This concentration corresponded with the cell density in a monolayer. The first day the medium contained only 10% FCS and next day wells were refilled for one containing 5% FCS and were kept under these conditions for all experiments. Cultures were maintained at 37°C and 5%CO_2 in open air.

3.4 RT-PCR

The RPE cells were collected and lyzed in the lysis buffer of the RNeasy Micro Kit (Qiagen, Hilden, Germany). Complete RNA from RPE cells were prepared from confluent cultures grown in a 12 well plate. The RNA (1 µg) was reverse-transcribed with following reaction mixture: 1 µg oligo dT primer (Invitrogen), 1 mM of each dNTP, 20 U RNAguard (Amersham Biosciences) and 20 U M-MLV reverse transcriptase (Invitrogen, Darmstadt, Germany). PCR experiments were performed as described in **Table IV** and **Table V** in 35 cycles. For porcine bestrophin-1, Stim-1-2 and Orai1-3 1 µl cDNA in 25 µl PCR reaction mixtures with Taq DNA polymerase (Stratagene), and 1.5 pmol of sense and antisense oligonucleotides specific to various Orai channels and Stim proteins was used (**Table VI**).

Table IV PCR Program used for bestrophin-1 RT-PCR

Cycles	Temperature	Time
1x	94°C	2 min
35x	94°C	30 sec
	56°C	30 sec
	72°C	30 sec
1x	72°C	2 min
1x	4°C	Final Hold

Table V PCR Program used for Orais and Stims RT-PCR

Cycles	Temperature	Time
1x	94°C	2 min
35x	94°C	30 sec
	60°C	30 sec
	72°C	30 sec
1x	72°C	2 min
1x	4°C	Final Hold

Table VI Primers used for RT-PCR

Gene	Acc.no.	sequence	length
BEST1	AY064707.1	Forward: AGTTTCGAGTTGCTCCCAGA Reverse: ATCAGTCTGGGTAAGGAGGA	212
ORAI1	NM_001173519.1	Forward: GTCAAGTTCTTGCCCCTCA Reverse: CGATAAAGATCAGGCCGAAG	177
ORAI2	NM_001191348.1	Forward: AACTGGTCACCTCCAACCAC Reverse: CTCGCTGATGGAGTTGAGGT	302
ORAI3	NM_001193202.1	Forward: GTCTGCTGCCTCACATTGAA Reverse: ACAAACTTGACCCAGCCAAC	171
STIM1	NM_003156.3	Forward: TGTGGAGCTGCCTCAGTATG Reverse: AAGAGAGGAGGCCCAAAGAG	183
STIM2	NM_020860.3	Forward: CTCTAACACGCCCACCTCAT Reverse: CTTCCTGTGCCTTTTCAAGC	207

3.5 qPCR

The RPE cells were collected and lyzed in the lysis buffer of the RNeasy Micro Kit (Qiagen, Hilden, Germany). Complete RNA from RPE cells were prepared from confluent cultures grown in a 12 well plate. The RNA (1 µg) was reverse-transcribed with following reaction mixture: 1 µg oligo dT primer (Invitrogen), 1 mM of each dNTP, 20 U RNAguard (Amersham Biosciences) and 20 U M-MLV reverse transcriptase (Invitrogen, Darmstadt, Germany). Quantitative PCR experiments were performed in 45 cycles (**Table VII**), for porcine bestrophin-1 with 5 µl diluted 1:5 cDNA in 15 µl PCR reaction mixtures SsoFast™ EvaGreen® Supermix (*BIO-RAD*), and 1.5 pmol of sense and antisense oligonucleotides specific for porcine bestrophin-1 (**Table VIII**).

Table VII PCR Program used for bestrophin-1 and GAPDH qPCR

Cycles	Temperature	Time
1x	94°C	2 min
45x	94°C	5 sec
	60°C	10 sec
1x	72°C	2 min
1x	4°C	Final Hold

Table VIII Primers used for qPCR

Gene	Acc.no.	sequence	length
BEST1	AY064707.1	Forward: AGTTTCGAGTTGCTCCCAGA Reverse: ATCAGTCTGGGTAAGGAGGA	212
GAPDH	NM_001206359	Forward: GGTGAAGGTCGGAGTGAACG Reverse: TGGGTGGAATCATACTGGAACA	150

3.6 siRNA

Duplexes of 25-nucleotide RNAi were designed and synthesized by Invitrogen (Paisley, UK). Both scrambled and siRNAs were labeled with Alexa 488 for detection and optimization of transfection condition. In the last step of cell isolation, just before seeding, cells were resuspended in the appropriated medium containing the duplexes RNAi and plated them on these conditions. We used for Orai-1siRNA and best-1siRNA a mixture of 3 different duplexes RNAi per each (**Table IX**).

Table IX Duplexes of 25-nucleotides RNAi labeled with Alexa 488 for the knock-down of bestrophin-1 and Orai-1 protein.

Gene	siRNA sequence	Position
BEST1	Sense: CCACACAACUCAUUCUGGAUGCCCU	72
	Antisense: AGGGCAUCCAGAAUGAGUUGUGUGG	
	Sense: CCCUCUUCACGUUCCUGCAGUUCUU	364
	Antisense: AAGAACUGCAGGAACGUGAAGAGGG	
	Sense: CCCAUGGAGCGAGAUAUGUACUGGA	534
	Antisense: UCCAGUACAUAUCUCGCUCCAUGGG	
ORAI1	Sense: CGGUGAGCAAUGUGCACAACCUCAA	470
	Antisense: UUGAGGUUGUGCACAUUGCUCACCG	
	Sense: CCUUUGGCCUGAUCUUUAUCGUCUU	764
	Antisense: AAGACGAUAAAGAUCAGGCCAAAGG	
	Sense: GGGCACUUCAGAGCUUUGGCCUUAA	950
	Antisense: UUAAGGCCAAAGCUCUGAAGUGCCC	

3.7 Western blot

Protein extracts from RPE were separated by 10% SDS-PAGE and transferred to a PVDF membrane, then blocked with buffer (PBS, 0.05% Tween 20) containing 5% non fat dried milk powder for 1 hour at room temperature. Membranes were incubated overnight at 4°C with primary antibodies anti-bestrophin-1 (1:3000; mouse monoclonal, abcam 2182, , Cambridge, UK), anti-stim-1 (1:1000; rabbit polyclonal, Santa Cruz laboratory, USA), anti-Orai-1 (1:300; rabbit polyclonal, Alomone laboratory, Israel) and anti-β-actin (1:5000; mouse monoclonal, abcam 6276, Cambridge, UK) diluted in PBS/Tween and 0.001% milk (5 % non fat dried milk powder). After washing the membranes three times for 10 minutes with PBS/Tween, the membranes were incubated with the appropriate anti-rabbit or anti-mouse IgG HRP-labeled antibody (1:5000; NEB, Frankfurt, Germany) for 1 hour at room

temperature. These were then washed again and visualized after 1–3 min incubation with enhanced chemiluminescence (ECL; Amersham Pharmacia Biotech, Freiburg, Germany). The experiments were performed three times each.

3.8 Immunoprecipitation and co-immunoprecipition

Confluent porcine RPE cells were divided into two groups: treated cells with thapsigargin and non-treated cells as control. Non-treated cells were kept in Ringer solution in parallel at the same time as the first group (treated cells). Cells in the treated group were washed with Ringer for 5 minutes and thenincubated for 5 minutes more with thapsigargin (1µM) which was followed by incubation inCa^{2+} free solution for 1 minute. Immediately after that cells of both groups were lysed in 6-well plate by shaking for 15 min at 4 ^{o}C with ice-cold lysis buffer (150 mM TriseHCl, pH 7.5, 150 mM NaCl, 1% Nonidet-P40, 0.5% natrium deoxycholate). Cell lysate was scraped and transferred to a new tube and lysed for additional 15 min at 4^{o}C with rocking. The lysates were clarified by centrifugation at 13,000 x g for 10 min at 4^{o}C.

3.8.1 Pre-clearing

Supernatants were applied to 50 ml of Protein G-Agarose (Sigma) and incubated 3 hours with rocking at 4^{o}C. After preclearing and centrifugation at 13,000xg for 1 minute the lysates were applied to new tubes with 50 ml of Protein G-Agarose already incubated for 1 hour with 3 mg of suitable/relevant antibody. Subsequently, after overnight incubation on a rotating wheel at 4^{o}C the beads were washed three times with washing buffer. All centrifugation steps were carried out at 1,200xg for 1 min at 4^{o}C. 1. Washing buffer (50 mM Tris-HCl, pH 7.5, 150 mM NaCl, 1% Nonidet-P40, 0.5% natrium deoxycholate, 1 tablet Complete Mini protein inhibitor mixture/10 ml (Roche Applied Science) and 0.7 mg/ml pepstatin). 2. Washing buffer (50 mM Tris-HCl, pH 7.5, 250 mM NaCl, 0.1% Nonidet-P40, 0.05% natrium deoxycholate). 3. Washing buffer (50 mM Tris-HCl, pH 7.5, 50 mM NaCl, 0.1% Nonidet-P40, 0.05% natrium deoxycholate). Protein complexes were dissociated from beads by incubation

at 37^{o}C for 30 min in 4xSDS loading buffer. The immunoprecipitates were subjected together with total lysates to 10% SDS-PAGE and Western blot was carried out.

3.9 Measurement of transepithelial resistance

Transepithelial electrical resistance of the porcine RPE monolayer was measured with the Endohm apparatus (World Precision Instruments, Sarasota, USA). Porcine RPE monolayer was grown on Transwell polycarbonate filters (0.4 mm pore size), which consist of tissue-culture-treated polyester membranes with an insert diameter of 12 mm and an effective growth area of 1 cm^2. The upper chamber (apical side) contained 0.5 ml medium and the lower one (basolateral side) contained 1.8 ml medium. Porcine RPE cells were seeded at a density of 10^6 cells per ml and were grown to reach a stable TER, representing a confluent monolayer, generally 10 days after seeding. The medium was changed every 2 days. The TER was calculated by correction for the background resistance of a blank filter submerged in medium only. The average TER measurement of polycarbonate filters in the absence of a cell monolayer was 120 Ω cm^2 (baseline).

3.10 Immunocytochemistry

Porcine RPE cells grown on *Transwell* polycarbonate filters or in cover glass 18-mm ø were washed with PBS and immediately fixed 4% (w/v) paraformaldehyde for 5 minutes at room temperature. After three-steps washing, with 1× PBS/Tween, porcine RPE cells were permeabilized with a blocking buffer (0.5 % Triton x 100, 10 % Goat serum, 1 x PBS pH 7.4, distilled H_2O) for 30 minutes. Then cells were labeled overnight against primary antibodies: anti-bestrophin-1 (1:500; abcam 2182, mouse monoclonal, Cambridge, UK) or anti-bestrophin-1 (1:500; Rabbit polyclonal, provided by Prof. Dr. Karl Kunzelmann, Regensburg university, Germany), anti-stim-1 (1:500; rabbit polyclonal, Santa Cruz laboratory, USA) and β-catenin (1:500; mouse monoclonal, BD transduction laboratories^{TM}) diluted in a anti-body buffer (0.1 % Triton x 100, 2 % Goat serum, 1 x PBS pH 7.4 and distilled H_2O). Next, after three additional washing steps, cells were incubated for 1 hour with appropriate secondary

antibodies (conjugated with Alexa Fluor 488 and Cy3; Invitrogen). Cells were mounted in an inverted microscope (Observer Z1; Carl Zeiss, Inc.) equipped with a confocal laser scanning microscope (LSM 710; Carl Zeiss, Inc.) operated with the ZEN 2008 software, the polychromatic illumination system VisiChrome (Visitron), and the MetaMorph software package (Universal Imaging Corp.)(Kindly provided by Prof. Dr. Witzgall, Molecular and cellular anatomy, Uni-Regensburg).

3.11 Electron Microscopy

Porcine RPE cells grown on *Transwell* polycarbonate filters were washed with PBS and immediately fixed 4% (w/v) paraformaldehyde for 5 minutes at room temperature. After three-steps washing, with 1× PBS/Tween, porcine RPE cells were permeabilized with a blocking buffer (0.5 % Triton x 100, 10 % Goat serum, 1 x PBS pH 7.4, distilled H_2O) for 30 minutes. After blocking, cells were labeled overnight against primary antibodies: anti-bestrophin-1 (1:100; abcam 2182, mouse monoclonal, Cambridge, UK) diluted in a anti-body buffer (0.1 % Triton x 100, 2 % Goat serum, 1 x PBS pH 7.4 and distilled H_2O). Then, next day cells were washed 3x with 1xPBS/tween containing 1% Goat serum and 7% non fat dried milk powder. After, cells were incubated for 1 hour at room temperature with the secondary antibody CF^{TM} 568 Fluor Nano Gold (BIOTREND) diluted (1:20) in a anti-body buffer (0.1 % Triton x 100, 2 % Goat serum, 1 x PBS pH 7.4, 5% non fat dried milk powder and distilled H_2O). After 4x washing steps 10 minutes each, the samples were divided in two groups. The first group was used for fluorescence microscopy, thus, cells were mounted in an inverted microscope (Observer Z1; Carl Zeiss, Inc.) equipped with a confocal laser scanning microscope (LSM 710; Carl Zeiss, Inc.) operated with the ZEN 2008 software, the polychromatic illumination system VisiChrome (Visitron), and the MetaMorph software package (Universal Imaging Corp.). The second group was used for electron microscopy, thus, Silver enhancement was done for 1 hour at room temperature (Aurion kit) in dark and then the sample was embedded in Epon. After embedding, Ultrasections were cut using a Leica Ultracut E, and the sections were analyzed with a Zeiss Libra 120 microscope (This technique was done by the technical assistance Margit Schimmel from Prof. Dr. Tamm at the department of Anatomy, Uni-Regensburg).

3.12 Calcium imaging (Fura-2 AM)

RPE cells grown on cover-slips were washed with Ringer solution (145 mM NaCl, 0.4 mM KH_2PO_4, 1.6 mM K_2HPO_4, 5 mM glucose, 1mM $MgCl_2x6H_2O$, 1.3 mM Ca-Gluconatex$1H_2O$, pH 7.4, with NaOH) and loaded with Fura-2-AM (invitrogen) for 45 min in Opti-MEM I containing 10 µM Fura-2 (at 37^oC). Cells were washed again and incubated for 15 min using a Ringer solution. The cover-slips were placed into a bath chamber superfused constantly with Ringer solution at 37°C which was mounted onto the stage of a Zeiss inverted microscope (Axiovert 35, Zeiss, Jena, Germany) equipped with a 40× Fluar objective. We performed ratiometric measurements with Fura-2 fluorescence at 0.5-s intervals using a high-speed polychromator system (Visitron Systems, Puchheim, Germany), altering the wavelength of excitation light between 340 and 380 nm. Emitted light was filtered with a 510 nm filter and detected by a cooled charged-coupled device camera (CoolSNAP). Data were recorded with MetaFlour software and analyzed with MetaAnalysis software (both from Universal Imaging Corporation, Puchheim, Germany). To calculate intracellular free Ca^{2+} ($[Ca^{2+}]i$), the cells were superfused with the Ringer solution, without Ca^{2+} supplement, with 5 mM EGTA and 2 µM ionomycin. The cells were then superfused with Ringer solution supplemented with 2 µM ionomycin and saturated Ca^{2+} concentration. $[Ca^{2+}]i$ was calculated according to Grynkiewicz et *al*. [201]:

$$[Ca^{2+}] = K_d*(R-R_{min}) / (R_{max}-R)*S_f/S_b$$

In this equation, R is the fluorescence intensity ratio [F (340)/F (380)], R_{min} the value where R is minimal (with EGTA) and R_{max} the value when R is maximal (with saturating Ca^{2+} and ionomycin). K_d represents the dissociation constant of Fura-2 (224 nM [201]), and S_f and S_b are the maximum and the minimum fluorescence, respectively, after excitation with 380 nm.

3.13 Statistical analysis

$[Ca^{2+}]_I$ data are presented in mean values ± SEM. Statistical significances are calculated using the Student's *t* test with *p* values [$^{*}p< 0.05$ (significant); $^{**}p< 0.01$ (highly significant) and $^{***}p< 0.001$ (highly significant)]. All calculations were performed in Microsoft office Excel 2007 (Microsoft, Munich, Germany). Experiments were performed as least three times. The phenotypic analysis of retinae or RPE cells from mouse models were performed as blinded study.

3.14 Equipments

General equipment

Equipment	**Model**
Weight	BP 1200
pH. Meter	Mettler Toledo
Pipettes	0.1µl-10µl,10µl-100µl, 100µl-1000µl (Eppendorf AG)
Incubator	Tüv GS
Centrifugator	Megafuge-Heraeus (Thermo scientific)
Centrifugator	Minispin Eppendorf
Centrifugator	Mikro 220 R –Hettich zentrifugen

Molecular biology

Equipment	**Model**
Thermocycler	Rotor Gene Q
Thermocycler	Cyclone gradient (peqlab)
Thermocycler	MJ Research,Inc (PTC-100^{TM})
Powerpack	BIORAD

Cell culture

Equipment	**Model**
Preparation microscope	Carl Zeiss Universal S3
Cell incubator	Hera cell 150 (Thermo scientific)
Cell Bank	Hera Safe (Thermo scientific)

Calcium-imaging

Equipment	**Model**
Microscope	Axiovert 35, Zeiss, Germany
Objective	Zeiss Fluor 40x / 1,3 Oil immersion objective, Zeiss, Germany
Imaging system	VisiChrome High Speed Polychromator System
Lamp	Xenon Kurzbogenlampe 75W, Visitron System GmbH
Shutter	Mac5000 PS-System
Software	Metafluor 5.0, Universal Imaging Corporation

4 Results

4.1 Bestrophin-1 mouse models

4.1.1 Light damage at threshold level

Light damage is a well established experiment to study mechanisms of retinal degeneration in which the retinal damage depends on the light intensity. The aim of this study was to detect changes in the mouse retina at threshold levels of damage to analyze whether the mutation of bestrophin-1 leads to an increased susceptibility. Therefore, animals were exposed only at 800 lux for 30 minutes. Under these conditions, 9 days after this experiment, wild type animals exposed to light (n=10) showed a tiny reduction of the outer segment (ONL) compared to those ones were not exposed (n=8). This reduction was not significant (**Fig. 7c**).

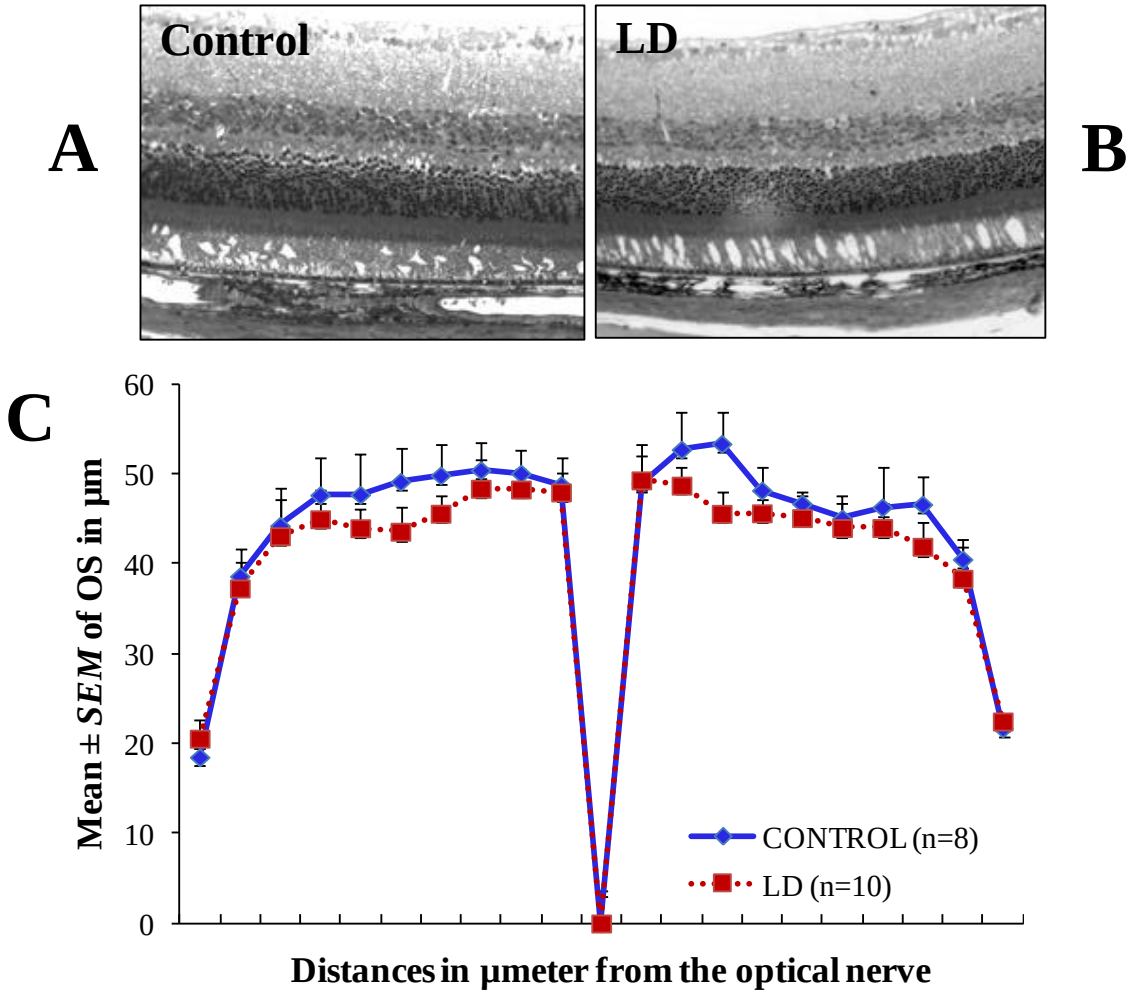

Fig. 7 Light damage at threshold level in mouse. a: Epon section from a black-6 wild type mouse without any light exposure. **b:** Epon section from a black-6 wild type mouse exposed to 800 lux light intensity for 30 minutes. **c**: Morphometric analysis of ONL retinas from exposed (LD; n=10) and non-exposed (control; n=8) mice.

4.1.2 Light damage in bestrophin-1 KI$^{+/Y227N}$ mouse model

In order to detect light-induced retinal degeneration due to a possible function of bestrophin-1, bestrophin-1 KI$^{+/Y227N}$ mice were exposed to light at threshold levels. By 9 days after this experiment, bestrophin KI$^{+/Y227N}$ animals exposed to light (n=5) showed an increase not significant of the ONL compared to not exposed KI animals (n=5)(**Fig. 8c**).

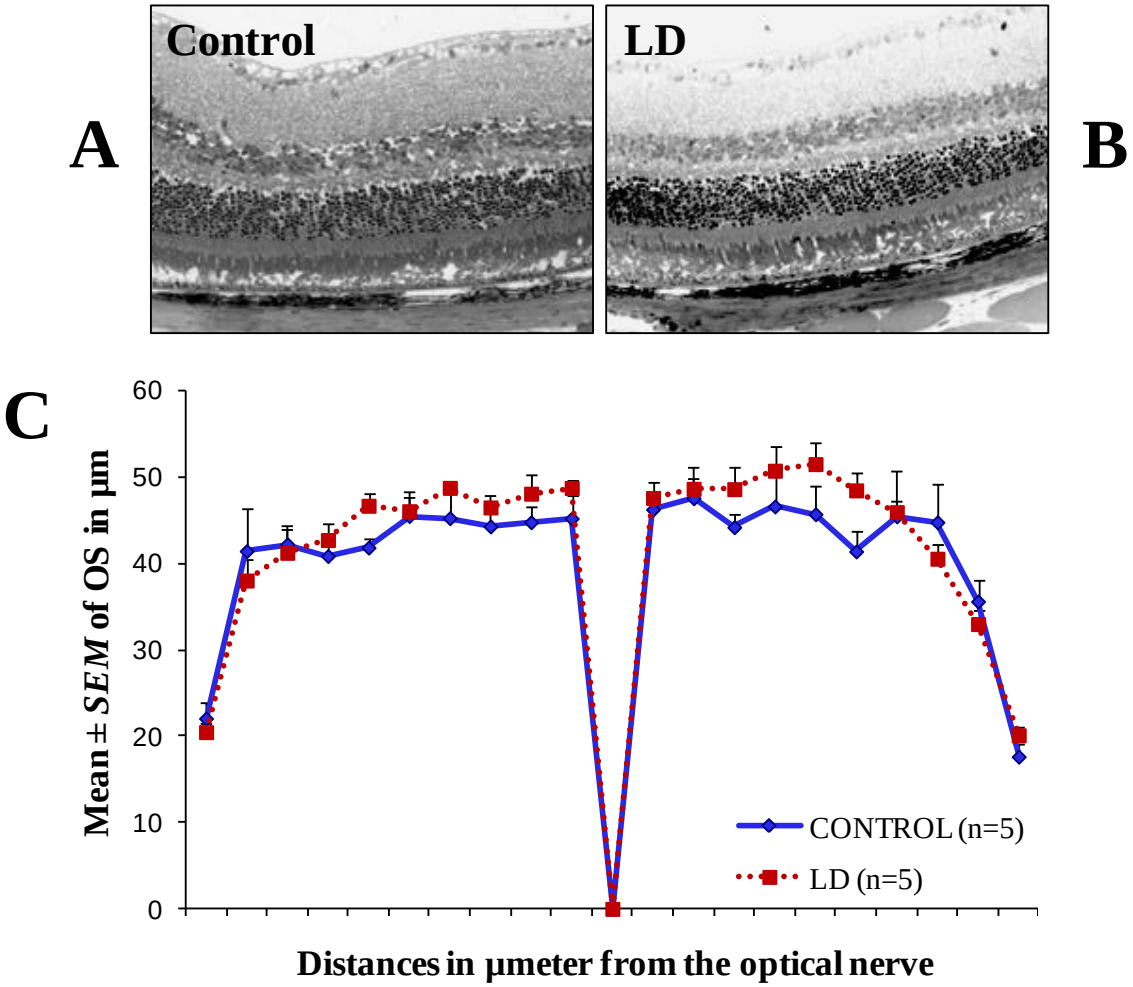

Fig. 8 Light damage at threshold level in bestrophin-1 KI$^{+/Y227N}$ mouse model. a: Epon section from a bestrophin-1 KI mouse without any light exposure. **b:** Epon section from a bestrophin-1 KI mouse exposed to 800 lux light intensity for 30 minutes. **c**: Morphometric analysis of ONL retinas from exposed (LD; n=5) and non-exposed (control; n=5) mice.

4.2 Calcium signalling in bestrophin-1$^{-/-}$ mouse model

In order to detect a possible intracellular function of bestrophin-1, ATP-induced Ca^{2+} responses were measured in primary retinal pigment epithelium (**Fig. 9**) cells from wild type (WT) and bestrophin-1$^{-/-}$ mice were isolated. In both cell types changes in intracellular Ca^{2+} level were trigged by application of ATP (100µM).

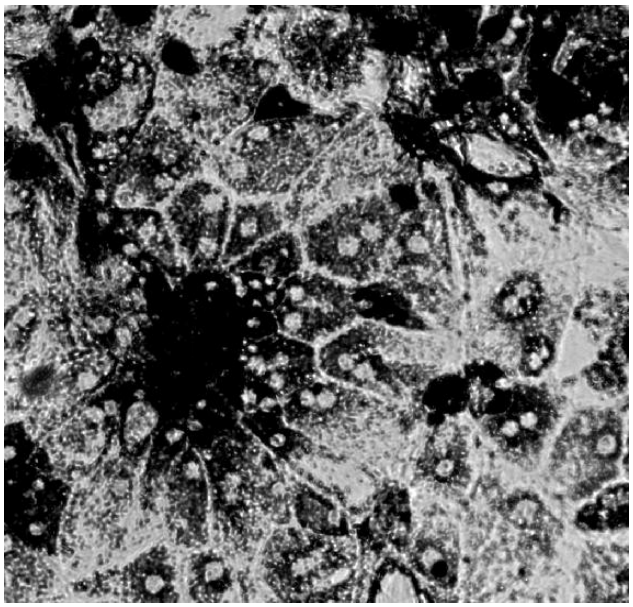

Fig. 9 Mouse RPE 1 week after isolation.

RPE cells from bestrophin-1$^{-/-}$ mice showed a resting intracellular Ca^{2+} concentration higher compared to that of RPE from wild type animals: Ca^{2+}(KO)=231.3 ± 20.5 (n=25) and Ca^{2+}(WT)=135.4 nM ± 28.4 (n=16) (**Fig. 10**). On the other hand, during application of ATP no differences were found between the peak amplitude trigged by ATP between wild type and bestrophin-1 KO RPE cells.

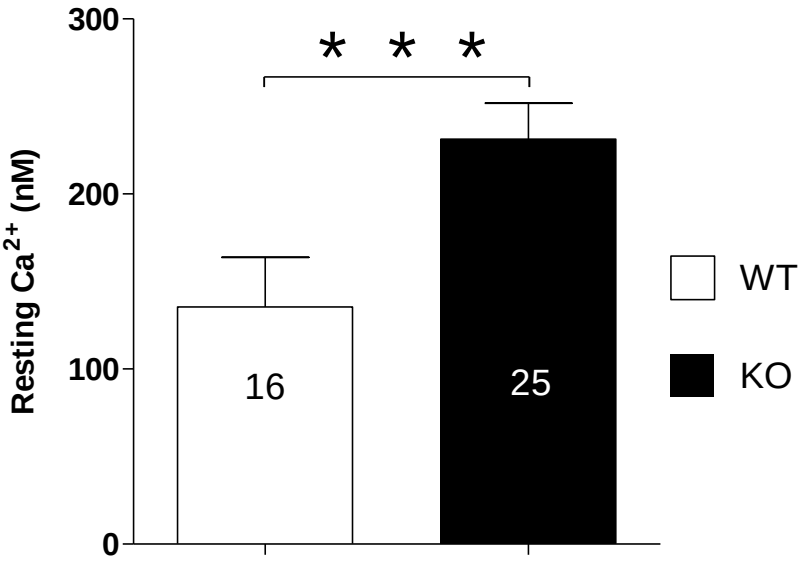

Fig.10 Comparison of resting Ca^{2+} levels between wild type and bestrophin-1 KO mice. Three independent experiments were done per group (WT=16; KO=25).

4.3 Porcine retinal pigmented epithelium cell model

Due to lack of reliable antibodies against mouse betrophin-1, together with the possible low expression of this protein in mouse, a new RPE cell model was developed for this study (**Fig. 11**).

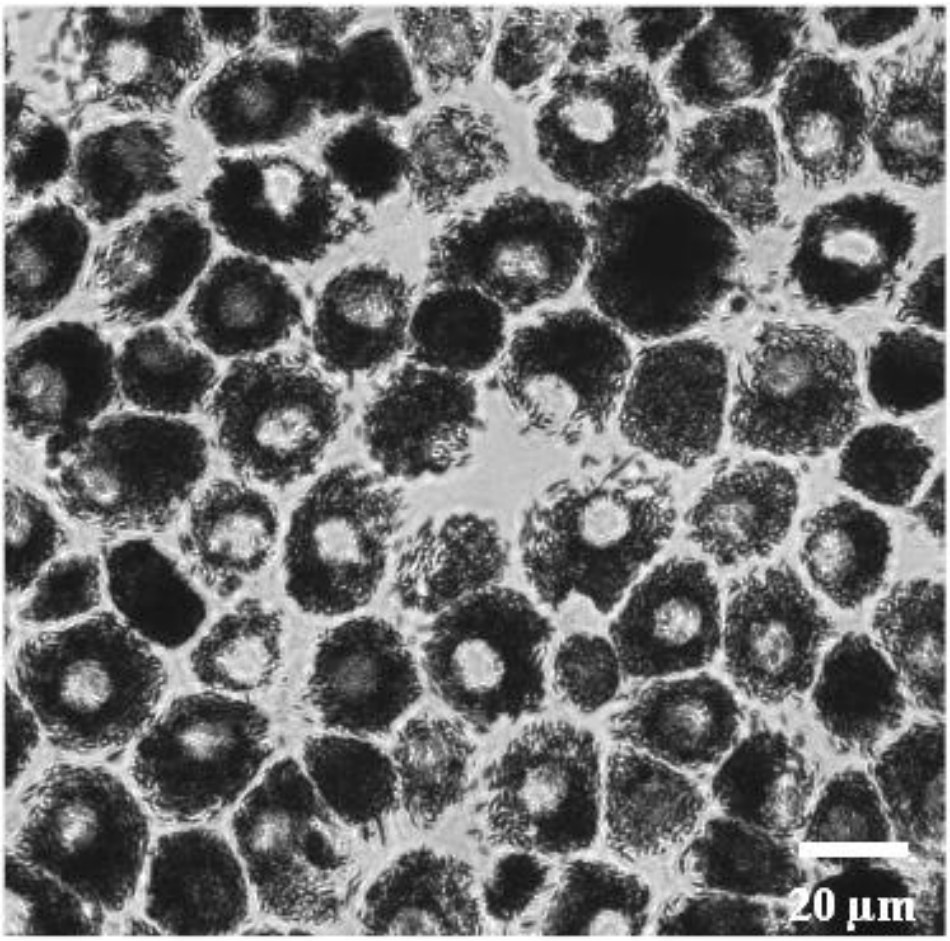

Fig. 11 Cell culture of porcine RPE cells. Cells were isolated and plated at the concentration of 1.0-1.2 x 10^6 cells per ml in a drop of 100µl medium containing 10% serum. Next day the wells were re-filled with medium containing 5% serum. Under these conditions, primary porcine RPE cells were confluent and semi-polarized in the range between 24-72 hours. In black the heavy typical pigmentation RPE cells have due to the presence of melanosomes.

Using a monoclonal mouse antibody against bestrophin-1, we were able to detect by mean of western blot and immunohistochemistry the presence of endogenously expressed bestrophin-1 in porcine retina (**Fig. 12**)

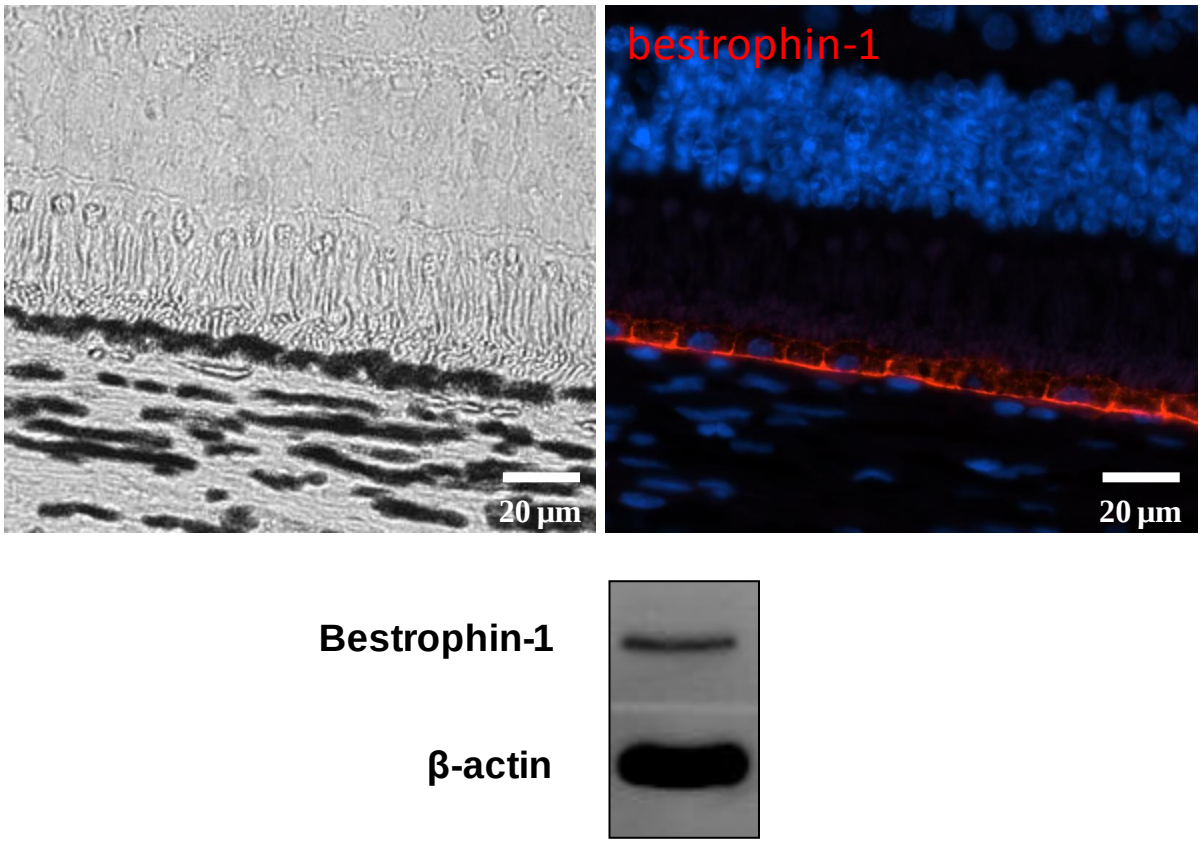

Fig. 12 Bestrophin-1 in porcine RPE cells. a: Paraffine section of the porcine retina; right panel: immunostaining of bestrophin-1 (**in red**); left panel: Light micrograph (DIC: Differential interference contrast). **b:** Western blot of bestrophin-1 from porcine RPE cells.

4.3.1 Bestrophin-1 expression in short-time porcine RPE cell culture

In native tissue bestrophin-1 protein has been shown to localize basolaterally in RPE cells.

Since the aim of this work was to study endogenously expressed bestrophin-1 by mean of knock down siRNA experiments, stable expression of bestrophin-1 in cell culture was needed. Thus, the effects of two cell culture conditions on bestrophin-1

expression were investigated. The first one was the cell density which was divided in two groups: confluent and non-confluent seeded cells. In both groups cells were treated with high percentage of serum in medium (20%). In the second condition confluent seeded cells treated with low percentage of serum in medium (5%) were analyzed. The expression of bestrophin-1 was investigated under these conditions at different time-points (24, 48 and 72 hour after cell isolation) by mean of qRT-PCR, western blot and immunocytochemistry.

As a first result it was found that non-confluent seeded cells showed a faster down-regulation of BEST1 compared with confluent seeded cells (**Fig. 13**). This effect was observed from 24 hours until 72 hours from cell isolation. On the other hand, confluent seeded cells treated with 5% serum showed a tendency to up-regulate BEST1 compared to confluent seeded cells treated with 20 % serum (**Fig. 13**). This tendency could be observed when confluent seeded cells treated with 20 % serum at 72 hours showed a reduction of BEST1 compared with those ones at 48 hours. In contrast, confluent seeded cells treated with 5 % serum showed an up-regulation of BEST1 at 72 hours compared with those ones at 48 hours isolated cells.

Comparable results were found at the protein level (**Fig. 14**). During the first 24 hours endogenously expressed bestrophin-1 showed similar levels in all cell culture conditions. After 48 hours non-confluent seeded cells showed a high reduction of bestrophin-1 expression compared to both confluent seeded cell groups. By 72 hours isolated porcine RPE cells in non-confluent seeded cells levels of bestrophin-1 has almost vanished. At this time point, it was also possible to observe that confluent seeded cells treated with 5 % serum showed higher levels of bestrophin-1 compared with confluent seeded cells treated with 20 % serum.

The western blot results were further confirmed by immunocytochemistry (**Fig. 15**). In immunocytochemistry experiments, bestrophin-1 in non-confluent cells was not added due to its low expression after 24 hours.

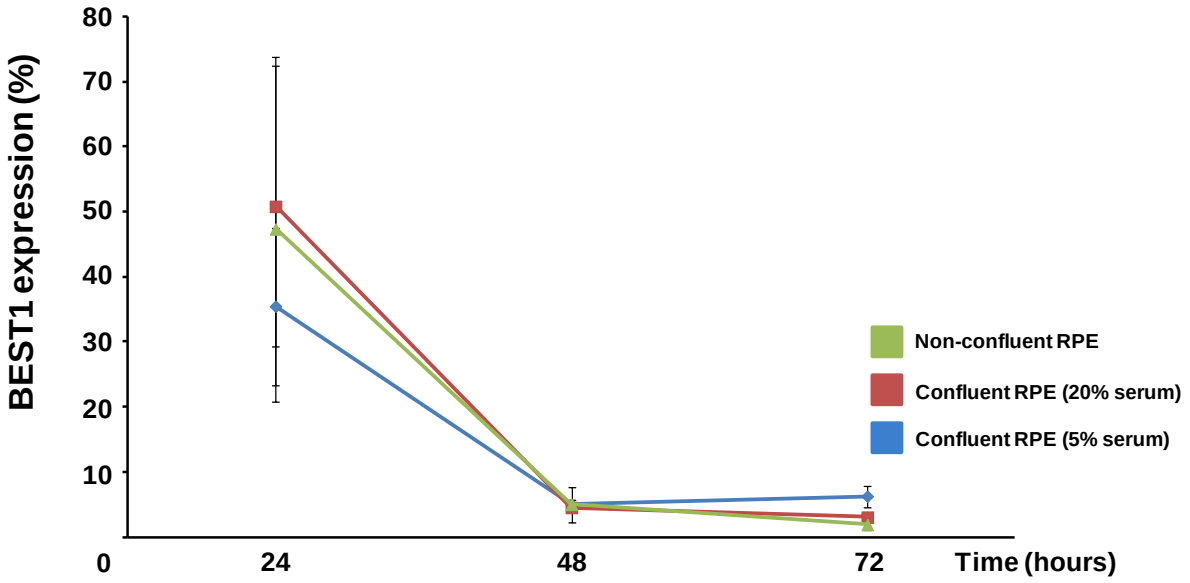

Fig. 13 Expression of BEST1 under different cell culture conditions in porcine RPE cells. Quantitative PCR was performed on three different cell culture groups. BEST1 expression was analyzed in non-confluent seeded cells, and confluent seeded cells. Confluent seeded cells were divided in two groups depending on the percentage of serum in medium, thus one used 5 % and the other one 20%. The analysis was done in 24, 48 and 72 hours isolated cells.

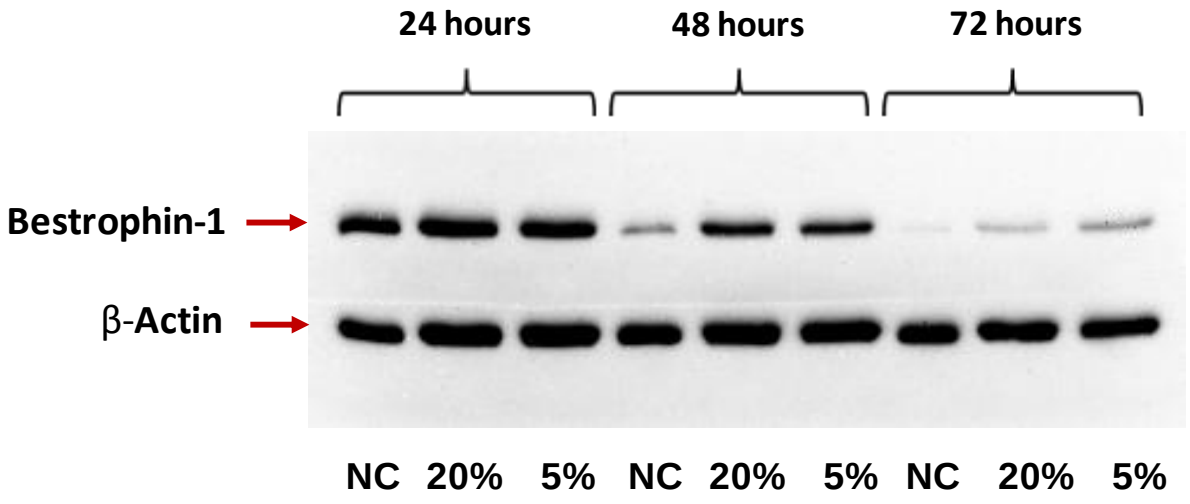

Fig. 14 Western blot experiments show different levels of endogenously expressed bestrophin-1 under different cell culture conditions. Three different groups of isolated primary porcine RPE cells were analyzed. One group consisted of non-confluent seeded cells (1.0-1.2 x 10^5 cells per ml) treated with 20% serum in medium. The second group of cultured cells was confluent plated (1.0-1.2 x 10^6 cells per ml) and treated with 20% serum in medium. The last group was confluent plated (1.0-1.2 x 10^6 cells per ml) but treated with 5% serum in medium. Equal amounts of protein were loaded to the blot. This experiment was replicated 3 times.

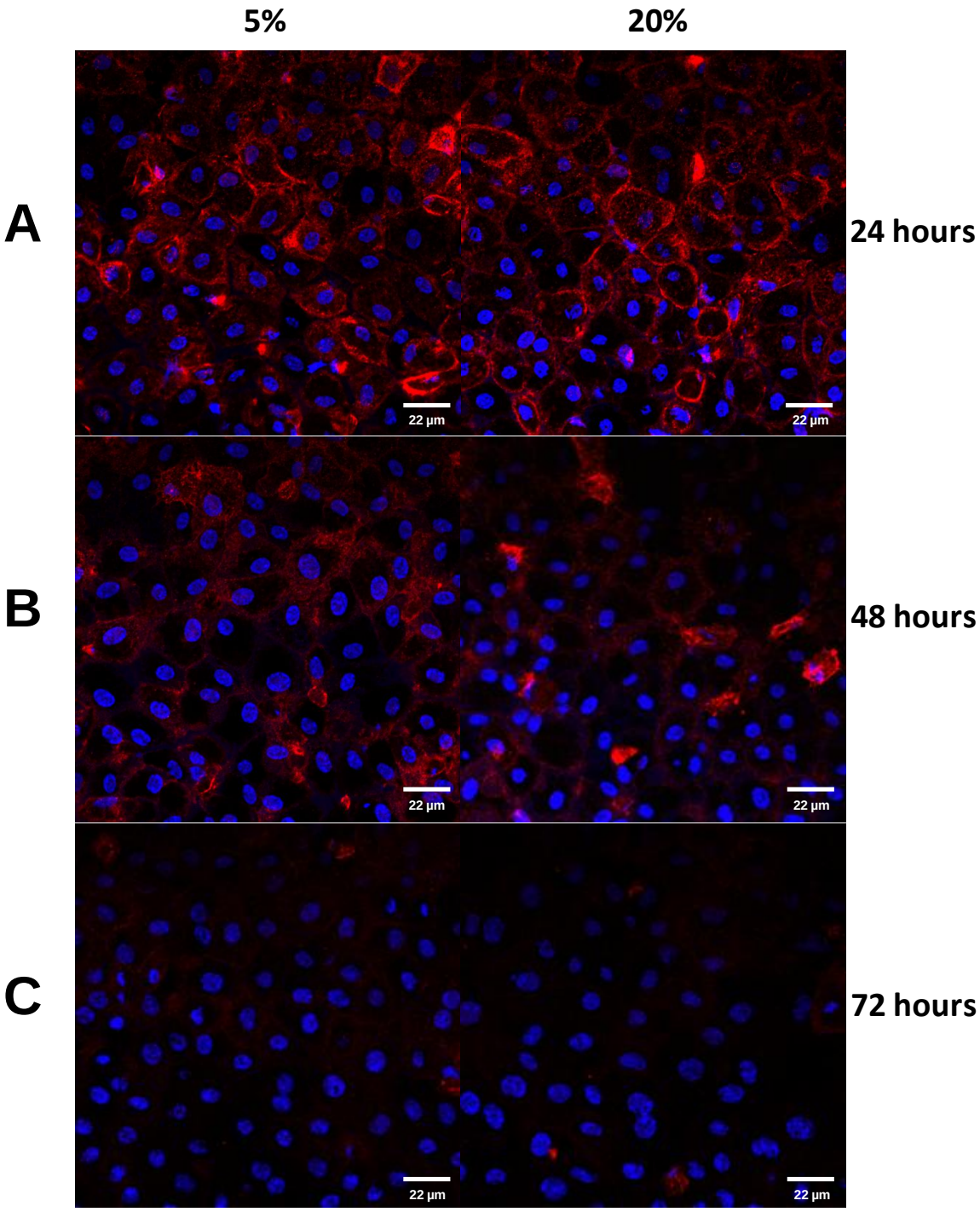

Fig. 15 Confocal microscopy in porcine RPE cells labeled against bestrophin-1 at different time points with different percentages serum. left row: RPE cells treated with 5% serum**. right row:** RPE cells treated with 20% serum **a:** Immunolabeling of bestrophin-1 after 24 hours RPE cells isolation. **b:** Immunolabeling of bestrophin-1 after 48 hours RPE cells isolation. **c:** Immunolabeling of bestrophin-1 after 72 hours RPE cells isolation.

4.4 Store-operated calcium entry (SOCE) in porcine RPE cells

Since store-operated calcium entry (SOCE) is a mechanism which involves the interaction of Stim and Orai proteins, their expression was analyzed in porcine RPE cells 48 hours in culture. Using RT-PCR the expression of I_{crac} channels: STIM 1,2 and ORAI 1,2,3 were found (**Fig. 16a**). Due to the lack of reliable antibodies for it was possible to detect orai-1 and stim-1 proteins in porcine cells (**Fig. 16b**).

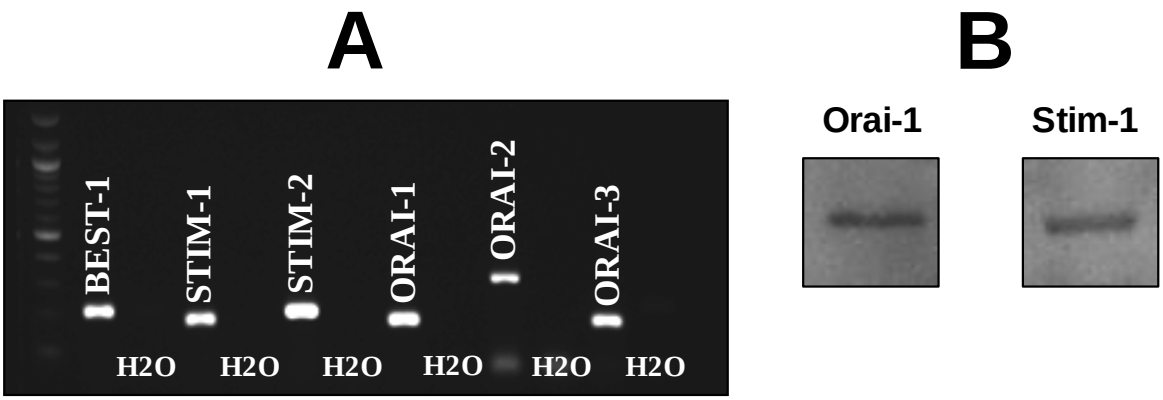

Fig. 16 Icrac channels in porcine RPE cells. a: After RNA isolation from 48 hours cultivated primary porcine RPE cells, RT-PCR showed the expression of BEST1 and the proteins involved in SOCE: STIM1, STIM2, ORAI, ORAI2 and ORAI3. **b:** Western blots showing the presence of stim-1 and orai-1 proteins

In order to show functional expression of Orai channel Ca^{2+} imaging experiments were performed in which store-operated Ca^{2+} entry (SOCE) was activated under influence of ion channel openers or blockers. An internal control was defined by using two subsequently activated SOCE. In this experiment the first store-operated calcium entry was regarded as a control (SOCE 1) and in the second one (SOCE 2) it was applied different drugs known to modulate Orai channels. To activate SOCE it was followed the protocol which has been described and shown in many studies before [137, 138, 145]. Thus, porcine RPE cells were treated first with a ringer solution until resting Ca^{2+} reached steady-state levels, later thapsigargin (1µM) was applied for 3 minutes and after a Ca^{2+} free solution for 1 minute. Later on ringer was re-added to the cells and ones SOCE was activated it was kept for 2 minutes. After this time a Ca^{2+} free solution was again applied for 1 minute and followed by ringer solution again keeping SOCE for 2 minutes more (**Fig. 17**).

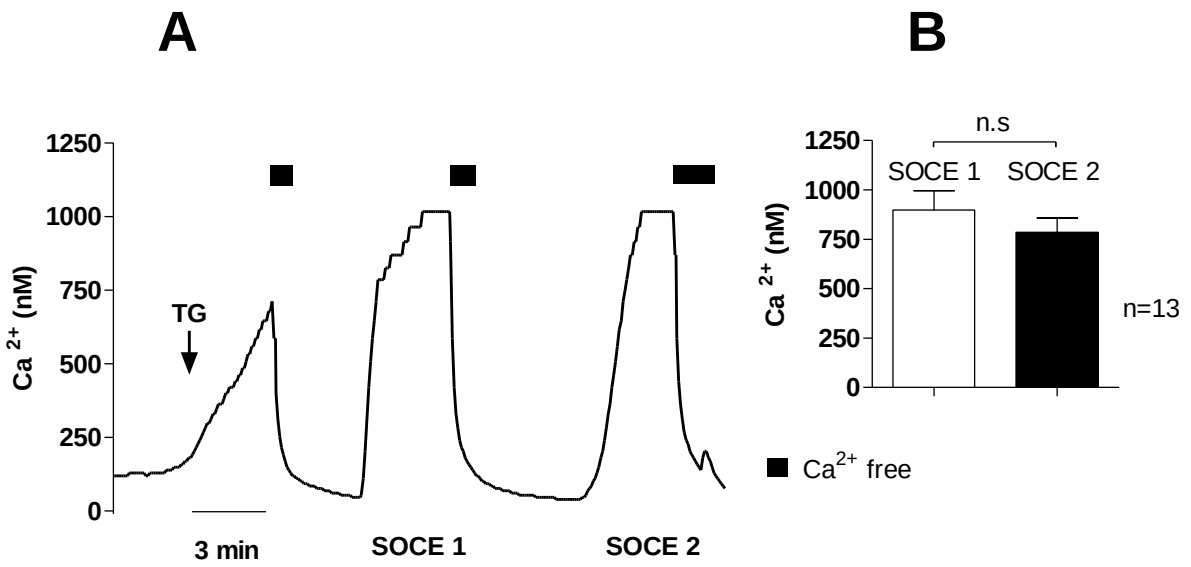

Fig. 17. **SOCE activation using the double paradigm in porcine RPE cells** (n=13); **a:** Cells were first treated with ringer solution untill the resting Ca^{2+} got stable, after that cells were treated with thapsigargin (1µM) for 3 minutes and followed by the application of a Ca^{2+}-free solution for 1 minute, after, ringer solution was re-added to the cells. After 2 minutes of SOCE activation peak, Ca^{2+}-free solution was re-added for 1 minute and again followed by the re-addition of ringer solution, keeping this second SOCE activation peak for 2 minutes again. **b:** Statistic analysis of the SOCE in the double paradigm (n=13; n.s). Using the double paradigm experiment it was possible to take the first SOCE activation peak (SOCE1) as a control for further experiments.

In order to clarify whether TRP or voltage-gated Ca^{2+} channels were involved in SOCE mechanism SKF 96365 (50µM) was applied. With this blocker no significant effect was found in porcine RPE cells between both SOCE amplitudes (**Fig. 18;** n=10).

2-Aminoethoxydiphenyl borate (2-APB) is known to affect on Orai channels depending on its concentration. High concentrations of 2-APB inhibits and low concentrations potentiate Orai channel activation [138, 202]. After application of 2-APB at high concentration (75µM) SOCE2 was reduced by 87.3 ± 7.6 % compared to control SOCE1 (**Fig.18**; n=22; $p \leq 0.001$).

Due to the strong SOCE response in porcine RPE cells which could be achieved by the combination of thapsigargin application under Ca^{2+}-free conditions we changed the paradigm into one with less strong SOCE response. For that purpose SOCE activation was performed without thapsigargin application. Under these conditions t the application of 2-APB at 5µM increased SOCE2 amplitude by 106 ± 14.6 % compared to control SOCE1 (Fig. **18;** n=19; $p \leq 0.001$).

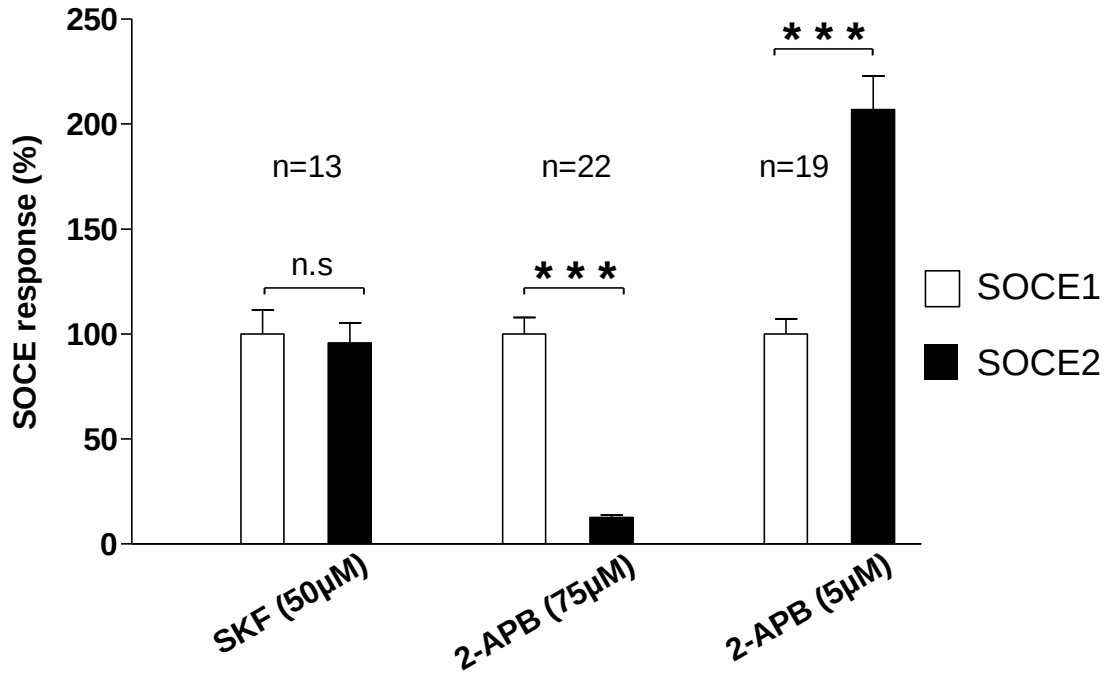

Fig. 18 Overview of different drugs effects that modulate SOCE response in porcine RPE cells. Using the double paradigm experiment in porcine RPE cells all drugs were applied in the second SOCE response (SOCE2). From the left to the right: SKF96365 (50µM) did not show any effect (n=10; n.s.), 2-APB (75µM) was highly significant (n=22; $p \leq 0.001$) as well as 2-APB (5µM)(n=19; $p \leq 0.001$).

In order to gain deeper insight into the mechanism that underlie SOCE activation in porcine RPE cells, siRNA knock-down experiments were performed against Orai-1 protein (Orai-1siRNA). Only in those cells which were transfected against Orai-1siRNA the expression of this protein was reduced by 80 ± 9,4 % (n = 3) compared to that in scrambled transfected cells (**Fig. 19**).

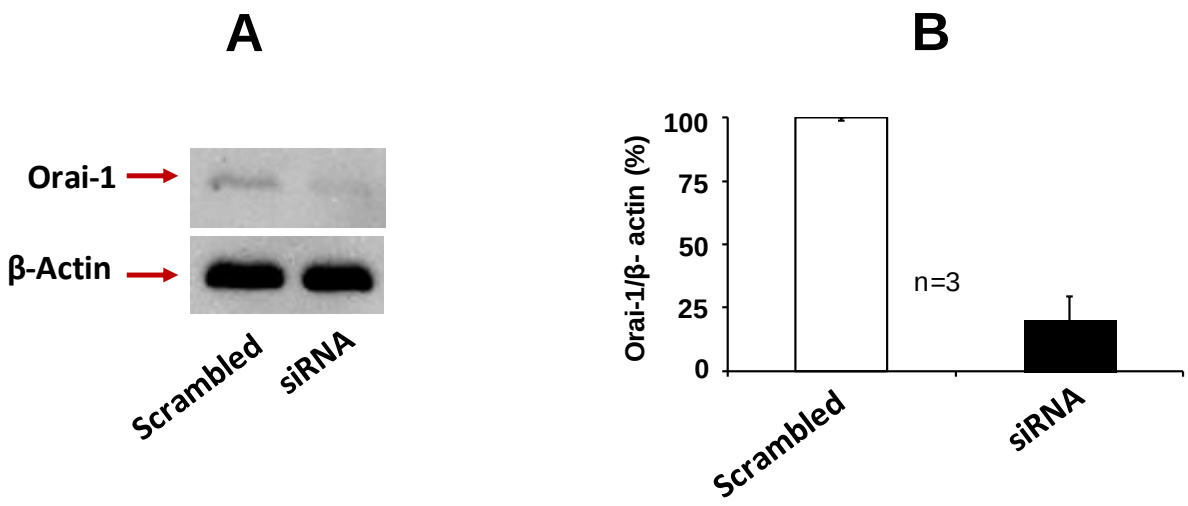

Fig. 19 Knock-down of Orai-1 protein. a: Western blot shows the knock-down of Orai-1 protein in Orai-1siRNA transfected cells compared to scrambled transfected cells. Equal amounts of protein were loaded to the blot. This experiment was replicated 3 times. **b:** Quantification of knock-down Orai-1 after a densitometric analysis

In calcium imaging experiments several differences were found between Orai-1siRNA (n=82) and scrambled transfected cells (n=86)(**Fig. 20**). First resting Ca^{2+} was higher in Orai-1siRNA transfected cells compared that of scrambled transfected cells: $Ca^{2+}_{Orai\text{-}1siRNA}$= 99.15 nM ± 4.9 and $Ca^{2+}_{scambled}$= 70.62 nM ± 3.1 (**Fig. 20**; $p \leq 0.001$). Furthermore, the amplitude of Ca^{2+} triggered by the application of thapsigargin differed between both groups: Ca^{2+}thapsi $_{Orai\text{-}1siRNA}$=197.58 ± 23.1 and Ca^{2+}thapsi $_{scrambled}$= 263.62 ± 15.2 (**Fig. 20**; $p \leq 0.05$). As a main result in cells transfected against Orai-1siRNA SOCE amplitude was reduced by 65.2% compared with scrambled transfected cells: amplitude of $SOCE_{Orai\text{-}1siRNA}$ = 174.4 ± 22.1 nM and amplitude of $SOCE_{scrambled}$ = 500.7 ± 31.5 nM (**Fig. 20**; $p \leq 0.001$).

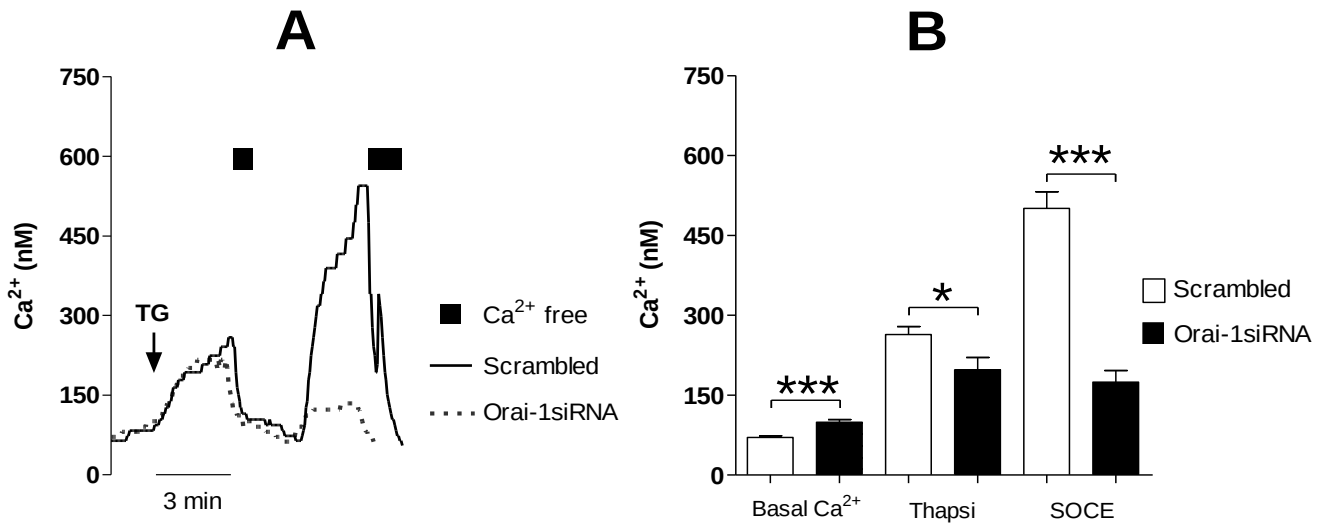

Fig. 20 Effect of Orai-1 knocked-down in SOCE in porcine RPE cells. a: Calcium tracing of scrambled and Orai-1siRNA (dashed line) transfected porcine RPE cells showing the effect of knock-down Orai-1 protein in the SOCE activation amplitude. Cells were treated first with ringer solution, after thapsigargin (1µM) was applied for 3 minutes and followed by Ca^{2+}-free solution for 1 minute, and later, extracellular Ca^{2+} was re-added to the cells. **b:** Statistic analysis of SOCE activation amplitude between scrambled and Orai-1siRNA transfected cells (***$P \leq 0{,}001$; $n_{scrambled}$= 86 and $n_{siOrai-1}$=82; all experiments were done in 3 different rounds of primary cells isolation; Number of scrambled experiments=8 and number of Orai-1siRNA experiments=6).

4.5 Bestrophin-1 influences SOCE in porcine RPE cells

In order to investigate whether bestrophin-1 could be involved in SOCE mechanism in primary porcine RPE cells siRNA experiments against bestrophin-1 protein (best-1siRNA) were performed. Densitometric analysis of western blots showed that bestrophin-1 expression in RPE cells was reduced by 81 ± 10.7 % (n = 3; **Fig. 21**). Using the same lysate from scrambled and best-1siRNA transfected cells, western-blots were stained against Orai-1 and Stim-1 which showed no effects in the expression levels of Orai-1 and Stim-1 (**Fig. 21**).

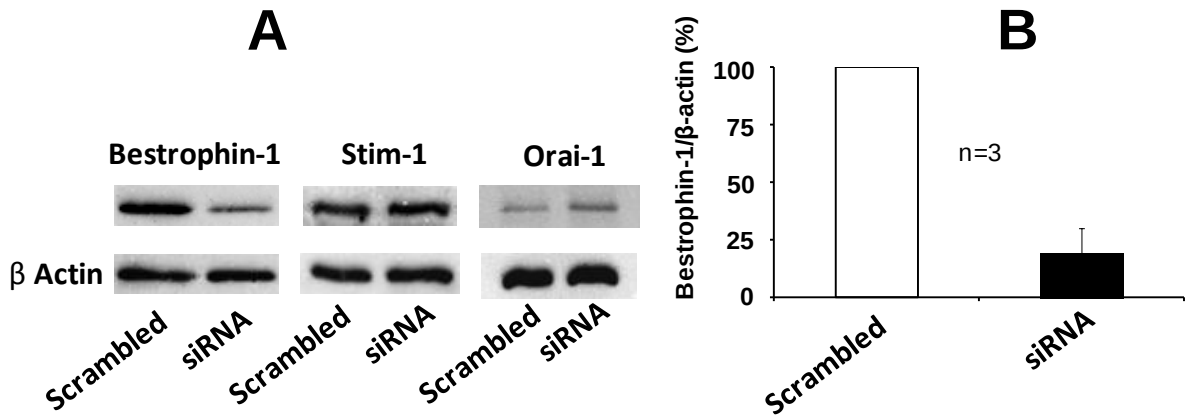

Fig. 21 Knock-down of bestrophin-1 protein a: Western blot shows the knock-down of bestrophin-1 protein in Best-1siRNA transfected cells compared to scrambled transfected cells. Stim-1 and Orai-1 proteins did not show any expression level changes due to Best-1siRNA. **b:** Quantification of knock-down Orai-1 after densitometric analysis..Equal amounts of protein were loaded into the blot. This experiment was replicated 3 times.

The labeling of the scrambled and the best-1siRNA with alexa 488 dye made it possible to identify transfected cells in Ca^{2+} imaging experiments. With this technique it was possible not only to compare SOCE response between best-1siRNA and scrambled transfected cells but also between cells which were not transfected. This second control gave us a more reliable insight into the function of bestrophin-1 in SOCE response. Thus, the experiments were divided in the following groups:

scrambled (n=86), best-1siRNA (n=109) and non transfected cells per scrambled (n=11) and best-1siRNA (n=16) (**Fig. 22b**).

As first observation it was found that porcine RPE cells transfected with best-1siRNA showed a significant higher resting Ca^{2+} compared to that of scrambled tranfected cells: $Ca^{2+}_{best\text{-}1siRNA}$= 81.64 nM ± 3.57 and $Ca^{2+}_{scrambled}$= 71.58 nM ± 3.32 (**Fig. 22a** and **b**;. $p \leq 0.05$). On the other hand, non-transfected cells per group did not significantly differ between each other (**Fig. 22 b**). The main finding of this study was that in those cells treated with best-1siRNA SOCE amplitude was remarkable reduced compared to those cells transfected with scrambled and non-transfected cells. Thus, best-1siRNA transfected cells showed SOCE amplitude reduced by 69.1 % compared with scrambled transfected cells: $SOCE_{best\text{-}1siRNA}$= 155.01 nM ± 17.06 and $SOCE_{scrambled}$= 500.7 nM ± 31.5. Furthermore, similar results were found between best-1siRNA and non-transfected cells per group (best-1siRNA and scrambled) differing significantly: $SOCE_{scrambled(n.t)}$= 734.22 nM ± 102.67 and $SOCE_{best\text{-}1siRNA(n.t)}$= 605.85 nM ± 81.27 (**Fig. 22a** and **b**; $p \leq 0.001$).

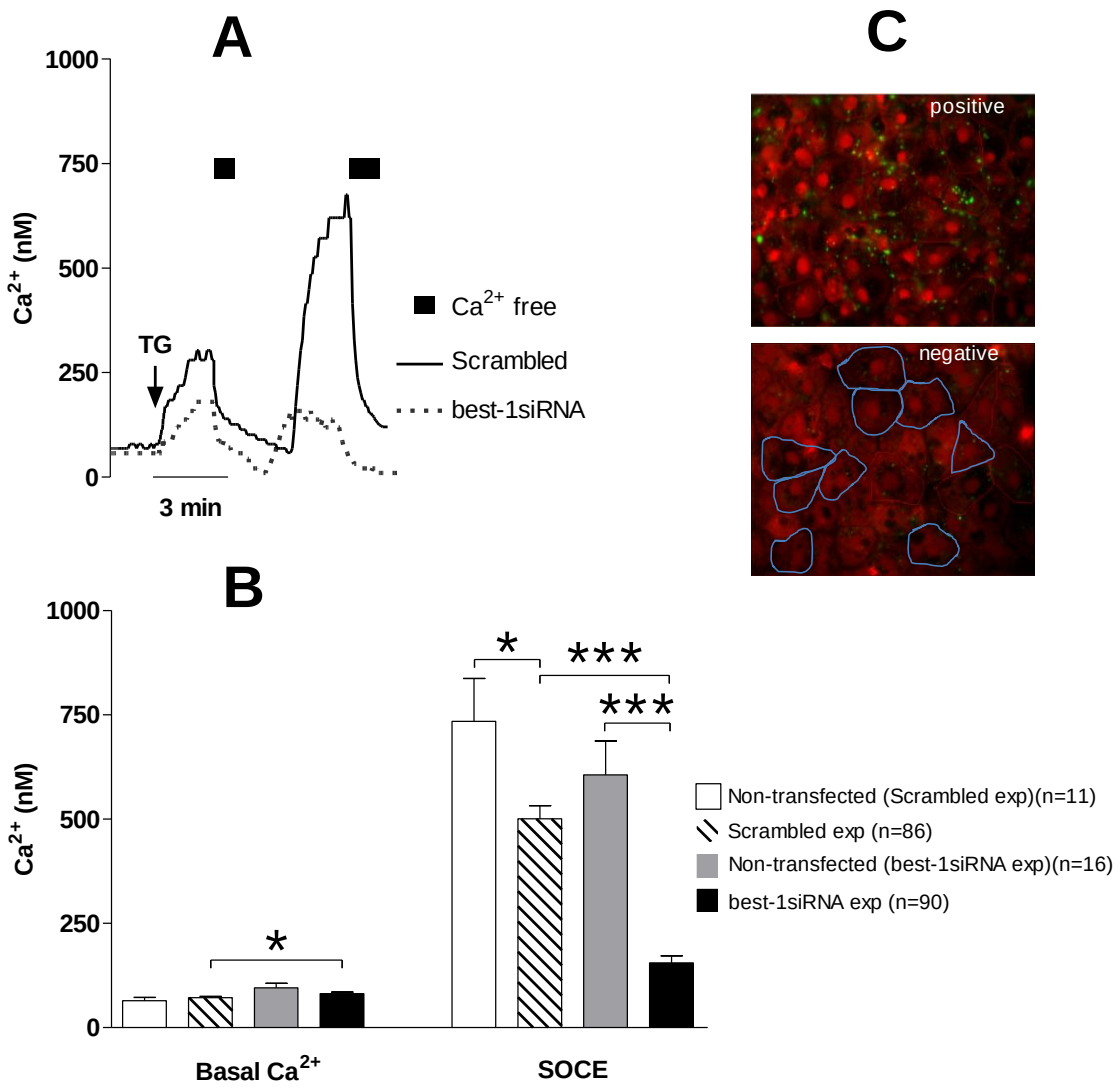

Fig. 22 Influence of bestrophin-1 protein in SOCE in porcine RPE cells. a: Calcium trace of SOCE in scrambled and best-1siRNA (dashed line) transfected cells. Cells were treated previously with a Ringer solution, after thapsigargin (1µM) was applied for 3 minutes and followed by Ca^{2+}-free solution for 1 minute, and later, extracellular Ca^{2+} was re-added to the cells. **b**: Statistic analysis of basal Ca^{2+}, thapsigargin effect and SOCE activation amplitude between scrambled and best-1siRNA transfected cells. Transfected cells and non-transfected (n.t) cells were also compared inside each group (best-1siRNA and scrambled) (*$P \leq 0{,}05$; **$P \leq 0{,}01$; ***$P \leq 0{,}001$; $n_{scrambled}$= 86 and $n_{scrambled(n.t)}$=11; $n_{best\text{-}1siRNA}$=90 and $n_{best\text{-}1siRNA(n.t)}$=16; all experiments were done in 3 different rounds of primary cells isolation; Number of scrambled experiment=8 and number of best-1siRNA experiment=6).**c**: Detection of best-1siRNA transfected cells. Best-1siRNA was labeled with Alexa 488 dye and therefore, it was possible to detect which cells were transfected (upper panel) and which ones were not (lower panel).

To obtain more information about the mechanism underlying the reduction of SOCE amplitude after knock-down of bestrophin-1 expression, the amplitude of Ca^{2+} released from ER stores by application of two different SERCA pump inhibitors was analyzed (**Fig. 23a** and **b**; $p \leq 0.001$). First, we applied cyclopiazonic acid (CPA) under physiological extracellular Ca^{2+} conditions for 2 minutes. After this short period of time we found that cells treated with best-1siRNA showed a significant reduction in the amplitude of Ca^{2+} released compared to control cells : $CPA_{best\text{-}1siRNA}$=292,73 ± 23,18 and $CPA_{scrambled}$=364,95 ± 19,36: (**Fig. 23a**; $p \leq 0.05$). In addition, this finding was supported in SOCE experiments in which the application of thapsigargin for 3 minutes showed a remarkable reduction of Ca^{2+} amplitude in those cells treated with best-1siRNA compared to control cells: $Ca^{2+}thapsi_{best\text{-}1siRNA}$=100.21 nM ± 6.40 and $Ca^{2+}thapsi_{scrambled}$=290.10 nM ± 18.25 (**Fig. 23b**; $p \leq 0.001$). This reduction was also significant against the non-transfected controls: amplitude $thapsi_{scrambled(n.t)}$= 317.09 ± 58.47 nM in scrambled siRNA experiments and amplitude $thapsi_{best\text{-}1siRNA(n.t)}$= 206.58 ± 15.37 nM in bestrophin-1 siRNA experiments (**Fig. 23b**; $p \leq 0.001$).

Because of the strong reduction in the amplitude of the Ca^{2+} response to SERCA inhibition in cells with decreased bestrophin-1 expression we hypothesized that the SOCE response depended on the amount of Ca^{2+} released from stores. In order to elucidate this, the total amount of Ca^{2+} released upon SERCA inhibition by thapsigargin was quantified. Here best-1siRNA treated cells showed 67.1 ± 5.9 % reduction of Ca^{2+} released from ER store compared to that of scrambled and Orai-1siRNA groups. In contrast, neither scrambled nor Orai-1siRNA treated cells showed significant differences between the amounts of Ca^{2+} released from ER store (**Fig. 23c**; $p \leq 0.001$).

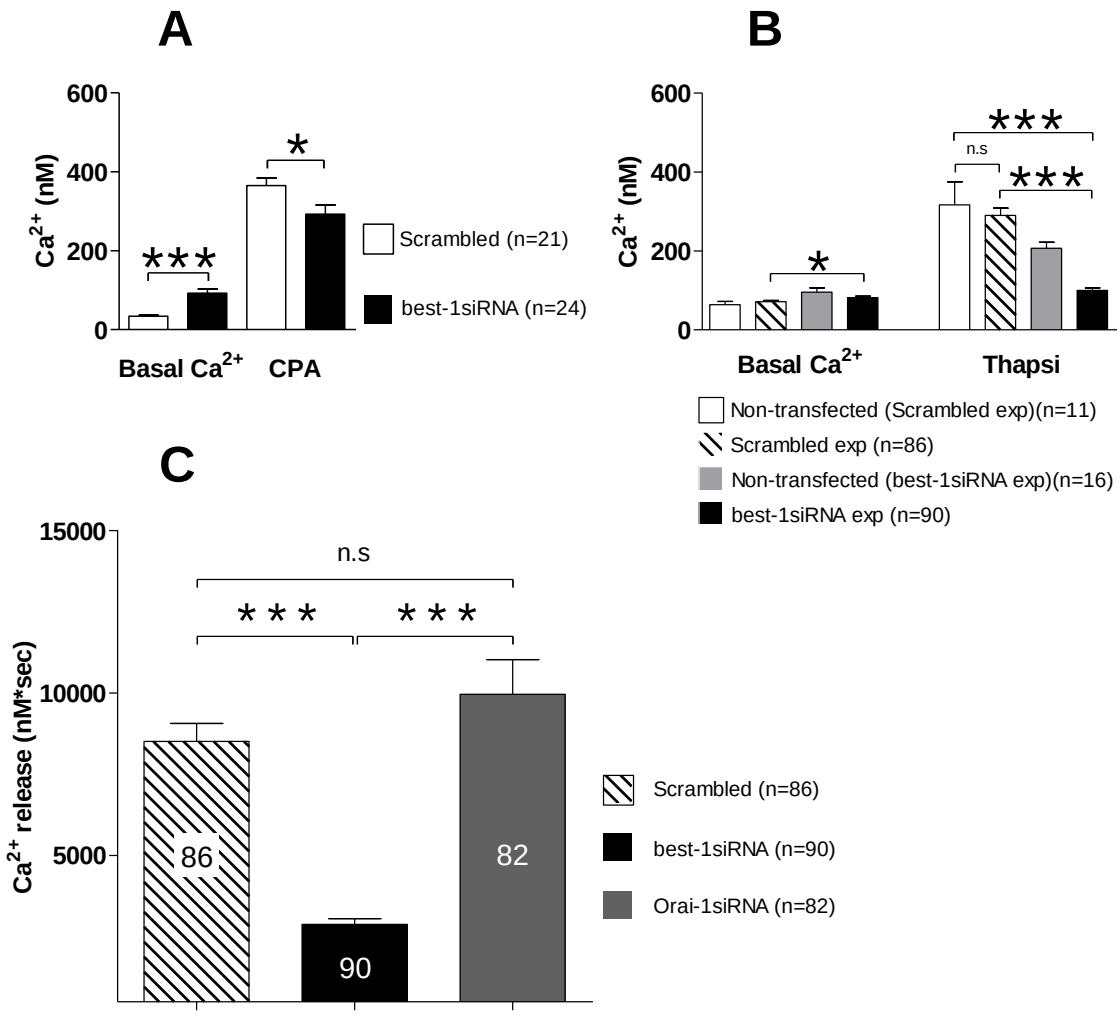

Fig. 23 Comparison of Ca^{2+} release from cytosolic stores in response to application of different SERCA inhibitors. a: Statistic analysis of basal Ca^{2+} and cyclopiazonic acid (CPA)(10µM) effect between scrambled and best-1siRNA transfected cells (*$P \leq 0{,}05$;$n_{scrambled}$=21 and $n_{best\text{-}1siRNA}$=24) **b**: Statistic analysis of basal Ca^{2+} and thapsigargin (1µM) between scrambled and best-1siRNA transfected cells. Transfected cells and non-transfected (n.t) cells were also compared inside each group (best-1siRNA and scrambled) (*$P \leq 0{,}05$; **$P \leq 0{,}01$; ***$P \leq 0{,}001$; $n_{scrambled}$= 86 and $n_{scrambled(n.t)}$=11; $n_{best\text{-}1siRNA}$=90 and $n_{best\text{-}1siRNA(n.t)}$=16; all experiments were done in 3 different rounds of primary cells isolation; Number of scrambled experiment=8 and number of best-1siRNA experiment=6). **c**: Comparison of Ca^{2+} release from cytosolic stores in response to application of thapsigargin in scrambled, Orai-1siRNA or best-1siRNA transfected cells. The amount of Ca^{2+} released was quantified by integration of the area below the curve of Ca^{2+} increases during thapsigargin (1µM) application. In every experiment thapsigargin was applied for 3 minutes (***$P \leq 0{,}001$; $n_{scrambled}$=86; $n_{best\text{-}1siRNA}$=90 and $n_{Orai\text{-}1siRNA}$=82).

Since the amount of Ca^{2+} in stores seems to be dependent on the presence of bestrophin-1, we investigated whether there is a possible physical interaction between bestrophin-1 and Stim-1. For this aim, polarized porcine RPE cells were grown on filters at a transepithelial resistance of 451.7 ± 14.6 Ωcm^2. Cells were double-immunolabeled against different proteins in the following way: bestrophin-1 with β-catenin, Stim-1 with β-catenin, and bestrophin-1 with Stim-1 (**Fig. 24a, b** and **c**; n=3). β-catenin was used as a plasma membrane protein control. In order to quantify possible co-localization pattern between these proteins Pearson's co-localization coefficients were calculated as done by Milenkovic et *al*.2011. Thus, we found that the highest co-localization coefficient between bestrophin-1 and Stim-1 co-localizing in 44.6 ± 0.013 % (**Fig. 25**; n=10; $P \leq 0{,}001$). However, comparing bestrophin-1 and Stim-1 against β-catenin, bestrophin-1 showed higher co-localization coefficient by 29 ± 0.006 % (**Fig. 25**, n=10, $P \leq 0{,}001$) compared to that with Stim-1 with 22 ± 0.01 (**Fig. 25**; n=10; $P \leq 0{,}001$).

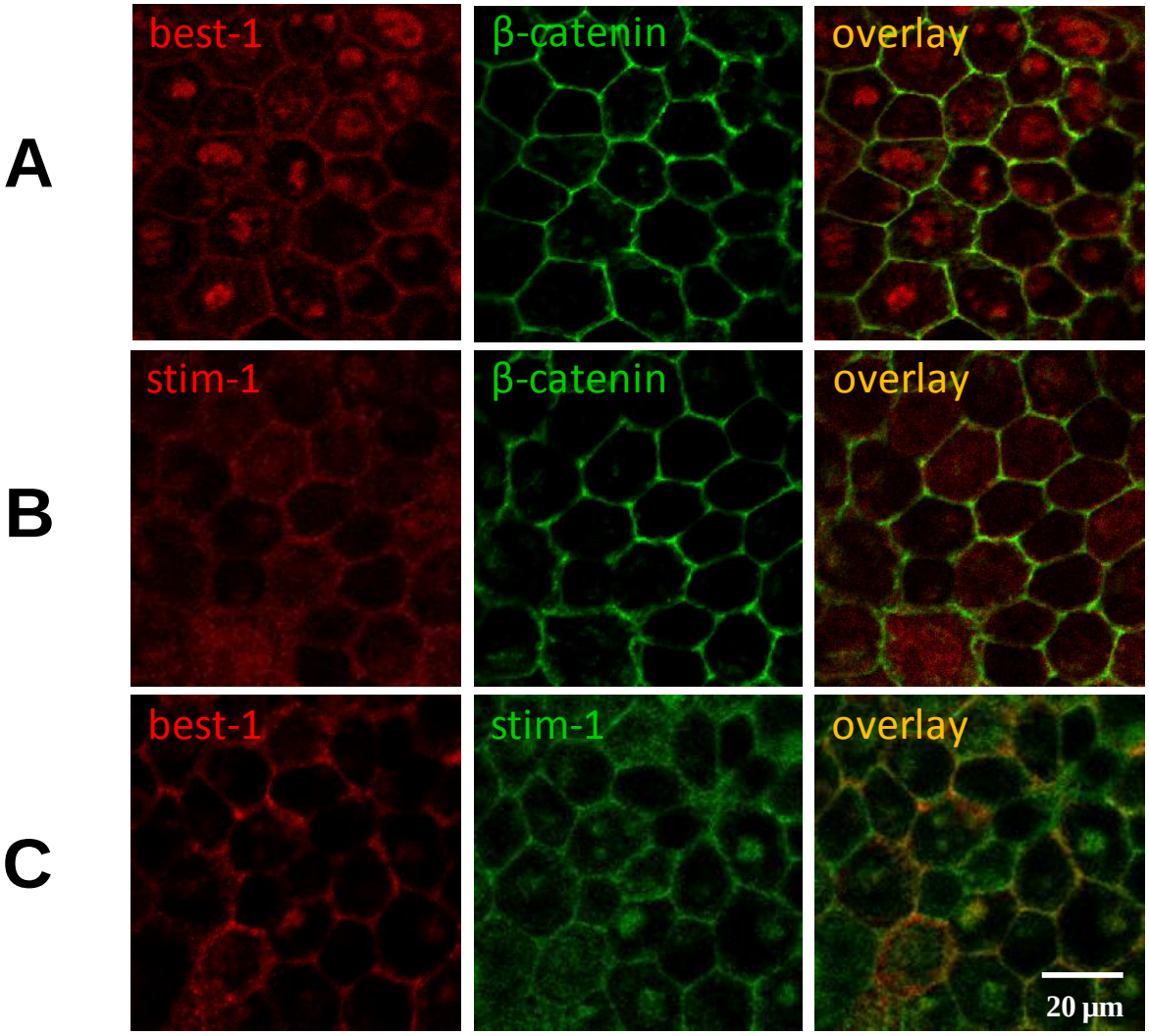

Fig. 24 Confocal microscopy of resting polarized porcine RPE cells on filter Porcine RPE cells were directly isolated from the eye and seeded on filters and used for immunocytochemistry when the transepithelial electrical resistance was above 400 Ωcm^2. **a: upper left panel:** immunostaining of bestrophin-1 (**in red**); **upper center panel**: immunostaining of β-catenin (**in green**) and **upper right panel**: overlay of both proteins. **b**: **middle left panel**: immunostaining of Stim-1 (**in red**), **middle center panel**: immunostaining of β-catenin (**in green**) and **middle right panel**: overlay of both proteins. **c: lower left panel:** immunostaining of bestrophin-1 (**in red**), **lower center panel**: immunostaining of Stim-1 (**in green**) and **lower right panel**: overlay of both proteins.

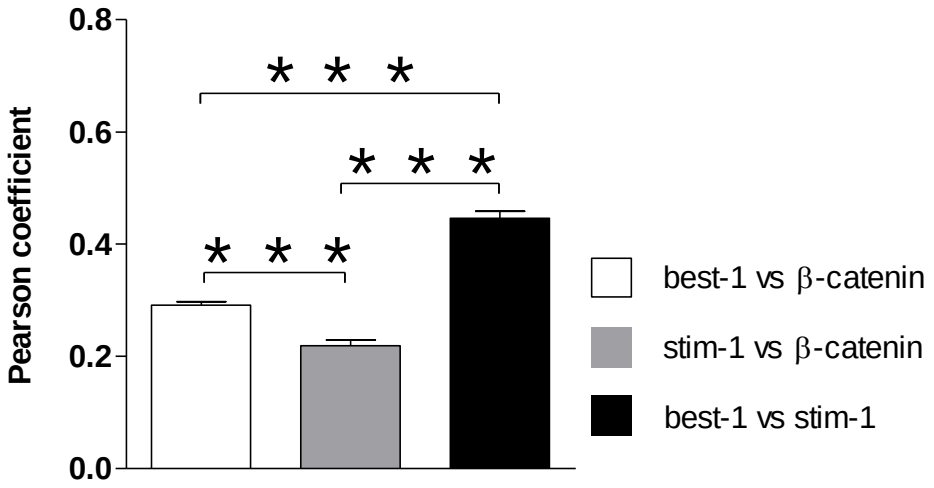

Fig. 25 Pearson's co-localization analysis between bestrophin-1, Stim-1 and β-catenin (*** $P \leq 0{,}001$; n=10 per group; these experiments were replicated 3 times).

Furthermore, since bestrophin-1 co-localized only by 29% with β-catenin, a membrane marker, and by 44% with Stim-1, an intracellular marker from ER store, it is likely a large portion of bestrophin-1 localizes in intracellular compartments as it has been suggested before [203]. In order to demonstrate whether bestrophin-1is an intracellular membrane protein or not, electron microscopy techniques were used (**Fig. 26**). Cells were grown on filter until they reached polarity. A Fluoro Nano Gold second antibody was used to correlate the signal detected in fluorescence confocal microscopy with electron microscopy. In immunohistochemical analysis in conjunction with a confocal microscope bestrophin-1 was basolaterally detected in polarized porcine RPE cells (**Fig. 26**, left and upper panel). Samples at the electron microscopy level showed that bestrophin-1 does not localize in the plasma membrane but very in the near (**Fig. 26**).

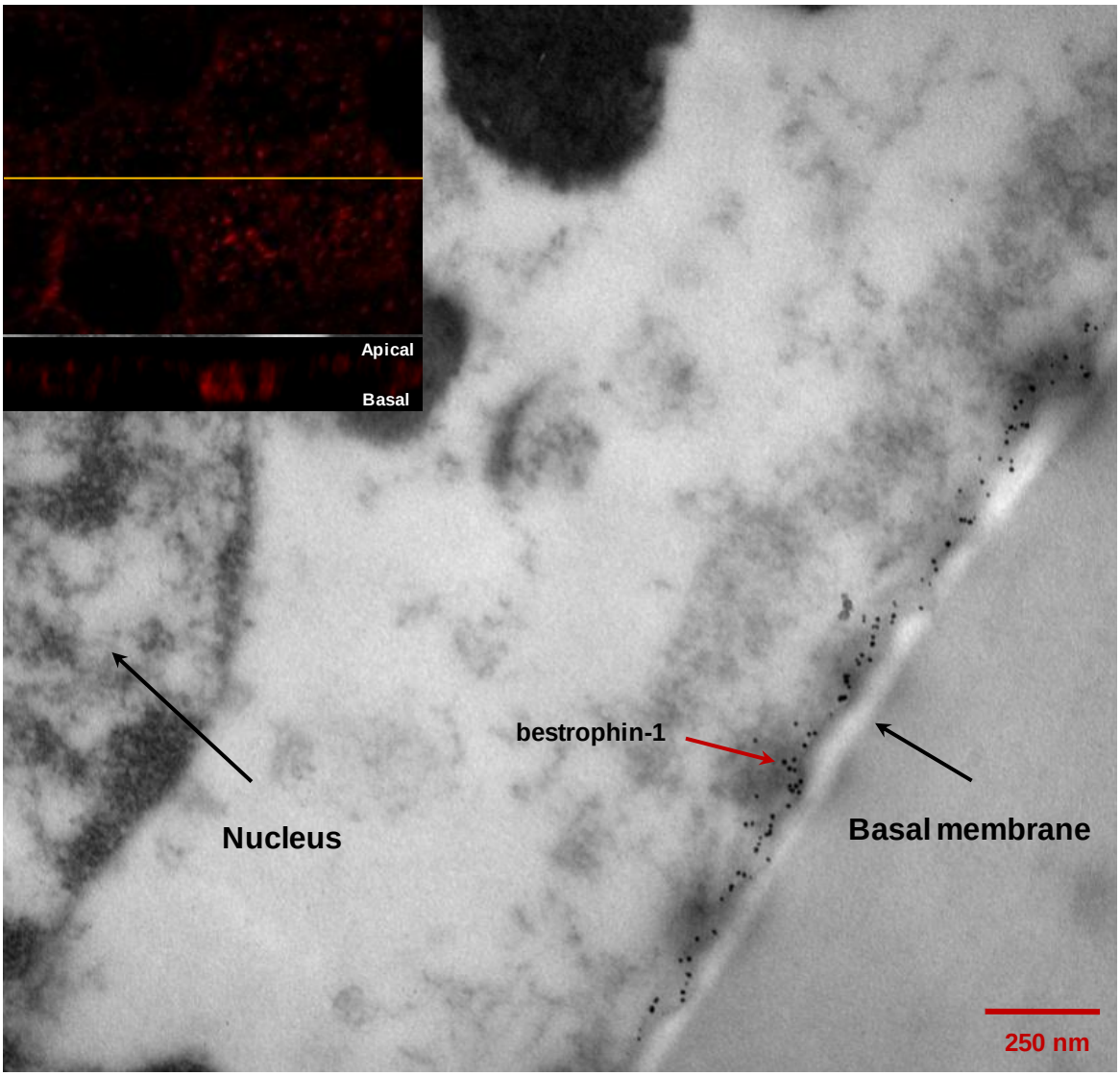

Fig. 26 Bestrophin-1 does not localize in the basal membrane of RPE cells. Polarized primary porcine RPE cells growing on filter were labeled against bestrophin-1. **left and up panel:** Using Fluor Nano Gold as a second antibody together with confocal microscopy was possible to detect bestrophin-1 localizing basolaterally in the RPE (in red). Using Fluor Nano Gold as a second antibody together with electron microscopy was possible to detect that bestrophin-1 localizes close to the basal plasma membrane but not in the plasma membrane. The right black arrow is pointing where the basal plasma membrane is and the left arrow is pointing where the nucleus is. The red arrow is pointing where bestrophin-1 is (black spots).

On the other hand, to test whether bestrophin-1 and Stim-1 have a functional interaction, we triggered SOCE activation in polarized porcine RPE cells grown on filters (**Fig .27a, b and c**). So, cells were incubated with ringer solution for 5 minutes, after cell were treated with thapsigargin (1µM) for 5 minutes and later this solution was replaced by a Ca^{2+} free solution for 1 minute. Both, the immunolabeling and the co-localization analysis were performed as described in resting polarized porcine RPE cells above. In this experiment we observed again that the highest co-localization coefficient was between bestrophin-1 and Stim-1 co-localizing in 44.5 ± 0.006 % (**Fig. 28**; n=10; $P \leq 0{,}001$). The comparison between bestrophin-1 and Stim-1 against β-catenin, exhibited that bestrophin-1 had higher co-localization coefficient by 38.2 ± 0.009 % compared with Stim-1 that showed 32 ± 0.02 (**Fig. 28**; n=10; $P \leq 0{,}001$). After analyzing resting and treated polarized cells, no differences in co-localization pattern between bestrophin-1 and stim-1were found (**Fig. 29**). However, both, bestrophin-1 and Stim-1 increased significantly their co-localization coefficient against β-catenin (**Fig. 29**; $P \leq 0{,}001$).

Over-expressing human Stim-1 and human bestrophin-1 in HEK293 cells revealed physical interaction of these proteins by means of immuno and co-immunoprecipitation experiments [203]. Therefore immunoprecipitation experiments with endogenously expressed bestrophin-1 and stim-1 were performed (**Fig. 30**). In order to show whether co-immunoprecipitation indicates physiological interaction, immunoprecipitation was performed under two different conditions: RPE cells seeded in 6-wells plate were treated with thapsigargin and Ca^{2+} free solution and non-treated cells. The experiment itself was performed in the following way: treated cells were incubated for 5 minutes in Ringer solution, later on the solution was substituted by a solution containing thapsigargin (1µM) for 5 minutes and after that time this solution was replaced by Ca^{2+} free solution for 1 minute application. We found that neither in RPE cells treated with thapsigargin nor non-treated RPE cells, bestrophin-1 and stim-1 showed co-immunoprecipitation.

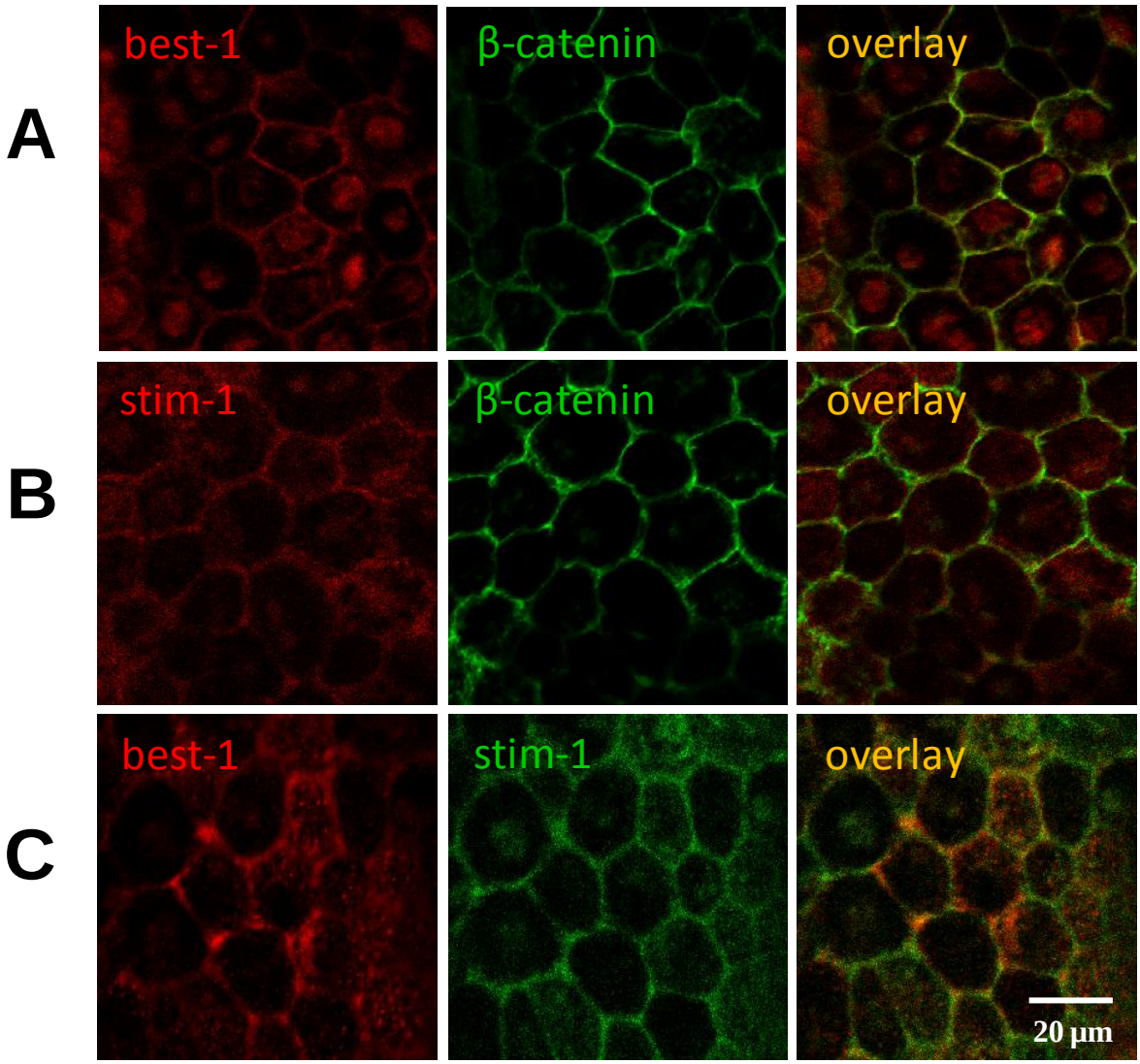

Fig. 27 Confocal microscopy of treated polarized porcine RPE cells on filter Porcine RPE cells were directly isolated from the eye and seeded on filters and used for immunocytochemistry when the transepithelial electrical resistance was above 400 Ωcm^2. **a: upper left panel:** immunostaining of bestrophin-1 (**in red**); **upper center panel**: immunostaining of β-catenin (**in green**) and **upper right panel**: overlay of both proteins. **b: middle left panel**: immunostaining of Stim-1 (**in red**), **middle center panel**: immunostaining of β-catenin (**in green**) and **middle right panel**: overlay of both proteins. **c: lower left panel:** immunostaining of bestrophin-1 (**in red**), **lower center panel**: immunostaining of Stim-1 (**in green**) and **lower right panel**: overlay of both proteins.

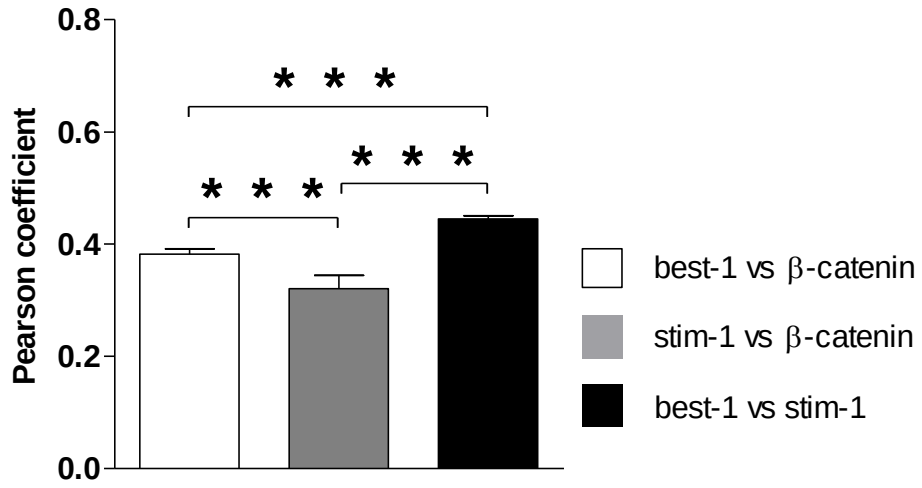

Fig. 28 Pearson's co-localization analysis between bestrophin-1, Stim-1 and β-catenin. Polarized porcine RPE cells on filters were treated with thapsigargin (1µM) for 5 minutes and after with Ca^{2+} free solution for 1 minute (*** $P \leq 0{,}001$; n=10 per group; these experiments were replicated 3 times).

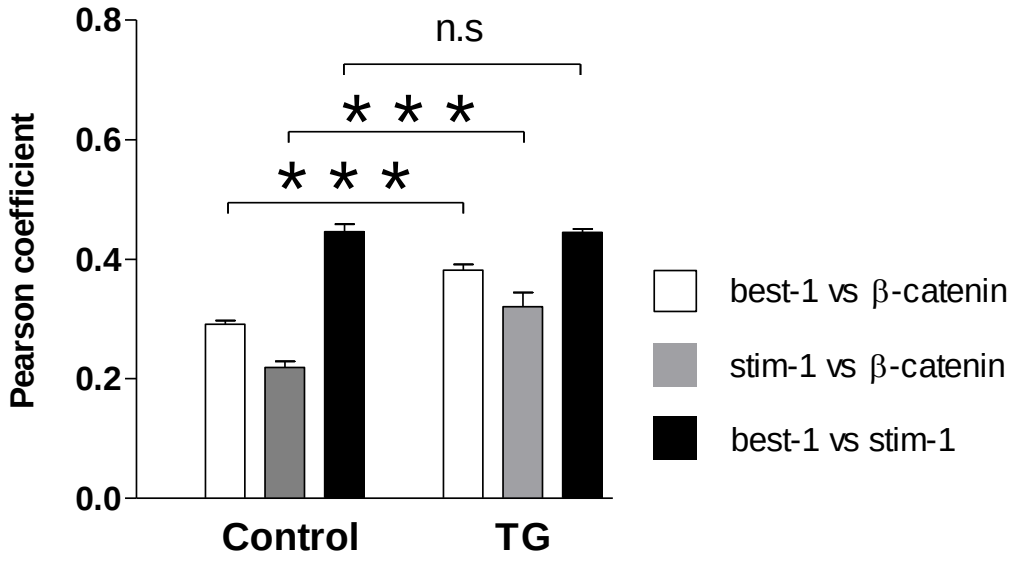

Fig. 29 Pearson´s co-localization analysis between resting and treated polarized porcine RPE cells on filter. The comparison between treated and non-treated polarized porcine RPE cells shows that bestrophin-1 and stim-1 do not change their co-localization pattern. In treated cells bestrophin-1 and stim-1 increase significantly their co-localization coefficients against β-catenin compared to resting cells.

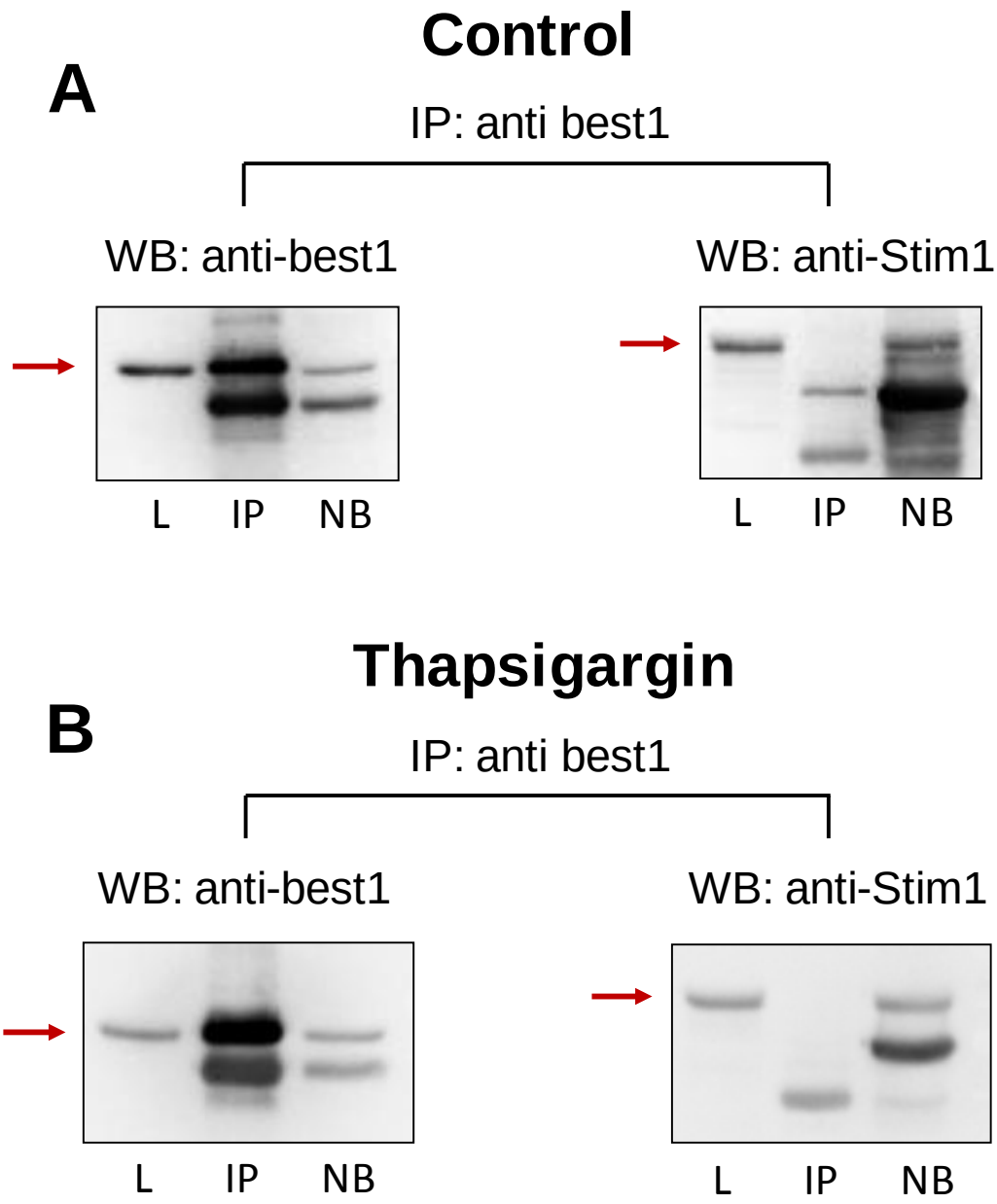

Fig. 30 Immunoprecipitation and co-immunoprecipitation of bestrophin-1 and Stim-1 respectively in treated and non-treated porcine RPE cells Porcine RPE cells were divided in two experiment groups (treated and non-treated) in the following way: treated cells were washed for 5 minutes with Ringer solution, later it was applied thapsigargin (1µM) for 5 minutes and after that it was added Ca^{2+} free solution for 1 minute. Non-treated cells were only bathed by a Ringer solution the same time in parallel to the treated cells**. a**: Non-treated cells showed in resting conditions no co-immunoprecipitation between bestrophin-1 and Stim-1 proteins. **b**: Treated cells showed during SOCE activation state no functional interaction bestrophin-1 and Stim-1 proteins.

5 Discussion

5.1 Bestrophin-1 mouse models

5.1.1 Light damage paradigm in bestrophin-1 KI$^{+/Y227N}$ mouse

In the present study the strategy of the experiment was to find light-induced damage at threshold levels. This means we aimed the susceptibility for damage of the retina. So first we investigated this idea in wild type Black 6 mice and later in bestrophin-1 KI$^{+/Y227N}$ animals. In control experiments with wild type black 6 mice it was found a tiny reduction of the outer nuclear layer (ONL) in those mice exposed to light. Although this reduction was not significant we wanted to explore further the same paradigm in the bestrophin-1 KI$^{+/Y227N}$ animals. Here it was likely in those mice exposed to light the thickness of ONL showed a tendency to be thicker compared to non-light exposed animals.

The light damage paradigm is a well established method which revealed the role of many proteins involve in retina degeneration [204-206]. In combination with this, several animal models have been developed to show possible mechanisms of degeneration [204-206]. In many mice models where the light-mediated retina damage has been studied some of them have shown a clear phenotype. This is the case of RPE65-deficient mice which were protected against light exposure [207]. In this study, as a conclusion, we did not find any clear light-induced damage in these groups of animals under these experimental conditions.

5.1.2 Calcium signaling in bestrophin-1 KO mouse

In our study comparing cultured RPE cells from bestrophin-1$^{-/-}$ mice against RPE cells from wild type animals we did not find any function of endogenously expressed bestrophin-1. We observed that RPE cells from bestrophin-1$^{-/-}$ mice showed significant higher levels of resting Ca^{2+} compared with that in wild type RPE cells. This result agrees with a study done with another bestrophin-1$^{-/-}$ mouse model in

which RPE cells from bestrophin-1 deficient mice showed also higher levels of resting Ca^{2+} compared with wild type RPE cells [180].

On the other hand, studying the mechanism of ATP-dependent Ca^{2+} signaling we found that in both, RPE cells from wild type and from bestrophin-$1^{-/-}$ mice the increase of intracellular Ca^{2+} was randomly in response and amplitude. On the contrary, in the other study named above, application of ATP resulted in a fast transient rise of intracellular Ca^{2+} in both RPE cells from wild type and bestrophin-$1^{-/-}$ mice. Therefore, accordingly with our results, using this bestrophin-1 deficient mouse model, we could not investigate further the involvement of endogenously expressed bestrophin-1 in calcium signaling.

5.2 Porcine RPE cell model

I developed a short-time cell culture model of porcine RPE cells which is useful to study the function of endogenously expressed bestrophin-1 in the RPE using siRNA technqiues. Here I found the following i) primary porcine RPE cells confluent seeded showed a longer expression of bestrophin-1 compared to non-confluent seeded cells and ii) primary porcine confluent seeded cells treated with serum at 5% compared to those ones treated with serum at 20% showed a longer expression of bestrophin-1.

As a first step developing this porcine RPE cell culture model, I hypothesized that cells seeded at a high density could maintain a longer the bestrophin-1 expression compared to those cells seeded at low density. Indeed, this hypothesis was proven in this study by mean of qPCR and western blot when non-confluent seeded cells showed a faster down regulation of bestrophin-1 protein compared with confluent seeded cells in the range from 24 hours until 72 hours.

Fundamental feature of all epithelial cells is their apical to basal polarization. The presence of tight junctions not only gives to the cell sheet a selective barrier function

but also divides chemically and structurally the apical from the basolateral side. Epithelial cells are also attached by other cell-cell with tight junctions to maintain the structural integrity of this tissue. RPE cells as a typical epithelia share all these features above named [8].

In cell culture, there are many factors that can change the biology of the RPE cells. As RPE monolayer cells are closely associated *in vivo* is expectable to find that they tend to survive better *in vitro* as clusters or sheet of cells than alone. This is due partly to the cell-cell contact which supports the cell differentiation in vitro conditions. When cells are highly densely seeded they can re-establish easier the morphology because no proliferation is needed. This means that cells can be semi-polarized and keep working as a monolayer. On the other hand, the cell-cell contacts as gap junctions, it is likely allow the transfer of second-messenger cyclic AMP between adjacent cells inhibiting proliferative process. In contrast, single cells immediately change from differentiated cells to flatted proliferative cells losing many properties as a RPE cell.

On the other hand, in the second part of this study, I hypothesized that the reduction of serum in medium could make slower proliferation processes and thus keeps longer the expression of bestrophin-1 protein in porcine RPE cells. Indeed, the results reached in this study supported strongly this hypothesis when cultured porcine RPE cells treated with serum at 5% show a longer expression of bestrophin-1 compared with those ones treated with serum at 20%.

RPE cells are known to produce and to secret a variety of growth factors as fibroblast growth factor (FBF), transforming growth factors-β (TGF-β), insulin -like growth factor–I (IGF-I), pigment epithelium- derived factor (PEDF), etc [2]. There are some studies which have shown the effect of growth factors on RPE cells [208-210]. In one of these studies it was demonstrated that epidermal growth factor stimulates proliferation of human RPE cells in vitro. In other study also was observed stimulation of proliferation after application of different growth factors together. The fetal calf

serum (FCS) which was the one I used in this study it is known to have a mixture of different growth factors. Therefore, it is expectable to find in those cells treated with 20% serum in medium a higher rate of proliferation compared to those ones treated with only 5%.

5.3 Store-operated calcium entry (SOCE) in porcine RPE cells.

5.3.1 Orai-1 is involved in SOCE activation in porcine RPE cells

The present work reveals the presence of store-operated calcium entry in porcine RPE cells mediated by Orai-1 protein and Stim-1 protein activation. This conclusion is based on the following findings i) porcine RPE cells expressed all homologous ORAI and STIM transcripts and Orai-1 and Stim-1 proteins; ii) treatment of the porcine RPE cells with Icrac modulators or a siRNA against Orai-1 protein decreased remarkable SOCE activation.

The finding that primary porcine RPE cells express the molecular basis of SOCE with all homologous (ORAI1-3 and STIM1-2) agrees with a previous study done in freshly isolated human RPE cells and ARPE-19 cell line [153]. In that study, in both, fresh isolated human RPE and ARPE-19 cell line also were detected all members of the family of Orai and Stim. In addition, in our study, we detected for the first time in RPE cells the proteins Orai-1 and Stim-1 by mean of western blot. The other members of the STIM or ORAI family could not be detect due to the lack of reliable antibodies for porcine species.

In porcine RPE cells, using the established protocol for SOCE activation described in many studies which involves the depletion of ER store, a remarkable increase in intracellular $Ca^{2+}$was induced. So, porcine RPE cells show SOCE response. This result was also observed in freshly isolated human RPE cells and ARPE-19 cell line in which the application of thapsigargin in free Ca^{2+} solution and the re-addition of extracellular Ca^{2+} led to an increased in intracellular Ca^{2+} [153].

In order to identify mechanisms involved in SOCE we performed on one hand a pharmacological study to discriminate whether Orai or TRP channels were part of this mechanism and on the other hand by specific targeting of Orai-1 protein using an siRNA (Orai-1siRNA).

So we demonstrated the Orai-1 activation in porcine RPE cells by pharmacological criteria. 2-APB is known to block Orai channels and TRP channels in different cell types including ARPE-19 at a high concentration (75µM). Application of 75 µM 2-APB almost completely blocked the SOCE activation in the porcine RPE cells. In order to discriminate between TRP and Orai channels we used 2-APB at low concentration (5µM) which is known to potentiate Orai-1 channel activation in many cells including ARPE-19 cells [138, 153, 202]. In order to detect the enhancing effect of 2-APB we used SOCE activation paradigm leading to less stronger activation of SOCE by not using thapsigargin. Since RPE cells display a strong resting Ca^{2+}-conductance, probably through TRPC channels [124], store-depletion can be achieved simply by exposure to extracellular Ca^{2+}-free conditions. Using this maneuver, we could confirm the enhancing effect of 2-APB indicating a predominant role Orai-1 in SOCE activation. Regarding the possible involvement of TRP channels in SOCE activation we found negligible contribution because the blocker of TRP and voltage-dependent channels SKF 96365 showed no effect.

The contribution of Orai-1 was confirmed using Orai-1siRNA. In our hands the Orai-1siRNA led to strongly decreased levels of Orai-1 protein and strong inhibition of the SOCE amplitude which underlines that Orai-1 predominantly mediates SOCE. This finding agrees with the study done in freshly isolated human RPE cells and ARPE-19 which concluded that SOCE was mediated by Orai-1 or/and Orai-2 [153].

In addition, we found that in polarized porcine RPE cells treated with thapsigargin and free-Ca^{2+} solution the co-localization coefficient between Stim-1 and β-catenin, a

membrane market protein increased significantly compared with resting polarized porcine RPE cells. This result could mean that Stim-1 approached to the plasma membrane after the depletion of the ER store. This feature of Stim-1 has been already described in other cells [145, 148] but not in the RPE. Stim-1 is known to be activated by depletion of ER store and its subsequent translocation in turn leads to the activation of Orai-1 by directly interaction. With our result we could speculate that this approach of Stim-1 to the plasma membrane could involve the activation of Orai-1 protein after the depletion of the ER store, but additional experiments like for example immune and co-immunoprecipitation most be done in order to confirm this mechanism here.

SOCE has been observed in a variety of non-excitable and some excitable cells including lymphocytes, pancreatic acinar, vascular endothelial, neurons and smooth muscle cells [137, 138, 211, 212]. The activation of SOCE through Orai channels can induce both, short-term changes in the cell such as: secretion, enzyme activation, maintainance of cytoplasmic Ca^{2+} oscillation and safeguarding Ca^{2+} content in the ER and also long-term changes as gene expression. Although, very few it is known about the physiological function of SOCE in the RPE, it is likely it could play an important role in these cells. In the RPE many functions are controlled by increases in intracellular Ca^{2+} [111]. The daily phagocytosis of photoreceptor outer segments is one of the most important processes which take place in the RPE and it is depending on increases of intracellular Ca^{2+} by the second-messenger $InsP_3$. In addition, the stimulation of RPE by ATP or growth factors leads to increases in intracellular Ca^{2+} and this in turn induces secretion of other growth factors [127, 130]. So, Orai-1 provides also a pathway to refill the ER Ca^{2+} store after activation of IP_3 and ryanodine receptors. Furthermore, since $InsP_3$-dependent rises in intracellular Ca^{2+} were found to induce sustain activation of Ca^{2+}-dependent Cl channels [213, 214], can be that Orai-1 supports this sustain activation and thus the transepithelial transport of water by the RPE.

So far in this study we have found that porcine RPE cells show all homologous ORAI and STIM genes. Both, the pharmacological study together with the further knock-

down of Orai-1 protein demonstrate that the SOCE activation found in porcine RPE cells is mediated by Orai-1 protein. This predominant involvement of Orai-1 in SOCE has been described in different cell types as well [140, 141, 215-217]. Moreover, the expression of the other members of Orai family has been also found in many cell types [218, 219]. Over-expressing Orai-2 with Stim-1 and Orai-3 with Stim-1 in HEK293, I_{crac} currents have been identified [220]. In HEK293 cells, it is likely Orai-2 and Orai-3 can partly replace Orai-1 in mediating SOCE [220]. In porcine RPE cells we did not find any replacement function in cells treated with Orai-1siRNA. On the other hand, we found the expression of STIM2 transcript but not Stim-2 protein in porcine RPE cells. Regarding Stim-2 function, it has been described to have higher affinity for Ca^{2+} than Stim-1, and therefore requires less depletion of the ER store to activate Orai channels [221]. Thus, it is likely Stim-2 has a homeostasis role that it ensures that ER Ca^{2+} levels are maintained [221].

5.4 Bestrophin-1 influences SOCE pathway in porcine RPE cells

I used a 48 hours porcine RPE cell culture model which appeared to be close to the *in vivo* situation. This model showed high levels of endogenous bestrophin-1 expression which could be influenced by transfection with siRNA (best-1siRNA). The reduction of bestrophin-1 protein in those cells treated with best-1siRNA it was detected by western-blot analysis which also confirms the specifity of the anti-bestrophin-1 antibody used in this study.

In order to analyze the possible involvement of bestrophin-1 in SOCE mechanism we performed siRNA against bestrophin-1 protein. First of all, we found higher levels of resting $[Ca^{2+}]_I$ in cells with reduced bestrophin-1 expression compared with that in corresponding control cells .A low level of resting $[Ca^{2+}]_I$ is normally achieved by the activity of either Ca^{2+}-ATPases and exchangers in the plasma membrane which transport Ca^{2+} out of the cells or by Ca^{2+}-ATPases in the ER (SERCA) which take up Ca^{2+} into cytosolic Ca^{2+} stores. Bestrophin-1 was described to function as a Cl channel. In two independent publications a cytosolic function of bestrophin-1 was suggested [180, 203]. Here, Barro-Soria et *al*. suggested that bestrophin-1 function

as a Cl channel in the ER which transports Cl^- as counter-ion for the Ca^{2+} transport into Ca^{2+} stores [203]. Thus the higher levels of resting $[Ca^{2+}]_I$ in cells with reduced bestrophin-1 expression can be explained by a less efficient Ca^{2+} uptake into cytosolic Ca^{2+} stores. This observation was also supported in a recent study in which we showed that in cultured RPE cells from *Best1*$^{-/-}$ mice the level of resting Ca^{2+} was also higher compared with cells from *Best1*$^{+/+}$ animals [180]. Indeed, in our study also RPE cells from bestrophin-1 -/- showed higher level of resting Ca^{2+} compared to the wild type.

By comparing the levels of SOCE amplitude between best-1siRNA treated cells and control cells, we found that cells with reduced bestrophin-1 expression showed a large reduction of SOCE Ca^{2+} influx. This is not due to reduced expression levels of Orai-1 or Stim-1 in best-1siRNA treated cells. Another explanation could also be a reduction of the amount of Ca^{2+} in cytosolic Ca^{2+} stores due to the absence of bestrophin-1. Indeed, we found that the amplitude of Ca^{2+} release from ER store by thapsigargin was remarkable reduced in those cells treated with best-1siRNA. In the current model for the SOCE mechanism, Orai-1 channel in the plasma membrane is activated by interaction with Stim-1 in the ER Ca^{2+}-store [151]. Stim-1 becomes activated by release of Ca^{2+} from the Ca^{2+} store into the cytoplasm. Activated Stim-1 undergoes a translocation to the cell membrane by a so far unknown mechanism and can bind to Orai at the crac motif of Orai leading to its activation and Ca^{2+} influx into the cell [145]. Therefore, it is likely that in RPE cells treated with best-1siRNA, less Ca^{2+} is released from the stores and less Stim-1 can translocate and in subsequence also less Orai-1 channels can be activated. To prove this hypothesis, we measured the amount of Ca^{2+} which can be released from cytosolic Ca^{2+} stores in response to the treatment by thapsigargin under extracellular Ca^{2+} conditions. As a result we found that cells treated with best-1siRNA showed a strongly reduced amount of Ca^{2+} released from stores compared to that from the corresponding control cells: cells treated with scrambled siRNA or cells treated with Orai-1siRNA. Thus the reduction of SOCE amplitude is due to a reduction of the amount of Ca^{2+} released from the ER. This is supported by other studies which found that bestrophin-1 modulates the release of calcium from ER store after application of thapsigargin or CPA [181]. For

example in HEK cells over-expressing human bestrophin-1, application of CPA trigged a released of Ca^{2+} from ER store faster than in those cells which did not over-express human bestrophin-1 [181]. In addition, we showed in a previous study that in RPE cells from *Best1*$^{-/-}$ mice ATP-induced Ca^{2+} signals were generated by a the use of different Ca^{2+} stores compared to *Best1*$^{+/+}$ animals [180].

The observation that bestrophin-1 helps to accumulate Ca^{2+} into ER Ca^{2+} stores by its Cl^- channel function implies that the physiological localization of bestrophin-1 is in cytosolic membranes, in close proximity to the cell membrane. To test this, we used pixel-analysis in immunocytochemistry against bestrophin-1, against Stim-1 as a marker for ER Ca^{2+} stores and β-catenin as a marker for plasma membrane localization in polarized porcine RPE cells grown on filter. We found that bestrophin-1 co-localized very little with β-catenin but much better with Stim-1 whereas β-catenin and Stim-1 showed less co-localization. This points out that bestrophin-1 has a prevalent cytosolic localization when endogenously expressed. Indeed, we confirmed this result when using electron microscopy technique, bestrophin-1 protein was detected close to the plasma membrane but not in the plasma membrane. This result supports the data from a recent study, also in fresh porcine RPE cells, in which after differential centrifugation, bestrophin-1 co-precipitated with ClC-3, a native ER Cl^- channel [180].

Although the effect of bestrophin-1 reduction onto SOCE activation seems to rely on the amount of Ca^{2+} released from ER calcium store it could also be that bestrophin-1 interacts with Stim-1. An interaction between bestrophin-1 and Stim-1 was suggested by a study which analyzed the contribution of bestrophin-1 for Ca^{2+}-signaling in lung epithelial airway cells [203]. However, although bestrophin-1 and Stim-1 showed a similar pattern of distribution inside the cell they co-localized only by 45 %. In order to test whether there is a Stim-1/bestrophin-1 interaction as endogenously expressed proteins or not we performed two experiments. The first one was the stimulation of SOCE activation in polarized porcine RPE cells and the analysis was done as described above for cytosolic localization of bestrophin-1 and stim-1. For the second experiment we made immunoprecipitation of bestrophin-1 and analyzed for co-

immunoprecipitation with Stim-1. In this one, in order to test whether co-immunoprecipitation reflects functional interaction between these two proteins, this experiment was divided in two groups: cells which were treated following the paradigm for SOCE activation and non-treated cells. In the first experiment after triggering SOCE activation the co-efficient analysis showed the same result found in polarized resting cells, so bestrophin-1 and stim-1 co-localized by 45%. In contrast, as we said before in this experiment we were able to detect the approach of stim-1 to the plasma membrane by the increasing of co-localization against β-catenin from 22% to 32 %. Surprisingly the same behavior was also found in bestrophin-1 when increased its co-localization coefficient against β-catenin from 29% to 38%.This observation opens a new gate to understand future molecular mechanisms of bestrophin-1 and interaction partner as L-type calcium channels. Since stim-1 can translocate to areas close to the plasma membrane and interact with orai channels in the plasma membrane, bestrophin-1 could do similar mechanism modulating other interactions. On the other, neither resting cells nor treated cells, no interaction it was found between endogenously expressed bestrophin-1 and Stim-1 proteins in porcine RPE cells.

In this study we have shown that with the reduction of bestrophin-1, the amount of Ca^{2+} released from ER is strongly reduced and thus the subsequent reduction of the SOCE activation. This result means indeed that bestrophin-1 as an intracellular Cl channel can regulate different processes Ca^{2+}-dependent from Ca^{2+} stores in the RPE. Thus, bestrophin-1 works as a counter-ion for Ca^{2+} uptake into ER Ca^{2+} stores. This function of bestrophin-1 not only involves the recruitment of Ca^{2+} into cytosolic Ca^{2+} stores but also indirectly, the release of Ca^{2+} in the cytosol. Increase in cytosolic free Ca^{2+} modulates many cellular processes in the RPE such as secretion, gene expression, phagocytosis or transepithelial transport [111]. Mutations of bestrophin-1 lead to Best's vitelliforme macular dystrophy [157, 158] an autosomal dominant inherited form of macular degeneration associated with a strong lipofuscin accumulation in the RPE [157, 158]. So, it might be possible that bestrophin-1 could play a role in the Ca^{2+}-dependent regulation of the phagocytosis process in the RPE. A reduction or loss of bestrophin-1 in RPE cells would lead to reduced SOCE

activation and therefore to a change in the regulation of phagocytosis. Since, the photoreceptor outer segment binding leads to an increase in intracellular Ca^{2+} generated by the second messenger IP_3 , a proper refilling and release of Ca^{2+} from ER store is needed. This hypothesis could be supported by the fact that human Best patients show a strong accumulation of lipofuscin in the RPE. In addition, bestrophin-1 KI $^{+/W93C}$ and bestrophin-1 KI $^{W93C/W93C}$ mice also show higher accumulation of lipofuscin compared with wild type animals.

Mutations in the BEST1 gene lead to a loss of function of bestrophin-1. The reason is that mutant bestrophin-1 does not properly traffic into the periphery of the cell [192]. This is also supported by a study done in dogs carrying mutations in BEST1 gene. Here the author showed *in vivo*, mislocalization of bestrophin-1 protein [222]. In addition, in histological analysis of the retina of Best patients indicated a loss of peripheral localization of mutant bestrophin-1 [223]. The periphery of the cell would be the area of the ER Ca^{2+} stores which involves SOCE. Thus we should expect a reduced activation of SOCE in cells which express mutant bestrophin-1 as well. So following this idea it is likely that mutant bestrophin-1 also affect SOCE in human patients. Therefore our finding opens a new route to understand how mutant bestrophin-1 can modulate the calcium homeostasis in RPE.

6 References

1. Lamb, T.D., S.P. Collin, and E.N. Pugh, Jr., *Evolution of the vertebrate eye: opsins, photoreceptors, retina and eye cup.* Nat Rev Neurosci, 2007. **8**(12): p. 960-76.
2. Strauss, O., *The retinal pigment epithelium in visual function.* Physiol Rev, 2005. **85**(3): p. 845-81.
3. Steinberg, R.H., *Interactions between the retinal pigment epithelium and the neural retina.* Doc Ophthalmol, 1985. **60**(4): p. 327-46.
4. Sparrow, J.R., D. Hicks, and C.P. Hamel, *The retinal pigment epithelium in health and disease.* Curr Mol Med. **10**(9): p. 802-23.
5. Bok, D., *The retinal pigment epithelium: a versatile partner in vision.* J Cell Sci Suppl, 1993. **17**: p. 189-95.
6. Rizzolo, L.J., *Polarity and the development of the outer blood-retinal barrier.* Histol Histopathol, 1997. **12**(4): p. 1057-67.
7. Marmorstein, A.D., et al., *Morphogenesis of the retinal pigment epithelium: toward understanding retinal degenerative diseases.* Ann N Y Acad Sci, 1998. **857**: p. 1-12.
8. Boulton, M. and P. Dayhaw-Barker, *The role of the retinal pigment epithelium: topographical variation and ageing changes.* Eye (Lond), 2001. **15**(Pt 3): p. 384-9.
9. Chaitin, M.H. and M.O. Hall, *Defective ingestion of rod outer segments by cultured dystrophic rat pigment epithelial cells.* Invest Ophthalmol Vis Sci, 1983. **24**(7): p. 812-20.
10. Delori, F.C., et al., *Autofluorescence distribution associated with drusen in age-related macular degeneration.* Invest Ophthalmol Vis Sci, 2000. **41**(2): p. 496-504.
11. Duncan, J.L., et al., *An RCS-like retinal dystrophy phenotype in mer knockout mice.* Invest Ophthalmol Vis Sci, 2003. **44**(2): p. 826-38.
12. Duncan, J.L., et al., *Inherited retinal dystrophy in Mer knockout mice.* Adv Exp Med Biol, 2003. **533**: p. 165-72.
13. Gollapalli, D.R., P. Maiti, and R.R. Rando, *RPE65 operates in the vertebrate visual cycle by stereospecifically binding all-trans-retinyl esters.* Biochemistry, 2003. **42**(40): p. 11824-30.
14. Gollapalli, D.R. and R.R. Rando, *All-trans-retinyl esters are the substrates for isomerization in the vertebrate visual cycle.* Biochemistry, 2003. **42**(19): p. 5809-18.
15. Gu, S.M., et al., *Mutations in RPE65 cause autosomal recessive childhood-onset severe retinal dystrophy.* Nat Genet, 1997. **17**(2): p. 194-7.
16. Rizzolo, L.J., *Development and role of tight junctions in the retinal pigment epithelium.* Int Rev Cytol, 2007. **258**: p. 195-234.
17. Cunha-Vaz, J.G., *The blood-retinal barriers.* Doc Ophthalmol, 1976. **41**(2): p. 287-327.
18. Ishida, K., et al., *Participation of pigment epithelium in ocular immune privilege. 3. Epithelia cultured from iris, ciliary body, and retina suppress T-cell*

activation by partially non-overlapping mechanisms. Ocul Immunol Inflamm, 2003. **11**(2): p. 91-105.
19. Finnemann, S.C., et al., *Phagocytosis of rod outer segments by retinal pigment epithelial cells requires alpha(v)beta5 integrin for binding but not for internalization.* Proc Natl Acad Sci U S A, 1997. **94**(24): p. 12932-7.
20. Dornonville de la Cour, M., *Ion transport in the retinal pigment epithelium. A study with double barrelled ion-selective microelectrodes.* Acta Ophthalmol Suppl, 1993(209): p. 1-32.
21. Alm, A. and A. Bill, *The oxygen supply to the retina. I. Effects of changes in intraocular and arterial blood pressures, and in arterial P O2 and P CO2 on the oxygen tension in the vitreous body of the cat.* Acta Physiol Scand, 1972. **84**(2): p. 261-74.
22. Alm, A. and A. Bill, *The oxygen supply to the retina. II. Effects of high intraocular pressure and of increased arterial carbon dioxide tension on uveal and retinal blood flow in cats. A study with radioactively labelled microspheres including flow determinations in brain and some other tissues.* Acta Physiol Scand, 1972. **84**(3): p. 306-19.
23. Alm, A. and A. Bill, *Blood flow and oxygen extraction in the cat uvea at normal and high intraocular pressures.* Acta Physiol Scand, 1970. **80**(1): p. 19-28.
24. Miceli, M.V., M.R. Liles, and D.A. Newsome, *Evaluation of oxidative processes in human pigment epithelial cells associated with retinal outer segment phagocytosis.* Exp Cell Res, 1994. **214**(1): p. 242-9.
25. Beatty, S., et al., *Macular pigment and age related macular degeneration.* Br J Ophthalmol, 1999. **83**(7): p. 867-77.
26. Boulton, M., *The role of melanin in the RPE. in: The retinal pigment epithelium, edited by Marmor MF and Wolfensberger. Oxford, UK: Oxford Univ. .* 1998: p. 65-68.
27. Handelman, G.J., et al., *Carotenoids in the human macula and whole retina.* Invest Ophthalmol Vis Sci, 1988. **29**(6): p. 850-5.
28. Bone, R.A., et al., *Distribution of lutein and zeaxanthin stereoisomers in the human retina.* Exp Eye Res, 1997. **64**(2): p. 211-8.
29. Ben-Shabat, S., et al., *Biosynthetic studies of A2E, a major fluorophore of retinal pigment epithelial lipofuscin.* J Biol Chem, 2002. **277**(9): p. 7183-90.
30. Ben-Shabat, S., et al., *Fluorescent pigments of the retinal pigment epithelium and age-related macular degeneration.* Bioorg Med Chem Lett, 2001. **11**(12): p. 1533-40.
31. Boulton, M., *Ageing of the retinal pigment epithelium. In: Progress in retinal research, edited by Osbourne NN and Chader GJ. New York: pergamon.* 1991: p. 125-151.
32. Newsome, D.A., *Antioxidants in the retinal pigment epithelium.* Prog Retin Eye Res, 1994. **13**: p. 101-123.
33. Beatty, S., et al., *The role of oxidative stress in the pathogenesis of age-related macular degeneration.* Surv Ophthalmol, 2000. **45**(2): p. 115-34.
34. Arking, R., *Biology of ageing.* 1998.
35. Hughes, B.A., R.P. Gallemore, and S.S. Miller, *Transport mechanism in the retinal pigment epithelium. In: The retinal pigment epithelium, edited by Marmor MF and Wolfensbenger TJ. New York: Oxford Univ. .* 1998: p. 103-134.

36. Gallemore, R.P., et al., *Basolateral membrane Cl- and K+ conductances of the dark-adapted chick retinal pigment epithelium.* J Neurophysiol, 1993. **70**(4): p. 1656-68.
37. Carlson, A. and D. Bok, *Polarity of 11-cis retinal release from cultured retinal pigment epithelium.* Invest Ophthalmol Vis Sci, 1999. **40**(2): p. 533-7.
38. Sugasawa, K., et al., *Immunocytochemical analyses of distributions of Na, K-ATPase and GLUT1, insulin and transferrin receptors in the developing retinal pigment epithelial cells.* Cell Struct Funct, 1994. **19**(1): p. 21-8.
39. Bergersen, L., et al., *Cellular and subcellular expression of monocarboxylate transporters in the pigment epithelium and retina of the rat.* Neuroscience, 1999. **90**(1): p. 319-31.
40. Ban, Y. and L.J. Rizzolo, *Regulation of glucose transporters during development of the retinal pigment epithelium.* Brain Res Dev Brain Res, 2000. **121**(1): p. 89-95.
41. Stamer, W.D., et al., *Aquaporin-1 channels in human retinal pigment epithelium: role in transepithelial water movement.* Invest Ophthalmol Vis Sci, 2003. **44**(6): p. 2803-8.
42. Hamann, S., et al., *Aquaporins in complex tissues: distribution of aquaporins 1-5 in human and rat eye.* Am J Physiol, 1998. **274**(5 Pt 1): p. C1332-45.
43. Gundersen, D., J. Orlowski, and E. Rodriguez-Boulan, *Apical polarity of Na,K-ATPase in retinal pigment epithelium is linked to a reversal of the ankyrin-fodrin submembrane cytoskeleton.* J Cell Biol, 1991. **112**(5): p. 863-72.
44. Marmorstein, A.D., *The polarity of the retinal pigment epithelium.* Traffic, 2001. **2**(12): p. 867-72.
45. Marmorstein, A.D., et al., *Apical polarity of N-CAM and EMMPRIN in retinal pigment epithelium resulting from suppression of basolateral signal recognition.* J Cell Biol, 1998. **142**(3): p. 697-710.
46. Ostwald, T.J. and R.H. Steinberg, *Localization of frog retinal pigment epithelium Na+-K+ ATPase.* Exp Eye Res, 1980. **31**(3): p. 351-60.
47. Adorante, J.S. and S.S. Miller, *Potassium-dependent volume regulation in retinal pigment epithelium is mediated by Na,K,Cl cotransport.* J Gen Physiol, 1990. **96**(6): p. 1153-76.
48. Hamann, S., *Molecular mechanisms of water transport in the eye.* Int Rev Cytol, 2002. **215**: p. 395-431.
49. Hughes, B.A., et al., *Apical electrogenic NaHCO3 cotransport. A mechanism for HCO3 absorption across the retinal pigment epithelium.* J Gen Physiol, 1989. **94**(1): p. 125-50.
50. Joseph, D.P. and S.S. Miller, *Apical and basal membrane ion transport mechanisms in bovine retinal pigment epithelium.* J Physiol, 1991. **435**: p. 439-63.
51. Keller, S.K., et al., *Regulation of intracellular pH in cultured bovine retinal pigment epithelial cells.* Pflugers Arch, 1988. **411**(1): p. 47-52.
52. Kennedy, B.G., *Na(+)-K(4)-Cl- cotransport in cultured cells derived from human retinal pigment epithelium.* Am J Physiol, 1990. **259**(1 Pt 1): p. C29-34.
53. La Cour, M., *Cl- transport in frog retinal pigment epithelium.* Exp Eye Res, 1992. **54**(6): p. 921-31.
54. Miller, S.S. and J.L. Edelman, *Active ion transport pathways in the bovine retinal pigment epithelium.* J Physiol, 1990. **424**: p. 283-300.
55. Blaug, S., et al., *Retinal pigment epithelial function: a role for CFTR?* Doc Ophthalmol, 2003. **106**(1): p. 43-50.

56. Bosl, M.R., et al., *Male germ cells and photoreceptors, both dependent on close cell-cell interactions, degenerate upon ClC-2 Cl(-) channel disruption.* EMBO J, 2001. **20**(6): p. 1289-99.
57. Hartzell, H.C. and Z. Qu, *Chloride currents in acutely isolated Xenopus retinal pigment epithelial cells.* J Physiol, 2003. **549**(Pt 2): p. 453-69.
58. Miller, S. and D. Farber, *Cyclic AMP modulation of ion transport across frog retinal pigment epithelium. Measurements in the short-circuit state.* J Gen Physiol, 1984. **83**(6): p. 853-74.
59. Crouch, R.K., et al., *Retinoids and the visual process.* Photochem Photobiol, 1996. **64**(4): p. 613-21.
60. Steinberg, R.H., R.A. Linsenmeier, and E.R. Griff, *Three light-evoked responses of the retinal pigment epithelium.* Vision Res, 1983. **23**(11): p. 1315-23.
61. Oakley, B., 2nd, *Potassium and the photoreceptor-dependent pigment epithelial hyperpolarization.* J Gen Physiol, 1977. **70**(4): p. 405-25.
62. Oakley, B., 2nd, S.S. Miller, and R.H. Steinberg, *Effect of intracellular potassium upon the electrogenic pump of frog retinal pigment epithelium.* J Membr Biol, 1978. **44**(3-4): p. 281-307.
63. Oakley, B., 2nd, et al., *The in vitro frog pigment epithelial cell hyperpolarization in response to light.* Invest Ophthalmol Vis Sci, 1977. **16**(8): p. 771-4.
64. Hughes, B.A. and M. Takahira, *Inwardly rectifying K+ currents in isolated human retinal pigment epithelial cells.* Invest Ophthalmol Vis Sci, 1996. **37**(6): p. 1125-39.
65. Segawa, Y. and B.A. Hughes, *Properties of the inwardly rectifying K+ conductance in the toad retinal pigment epithelium.* J Physiol, 1994. **476**(1): p. 41-53.
66. Shimura, M., et al., *Expression and permeation properties of the K(+) channel Kir7.1 in the retinal pigment epithelium.* J Physiol, 2001. **531**(Pt 2): p. 329-46.
67. Yuan, Y., M. Shimura, and B.A. Hughes, *Regulation of inwardly rectifying K+ channels in retinal pigment epithelial cells by intracellular pH.* J Physiol, 2003. **549**(Pt 2): p. 429-38.
68. la Cour, M., *Kinetic properties and Na+ dependence of rheogenic Na(+)-HCO3- co-transport in frog retinal pigment epithelium.* J Physiol, 1991. **439**: p. 59-72.
69. Kenyon, E., et al., *Apical and basolateral membrane mechanisms that regulate pHi in bovine retinal pigment epithelium.* Am J Physiol, 1997. **273**(2 Pt 1): p. C456-72.
70. Lin, H., E. Kenyon, and S.S. Miller, *Na-dependent pHi regulatory mechanisms in native human retinal pigment epithelium.* Invest Ophthalmol Vis Sci, 1992. **33**(13): p. 3528-38.
71. Lin, H. and S.S. Miller, *pHi regulation in frog retinal pigment epithelium: two apical membrane mechanisms.* Am J Physiol, 1991. **261**(1 Pt 1): p. C132-42.
72. Baylor, D., *How photons start vision.* Proc Natl Acad Sci U S A, 1996. **93**(2): p. 560-5.
73. Baylor, D.A. and M.E. Burns, *Control of rhodopsin activity in vision.* Eye (Lond), 1998. **12 (Pt 3b)**: p. 521-5.
74. Okada, T., et al., *Activation of rhodopsin: new insights from structural and biochemical studies.* Trends Biochem Sci, 2001. **26**(5): p. 318-24.
75. Hargrave, P.A., *Rhodopsin structure, function, and topography the Friedenwald lecture.* Invest Ophthalmol Vis Sci, 2001. **42**(1): p. 3-9.

76. Hofmann, K.P., *Signalling states of photoactivated rhodopsin.* Novartis Found Symp, 1999. **224**: p. 158-75; discussion 175-80.
77. Lamb, T.D. and E.N. Pugh, Jr., *Dark adaptation and the retinoid cycle of vision.* Prog Retin Eye Res, 2004. **23**(3): p. 307-80.
78. Baehr, W., et al., *The retinoid cycle and retina disease.* Vision Res, 2003. **43**(28): p. 2957-8.
79. Kevany, B.M. and K. Palczewski, *Phagocytosis of retinal rod and cone photoreceptors.* Physiology (Bethesda), 2010. **25**(1): p. 8-15.
80. LaVail, M.M., *Rod outer segment disk shedding in rat retina: relationship to cyclic lighting.* Science, 1976. **194**(4269): p. 1071-4.
81. Young, R.W., *The daily rhythm of shedding and degradation of cone outer segment membranes in the lizard retina.* J Ultrastruct Res, 1977. **61**(2): p. 172-85.
82. Finnemann, S.C., *Role of alphavbeta5 integrin in regulating phagocytosis by the retinal pigment epithelium.* Adv Exp Med Biol, 2003. **533**: p. 337-42.
83. Finnemann, S.C., *Focal adhesion kinase signaling promotes phagocytosis of integrin-bound photoreceptors.* EMBO J, 2003. **22**(16): p. 4143-54.
84. Finnemann, S.C. and R.L. Silverstein, *Differential roles of CD36 and alphavbeta5 integrin in photoreceptor phagocytosis by the retinal pigment epithelium.* J Exp Med, 2001. **194**(9): p. 1289-98.
85. Heth, C.A. and P.A. Marescalchi, *Inositol triphosphate generation in cultured rat retinal pigment epithelium.* Invest Ophthalmol Vis Sci, 1994. **35**(2): p. 409-16.
86. Ryeom, S.W., et al., *Binding of anionic phospholipids to retinal pigment epithelium may be mediated by the scavenger receptor CD36.* J Biol Chem, 1996. **271**(34): p. 20536-9.
87. Ryeom, S.W., J.R. Sparrow, and R.L. Silverstein, *CD36 participates in the phagocytosis of rod outer segments by retinal pigment epithelium.* J Cell Sci, 1996. **109 (Pt 2)**: p. 387-95.
88. Sparrow, J.R., et al., *CD36 expression is altered in retinal pigment epithelial cells of the RCS rat.* Exp Eye Res, 1997. **64**(1): p. 45-56.
89. Rakoczy, P.E., et al., *Distribution of cathepsin D in human eyes with or without age-related maculopathy.* Exp Eye Res, 1999. **69**(4): p. 367-74.
90. Tanihara, H., M. Inatani, and Y. Honda, *Growth factors and their receptors in the retina and pigment epithelium.* Progress in retina and eye research, 1997. **16**(10): p. 271-301.
91. Cao, W., et al., *Pigment epithelium-derived factor protects cultured retinal neurons against hydrogen peroxide-induced cell death.* J Neurosci Res, 1999. **57**(6): p. 789-800.
92. Steele, F.R., et al., *Pigment epithelium-derived factor: neurotrophic activity and identification as a member of the serine protease inhibitor gene family.* Proc Natl Acad Sci U S A, 1993. **90**(4): p. 1526-30.
93. Wenkel, H. and J.W. Streilein, *Evidence that retinal pigment epithelium functions as an immune-privileged tissue.* Invest Ophthalmol Vis Sci, 2000. **41**(11): p. 3467-73.
94. Relvas, L.J., et al., *Extracellular nucleotides and interleukin-8 production by ARPE cells: potential role of danger signals in blood-retinal barrier activation.* Invest Ophthalmol Vis Sci, 2009. **50**(3): p. 1241-6.

95. Kim, Y.H., et al., *Regulated secretion of complement factor H by RPE and its role in RPE migration.* Graefes Arch Clin Exp Ophthalmol, 2009. **247**(5): p. 651-9.
96. Austin, B.A., et al., *Biologically active fibronectin fragments stimulate release of MCP-1 and catabolic cytokines from murine retinal pigment epithelium.* Invest Ophthalmol Vis Sci, 2009. **50**(6): p. 2896-902.
97. Berridge, M.J., *The AM and FM of calcium signalling.* Nature, 1997. **386**(6627): p. 759-60.
98. Berridge, M.J., P. Lipp, and M.D. Bootman, *The versatility and universality of calcium signalling.* Nat Rev Mol Cell Biol, 2000. **1**(1): p. 11-21.
99. Lipp, P. and E. Niggli, *Fundamental calcium release events revealed by two-photon excitation photolysis of caged calcium in Guinea-pig cardiac myocytes.* J Physiol, 1998. **508 (Pt 3)**: p. 801-9.
100. Bootman, M., et al., *Imaging the hierarchical Ca2+ signalling system in HeLa cells.* J Physiol, 1997. **499 (Pt 2)**: p. 307-14.
101. Cheng, H., W.J. Lederer, and M.B. Cannell, *Calcium sparks: elementary events underlying excitation-contraction coupling in heart muscle.* Science, 1993. **262**(5134): p. 740-4.
102. Robb-Gaspers, L.D. and A.P. Thomas, *Coordination of Ca2+ signaling by intercellular propagation of Ca2+ waves in the intact liver.* J Biol Chem, 1995. **270**(14): p. 8102-7.
103. De Koninck, P. and H. Schulman, *Sensitivity of CaM kinase II to the frequency of Ca2+ oscillations.* Science, 1998. **279**(5348): p. 227-30.
104. Oancea, E. and T. Meyer, *Protein kinase C as a molecular machine for decoding calcium and diacylglycerol signals.* Cell, 1998. **95**(3): p. 307-18.
105. Fishman, M.L., et al., *Ultrastructural demonstration of calcium in retina, retinal pigment epithelium and choroid.* Exp Eye Res, 1977. **24**(4): p. 341-53.
106. Salceda, R. and J.R. Riesgo-Escovar, *Characterization of calcium uptake in chick retinal pigment epithelium.* Pigment Cell Res, 1990. **3**(3): p. 141-5.
107. Salceda, R. and G. Sanchez-Chavez, *Calcium uptake, release and ryanodine binding in melanosomes from retinal pigment epithelium.* Cell Calcium, 2000. **27**(4): p. 223-9.
108. Himpens, B., et al., *Intra- and intercellular Ca2+ signaling in retinal pigment epithelial cells during mechanical stimulation.* FASEB J, 1999. **13 Suppl**: p. S63-8.
109. Himpens, B. and J. Vereecke, *[Intra- and intercellular Ca(2+)-signal transduction].* Verh K Acad Geneeskd Belg, 2000. **62**(6): p. 501-63.
110. Pearson, R.A., et al., *Ca(2+) signalling and gap junction coupling within and between pigment epithelium and neural retina in the developing chick.* Eur J Neurosci, 2004. **19**(9): p. 2435-45.
111. Wimmers, S., M.O. Karl, and O. Strauss, *Ion channels in the RPE.* Prog Retin Eye Res, 2007. **26**(3): p. 263-301.
112. Cordeiro, S., et al., *Heat-sensitive TRPV channels in retinal pigment epithelial cells: regulation of VEGF-A secretion.* Invest Ophthalmol Vis Sci. **51**(11): p. 6001-8.
113. Karl, M.O., et al., *Endogenous Gas6 and Ca2+ -channel activation modulate phagocytosis by retinal pigment epithelium.* Cell Signal, 2008. **20**(6): p. 1159-68.
114. Catterall, W.A., *Voltage-gated calcium channels.* Cold Spring Harb Perspect Biol, 2011. **3**(8): p. a003947.

115. Catterall, W.A., et al., *International Union of Pharmacology. XLVIII. Nomenclature and structure-function relationships of voltage-gated calcium channels.* Pharmacol Rev, 2005. **57**(4): p. 411-25.
116. Striessnig, J., *Pharmacology, structure and function of cardiac L-type Ca(2+) channels.* Cell Physiol Biochem, 1999. **9**(4-5): p. 242-69.
117. Striessnig, J., et al., *L-type Ca2+ channels in Ca2+ channelopathies.* Biochem Biophys Res Commun, 2004. **322**(4): p. 1341-6.
118. Wimmers, S., et al., *Expression profile of voltage-dependent Ca2+ channel subunits in the human retinal pigment epithelium.* Graefes Arch Clin Exp Ophthalmol, 2008. **246**(5): p. 685-92.
119. Rosenthal, R., et al., *Ca2+ channels in retinal pigment epithelial cells regulate vascular endothelial growth factor secretion rates in health and disease.* Mol Vis, 2007. **13**: p. 443-56.
120. Strauss, O., et al., *Activation of neuroendocrine L-type channels (alpha1D subunits) in retinal pigment epithelial cells and brain neurons by pp60(c-src).* Biochem Biophys Res Commun, 2000. **270**(3): p. 806-10.
121. Rosenthal, R., et al., *Expression of bestrophin-1, the product of the VMD2 gene, modulates voltage-dependent Ca2+ channels in retinal pigment epithelial cells.* FASEB J, 2006. **20**(1): p. 178-80.
122. Koschak, A., et al., *alpha 1D (Cav1.3) subunits can form l-type Ca2+ channels activating at negative voltages.* J Biol Chem, 2001. **276**(25): p. 22100-6.
123. Michna, M., et al., *Cav1.3 (alpha1D) Ca2+ currents in neonatal outer hair cells of mice.* J Physiol, 2003. **553**(Pt 3): p. 747-58.
124. Wimmers, S. and O. Strauss, *Basal calcium entry in retinal pigment epithelial cells is mediated by TRPC channels.* Invest Ophthalmol Vis Sci, 2007. **48**(12): p. 5767-72.
125. Burnstock, G., *Introduction: P2 receptors.* Curr Top Med Chem, 2004. **4**(8): p. 793-803.
126. North, R.A., *Molecular physiology of P2X receptors.* Physiol Rev, 2002. **82**(4): p. 1013-67.
127. Peterson, W.M., et al., *Extracellular ATP activates calcium signaling, ion, and fluid transport in retinal pigment epithelium.* J Neurosci, 1997. **17**(7): p. 2324-37.
128. Reigada, D., et al., *Degradation of extracellular ATP by the retinal pigment epithelium.* Am J Physiol Cell Physiol, 2005. **289**(3): p. C617-24.
129. Reigada, D. and C.H. Mitchell, *Release of ATP from retinal pigment epithelial cells involves both CFTR and vesicular transport.* Am J Physiol Cell Physiol, 2005. **288**(1): p. C132-40.
130. Mitchell, C.H., *Release of ATP by a human retinal pigment epithelial cell line: potential for autocrine stimulation through subretinal space.* J Physiol, 2001. **534**(Pt 1): p. 193-202.
131. Conn, P.J., *Physiological roles and therapeutic potential of metabotropic glutamate receptors.* Ann N Y Acad Sci, 2003. **1003**: p. 12-21.
132. Kew, J.N. and J.A. Kemp, *Ionotropic and metabotropic glutamate receptor structure and pharmacology.* Psychopharmacology (Berl), 2005. **179**(1): p. 4-29.
133. Mayer, M.L., *Glutamate receptor ion channels.* Curr Opin Neurobiol, 2005. **15**(3): p. 282-8.
134. Feldman, E.L., et al., *Receptor-coupled phosphoinositide hydrolysis in human retinal pigment epithelium.* J Neurochem, 1991. **56**(6): p. 2094-100.

135. Fragoso, G. and A.M. Lopez-Colome, *Excitatory amino acid-induced inositol phosphate formation in cultured retinal pigment epithelium.* Vis Neurosci, 1999. **16**(2): p. 263-9.
136. Reigada, D., W. Lu, and C.H. Mitchell, *Glutamate acts at NMDA receptors on fresh bovine and on cultured human retinal pigment epithelial cells to trigger release of ATP.* J Physiol, 2006. **575**(Pt 3): p. 707-20.
137. Parekh, A.B., *Store-operated CRAC channels: function in health and disease.* Nat Rev Drug Discov, 2010. **9**(5): p. 399-410.
138. Parekh, A.B. and J.W. Putney, Jr., *Store-operated calcium channels.* Physiol Rev, 2005. **85**(2): p. 757-810.
139. Clapham, D.E., *Calcium signaling.* Cell, 2007. **131**(6): p. 1047-58.
140. Liou, J., et al., *STIM is a Ca2+ sensor essential for Ca2+-store-depletion-triggered Ca2+ influx.* Curr Biol, 2005. **15**(13): p. 1235-41.
141. Roos, J., et al., *STIM1, an essential and conserved component of store-operated Ca2+ channel function.* J Cell Biol, 2005. **169**(3): p. 435-45.
142. Zhang, S.L., et al., *STIM1 is a Ca2+ sensor that activates CRAC channels and migrates from the Ca2+ store to the plasma membrane.* Nature, 2005. **437**(7060): p. 902-5.
143. Prakriya, M., et al., *Orai1 is an essential pore subunit of the CRAC channel.* Nature, 2006. **443**(7108): p. 230-3.
144. Vig, M., et al., *CRACM1 multimers form the ion-selective pore of the CRAC channel.* Curr Biol, 2006. **16**(20): p. 2073-9.
145. Cahalan, M.D., et al., *Molecular basis of the CRAC channel.* Cell Calcium, 2007. **42**(2): p. 133-44.
146. Lewis, R.S., *The molecular choreography of a store-operated calcium channel.* Nature, 2007. **446**(7133): p. 284-7.
147. Dziadek, M.A. and L.S. Johnstone, *Biochemical properties and cellular localisation of STIM proteins.* Cell Calcium, 2007. **42**(2): p. 123-32.
148. Cahalan, M.D., *STIMulating store-operated Ca(2+) entry.* Nat Cell Biol, 2009. **11**(6): p. 669-77.
149. Hogan, P.G., R.S. Lewis, and A. Rao, *Molecular basis of calcium signaling in lymphocytes: STIM and ORAI.* Annu Rev Immunol, 2010. **28**: p. 491-533.
150. Vig, M., et al., *CRACM1 is a plasma membrane protein essential for store-operated Ca2+ entry.* Science, 2006. **312**(5777): p. 1220-3.
151. Yeromin, A.V., et al., *Molecular identification of the CRAC channel by altered ion selectivity in a mutant of Orai.* Nature, 2006. **443**(7108): p. 226-9.
152. Park, C.Y., et al., *STIM1 clusters and activates CRAC channels via direct binding of a cytosolic domain to Orai1.* Cell, 2009. **136**(5): p. 876-90.
153. Cordeiro, S. and O. Strauss, *Expression of Orai genes and I(CRAC) activation in the human retinal pigment epithelium.* Graefes Arch Clin Exp Ophthalmol, 2011. **249**(1): p. 47-54.
154. Allikmets, R., *A photoreceptor cell-specific ATP-binding transporter gene (ABCR) is mutated in recessive Stargardt macular dystrophy.* Nat Genet, 1997. **17**(1): p. 122.
155. Cideciyan, A.V., et al., *Mutations in ABCA4 result in accumulation of lipofuscin before slowing of the retinoid cycle: a reappraisal of the human disease sequence.* Hum Mol Genet, 2004. **13**(5): p. 525-34.
156. Delori, F.C., et al., *In vivo measurement of lipofuscin in Stargardt's disease--Fundus flavimaculatus.* Invest Ophthalmol Vis Sci, 1995. **36**(11): p. 2327-31.

157. Petrukhin, K., et al., *Identification of the gene responsible for Best macular dystrophy.* Nat Genet, 1998. **19**(3): p. 241-7.
158. Marquardt, A., et al., *Mutations in a novel gene, VMD2, encoding a protein of unknown properties cause juvenile-onset vitelliform macular dystrophy (Best's disease).* Hum Mol Genet, 1998. **7**(9): p. 1517-25.
159. Clemett, R., *Vitelliform dystrophy: long-term observations on New Zealand pedigrees.* Aust N Z J Ophthalmol, 1991. **19**(3): p. 221-7.
160. Mohler, C.W. and S.L. Fine, *Long-term evaluation of patients with Best's vitelliform dystrophy.* Ophthalmology, 1981. **88**(7): p. 688-92.
161. Wabbels, B., et al., *Genotype-phenotype correlation and longitudinal course in ten families with Best vitelliform macular dystrophy.* Graefes Arch Clin Exp Ophthalmol, 2006. **244**(11): p. 1453-66.
162. Renner, A.B., et al., *Late onset is common in best macular dystrophy associated with VMD2 gene mutations.* Ophthalmology, 2005. **112**(4): p. 586-92.
163. Frangieh, G.T., W.R. Green, and S.L. Fine, *A histopathologic study of Best's macular dystrophy.* Arch Ophthalmol, 1982. **100**(7): p. 1115-21.
164. Weingeist, T.A., J.L. Kobrin, and R.C. Watzke, *Histopathology of Best's macular dystrophy.* Arch Ophthalmol, 1982. **100**(7): p. 1108-14.
165. Boon, C.J., et al., *The spectrum of ocular phenotypes caused by mutations in the BEST1 gene.* Prog Retin Eye Res, 2009. **28**(3): p. 187-205.
166. Lorenz, B. and M.N. Preising, *[Best's disease. Overview of pathology and its causes].* Ophthalmologe, 2005. **102**(2): p. 111-5.
167. Brown, M., et al., *ISCEV Standard for Clinical Electro-oculography (EOG) 2006.* Doc Ophthalmol, 2006. **113**(3): p. 205-12.
168. Arden, G.B., A. Barrada, and J.H. Kelsey, *New clinical test of retinal function based upon the standing potential of the eye.* Br J Ophthalmol, 1962. **46**(8): p. 449-67.
169. Deutman, A.F., *Electro-oculography in families with vitelliform dystrophy of the fovea. Detection of the carrier state.* Arch Ophthalmol, 1969. **81**(3): p. 305-16.
170. Pollack, K., F.R. Kreuz, and L.E. Pillunat, *[Best's disease with normal EOG. Case report of familial macular dystrophy].* Ophthalmologe, 2005. **102**(9): p. 891-4.
171. Hartzell, H.C., et al., *Molecular physiology of bestrophins: multifunctional membrane proteins linked to best disease and other retinopathies.* Physiol Rev, 2008. **88**(2): p. 639-72.
172. Tsunenari, T., et al., *Structure-function analysis of the bestrophin family of anion channels.* J Biol Chem, 2003. **278**(42): p. 41114-25.
173. Milenkovic, V.M., et al., *Molecular evolution and functional divergence of the bestrophin protein family.* BMC Evol Biol, 2008. **8**: p. 72.
174. Marmorstein, A.D., et al., *Bestrophin, the product of the Best vitelliform macular dystrophy gene (VMD2), localizes to the basolateral plasma membrane of the retinal pigment epithelium.* Proc Natl Acad Sci U S A, 2000. **97**(23): p. 12758-63.
175. Marmorstein, L.Y., et al., *The light peak of the electroretinogram is dependent on voltage-gated calcium channels and antagonized by bestrophin (best-1).* J Gen Physiol, 2006. **127**(5): p. 577-89.
176. Milenkovic, V.M., et al., *Insertion and topology of normal and mutant bestrophin-1 in the endoplasmic reticulum membrane.* J Biol Chem, 2007. **282**(2): p. 1313-21.

177. Kramer, F., H. Stohr, and B.H. Weber, *Cloning and characterization of the murine Vmd2 RFP-TM gene family.* Cytogenet Genome Res, 2004. **105**(1): p. 107-14.
178. Park, H., et al., *Bestrophin-1 encodes for the Ca2+-activated anion channel in hippocampal astrocytes.* J Neurosci, 2009. **29**(41): p. 13063-73.
179. Stohr, H., et al., *Three novel human VMD2-like genes are members of the evolutionary highly conserved RFP-TM family.* Eur J Hum Genet, 2002. **10**(4): p. 281-4.
180. Neussert, R., et al., *The presence of bestrophin-1 modulates the Ca2+ recruitment from Ca2+ stores in the ER.* Pflugers Arch, 2010. **460**(1): p. 163-75.
181. Barro Soria, R., et al., *Bestrophin-1 enables Ca2+-activated Cl- conductance in epithelia.* J Biol Chem, 2009. **284**(43): p. 29405-12.
182. Sun, H., et al., *The vitelliform macular dystrophy protein defines a new family of chloride channels.* Proc Natl Acad Sci U S A, 2002. **99**(6): p. 4008-13.
183. Stanton, J.B., et al., *Hydrodynamic properties of porcine bestrophin-1 in Triton X-100.* Biochim Biophys Acta, 2006. **1758**(2): p. 241-7.
184. Marchant, D., et al., *New VMD2 gene mutations identified in patients affected by Best vitelliform macular dystrophy.* J Med Genet, 2007. **44**(3): p. e70.
185. Yu, K., et al., *Chloride channel activity of bestrophin mutants associated with mild or late-onset macular degeneration.* Invest Ophthalmol Vis Sci, 2007. **48**(10): p. 4694-705.
186. Barro-Soria, R., R. Schreiber, and K. Kunzelmann, *Bestrophin 1 and 2 are components of the Ca(2+) activated Cl(-) conductance in mouse airways.* Biochim Biophys Acta, 2008. **1783**(10): p. 1993-2000.
187. Constable, P.A., *Nifedipine alters the light-rise of the electro-oculogram in man.* Graefes Arch Clin Exp Ophthalmol. **249**(5): p. 677-84.
188. Yu, K., et al., *The best disease-linked Cl- channel hBest1 regulates Ca V 1 (L-type) Ca2+ channels via src-homology-binding domains.* J Neurosci, 2008. **28**(22): p. 5660-70.
189. Reichhart, N., et al., *Effect of bestrophin-1 on L-type Ca2+ channel activity depends on the Ca2+ channel beta-subunit.* Exp Eye Res, 2010. **91**(5): p. 630-9.
190. Milenkovic, V.M., et al., *Interaction of bestrophin-1 and Ca2+ channel beta-subunits: identification of new binding domains on the bestrophin-1 C-terminus.* PLoS One, 2011. **6**(4): p. e19364.
191. Schulz, H.L., *VMD2 database (Institute of Human Genetics, University of Regensburg,*
Germany). 2009.
192. Milenkovic, V.M., et al., *Disease-associated missense mutations in bestrophin-1 affect cellular trafficking and anion conductance.* J Cell Sci, 2011. **124**(Pt 17): p. 2988-96.
193. Zhang, Y., et al., *Suppression of Ca2+ signaling in a mouse model of Best disease.* Hum Mol Genet, 2010. **19**(6): p. 1108-18.
194. Bakall, B., et al., *Enhanced accumulation of A2E in individuals homozygous or heterozygous for mutations in BEST1 (VMD2).* Exp Eye Res, 2007. **85**(1): p. 34-43.
195. Nordstrom, S. and Y. Barkman, *Hereditary maculardegeneration (HMD) in 246 cases traced to one gene-source in central Sweden.* Hereditas, 1977. **84**(2): p. 163-76.

196. Nordstrom, S. and W. Thorburn, *Dominantly inherited macular degeneration (Best's disease) in a homozygous father with 11 children.* Clin Genet, 1980. **18**(3): p. 211-6.
197. Bakall, B., et al., *Expression and localization of bestrophin during normal mouse development.* Invest Ophthalmol Vis Sci, 2003. **44**(8): p. 3622-8.
198. Guziewicz, K.E., et al., *Bestrophin gene mutations cause canine multifocal retinopathy: a novel animal model for best disease.* Invest Ophthalmol Vis Sci, 2007. **48**(5): p. 1959-67.
199. Hoffmann, I., et al., *Canine multifocal retinopathy in the Australian Shepherd: a case report.* Vet Ophthalmol, 2012.
200. Zangerl, B., et al., *Assessment of canine BEST1 variations identifies new mutations and establishes an independent bestrophinopathy model (cmr3).* Mol Vis, 2010. **16**: p. 2791-804.
201. Grynkiewicz, G., M. Poenie, and R.Y. Tsien, *A new generation of Ca2+ indicators with greatly improved fluorescence properties.* J Biol Chem, 1985. **260**(6): p. 3440-50.
202. Putney, J.W., *Pharmacology of store-operated calcium channels.* Mol Interv. **10**(4): p. 209-18.
203. Barro-Soria, R., et al., *ER-localized bestrophin 1 activates Ca2+-dependent ion channels TMEM16A and SK4 possibly by acting as a counterion channel.* Pflugers Arch, 2010. **459**(3): p. 485-97.
204. Hafezi, F., et al., *Retinal degeneration in the rd mouse in the absence of c-fos.* Invest Ophthalmol Vis Sci, 1998. **39**(12): p. 2239-44.
205. Reme, C.E., et al., *Apoptotic cell death in retinal degenerations.* Prog Retin Eye Res, 1998. **17**(4): p. 443-64.
206. Wenzel, A., et al., *The genetic modifier Rpe65Leu(450): effect on light damage susceptibility in c-Fos-deficient mice.* Invest Ophthalmol Vis Sci, 2003. **44**(6): p. 2798-802.
207. Grimm, C., et al., *Protection of Rpe65-deficient mice identifies rhodopsin as a mediator of light-induced retinal degeneration.* Nat Genet, 2000. **25**(1): p. 63-6.
208. Kaven, C.W., et al., *Growth factor combinations modulate human retinal pigment epithelial cell proliferation.* Curr Eye Res, 2000. **20**(6): p. 480-7.
209. Spraul, C.W., et al., *Effect of insulin-like growth factors 1 and 2, and glucose on the migration and proliferation of bovine retinal pigment epithelial cellsin vitro.* Ophthalmic Res, 2000. **32**(5): p. 244-8.
210. Steindl-Kuscher, K., et al., *Epidermal growth factor: the driving force in initiation of RPE cell proliferation.* Graefes Arch Clin Exp Ophthalmol. **249**(8): p. 1195-200.
211. Feske, S., *CRAC channelopathies.* Pflugers Arch. **460**(2): p. 417-35.
212. Hogan, P.G., R.S. Lewis, and A. Rao, *Molecular basis of calcium signaling in lymphocytes: STIM and ORAI.* Annu Rev Immunol. **28**: p. 491-533.
213. Strauss, O., et al., *Involvement of protein tyrosine kinase in the InsP3-induced activation of Ca2+-dependent Cl- currents in cultured cells of the rat retinal pigment epithelium.* J Membr Biol, 1999. **169**(3): p. 141-53.
214. Strauss, O., M. Wiederholt, and M. Wienrich, *Activation of Cl- currents in cultured rat retinal pigment epithelial cells by intracellular applications of inositol-1,4,5-triphosphate: differences between rats with retinal dystrophy (RCS) and normal rats.* J Membr Biol, 1996. **151**(2): p. 189-200.

215. Feske, S., *ORAI1 and STIM1 deficiency in human and mice: roles of store-operated Ca2+ entry in the immune system and beyond.* Immunol Rev, 2009. **231**(1): p. 189-209.
216. Feske, S., et al., *A mutation in Orai1 causes immune deficiency by abrogating CRAC channel function.* Nature, 2006. **441**(7090): p. 179-85.
217. Zhang, S.L., et al., *Genome-wide RNAi screen of Ca(2+) influx identifies genes that regulate Ca(2+) release-activated Ca(2+) channel activity.* Proc Natl Acad Sci U S A, 2006. **103**(24): p. 9357-62.
218. Gross, S.A., et al., *Murine ORAI2 splice variants form functional Ca2+ release-activated Ca2+ (CRAC) channels.* J Biol Chem, 2007. **282**(27): p. 19375-84.
219. Gwack, Y., et al., *Biochemical and functional characterization of Orai proteins.* J Biol Chem, 2007. **282**(22): p. 16232-43.
220. Lis, A., et al., *CRACM1, CRACM2, and CRACM3 are store-operated Ca2+ channels with distinct functional properties.* Curr Biol, 2007. **17**(9): p. 794-800.
221. Brandman, O., et al., *STIM2 is a feedback regulator that stabilizes basal cytosolic and endoplasmic reticulum Ca2+ levels.* Cell, 2007. **131**(7): p. 1327-39.
222. Guziewicz, K.E., et al., *Molecular consequences of BEST1 gene mutations in canine multifocal retinopathy predict functional implications for human bestrophinopathies.* Invest Ophthalmol Vis Sci, 2011. **52**(7): p. 4497-505.
223. Mullins, R.F., et al., *Late development of vitelliform lesions and flecks in a patient with best disease: clinicopathologic correlation.* Arch Ophthalmol, 2005. **123**(11): p. 1588-94.